Geological Survey of Finland 2016

Electromagnetic Geotomographic Research on Attenuating Material Using the Middle Radio Frequency Band

Arto Korpisalo

Academic Dissertation

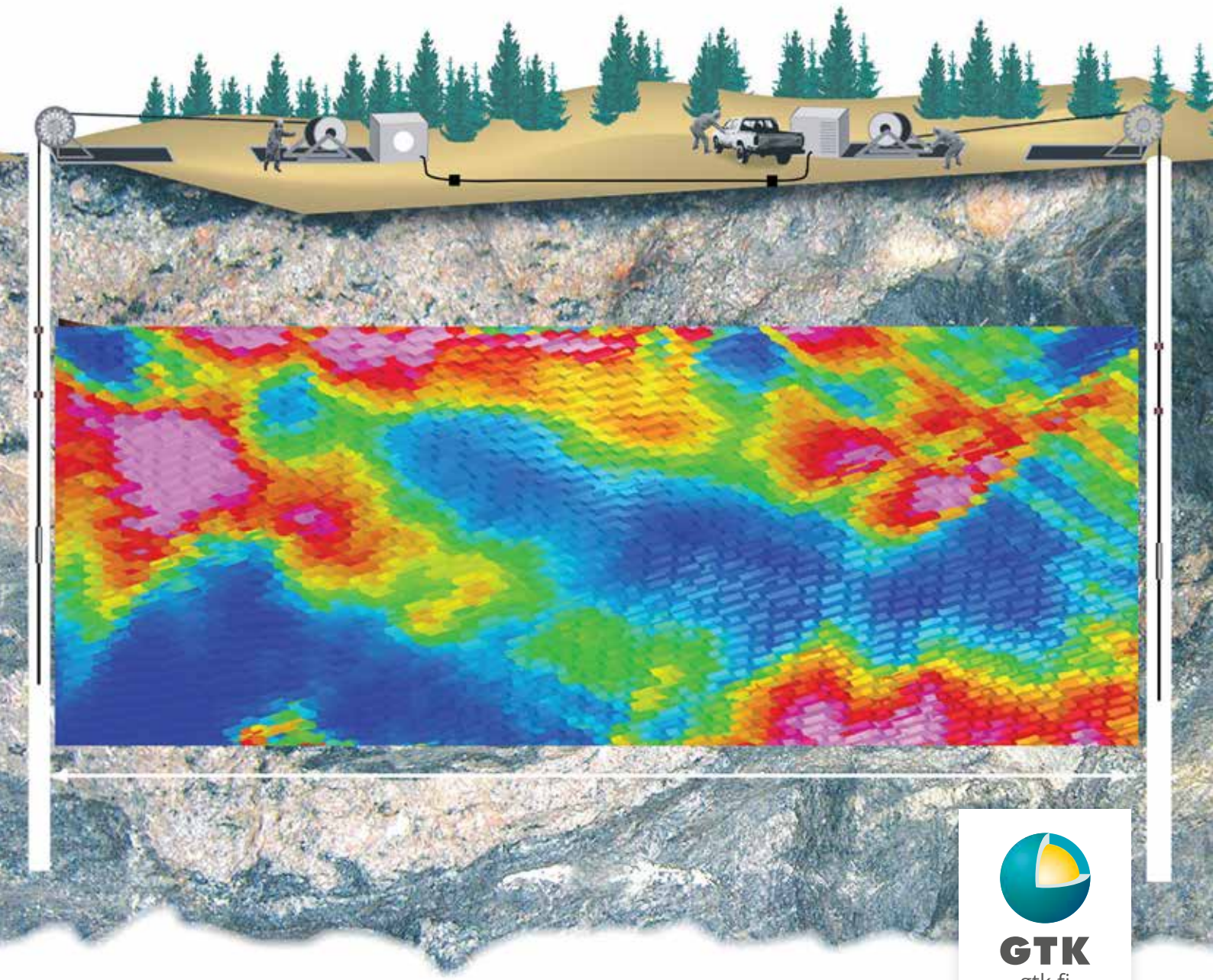

GTK
gtk.fi

ELECTROMAGNETIC GEOTOMOGRAPHIC RESEARCH ON ATTENUATING MATERIAL USING MIDDLE RADIO FREQUENCY BAND

by

Arto Korpisalo
Geological Survey of Finland
P.O. Box 96
FI-02151 Espoo, Finland

ACADEMIC DISSERTATION
Department of Physics, University of Helsinki

To be presented, with the permission of the Faculty of Science of University of Helsinki, for public criticism in Auditorium D101, Physicum, Gustaf Hällströmin katu 2a, on October 14th, 2016, at 12 o'clock noon.

Unless otherwise indicated, the figures have been prepared by the author of the publication.

Geological Survey of Finland
Espoo 2016

Supervisors
Professor Ilmo Kukkonen
University of Helsinki
Department of Physics
Finland

Professor Emeritus Folke Stenman
University of Helsinki
Department of Physics
Finland

Pre-examiners
Dosent Ville Viikari
Aalto University
School of Electric Engineering
Espoo, Finland

Dr Declan Vogt
University of the Witwatersrand
Faculty of Engineering and the Built Environment
Johannesburg, South Africa

Opponent
Professor Richard Smith,
Laurentian University
Department of Earth Sciences
Sudbury, Canada

Front cover: Geotomographic measurement and reconstruction (not to scale).
Photo: Harri Kutvonen, GTK.

Korpisalo, A. 2016. Electromagnetic Geotomographic Research on Attenuating Material Using Middle Radio Frequency Band. *Geological Survey of Finland*, Espoo. 68 pages, 30 figures, 1 table with original articles (I–IV).

ABSTRACT

The purpose of this thesis is to present the essential issues concerning the radio imaging method (RIM) and attenuation measurements. Although most of the issues discussed in this thesis are in no sense novel, the thesis provides an overview of the fundamental aspects of RIM and presents novel results from the combination of RIM with other borehole methods.

About 2.6 million years ago, early humans perhaps accidently discovered that sharp stone flakes made it easier to cut the flesh from around bones. From sharp flakes to the first handaxes took hundreds of thousands of years, and the development was thus extremely slow. Alessandro Volta's invention of the voltaic pile (battery) in 1800 started a huge journey, and only one hundred years later humans had all the necessary means to start examining the Earth's subsurface. Since then, the development has been rapid, resulting in numerous methods (*e.g. magnetic, gravimetric, electromagnetic and seismic*) and techniques to resolve the Earth's treasures.

The theoretical basis for the radio imaging method was established long before the method was utilized for exploration purposes. RIM is a geotomographic electromagnetic method in which the transmitter and receivers are in different boreholes to delineate electric conductors between the boreholes. It is a frequency domain method and the continuous wave technique is usually utilized. One of the pioneers was L.G. Stolarczyk in the USA in the 1980s. In the former Soviet Union, interest in RIM was high in the late 2000s. Our present device is also Russian based. Furthermore, in South Africa and Australian, a considerable amount of effort has been invested in RIM.

The RIM device is superficially examined. It is the essential part in our RIM system, referred to as electromagnetic radiofrequency echoing (EMRE). The idea behind the device is excellent. However, several poor solutions have been utilized in its construction. Many of them have possibly resulted from the lack of good electronic components. The overall electronic construction of the whole device is very complicated. At least two essential properties are lacking, namely circuits for measuring the input impedances of the antennas and the return loss to obtain the actual output power. Of course, the digitalization of data in the borehole receiver could give additional benefits in data handling. The measurements can be monitored in real time on a screen, thus allowing the operator to already gain initial insights into the subsurface geology at the site and also to modify the measurement plan if necessary. Even today, no practical forward modelling tool for examining the behaviour of electromagnetic waves in the Earth's subsurface is available for the RIM environment, and interpretation is thus traditionally based on linear reconstruction techniques. Assuming low contrast and straight ray conditions can generally provide good and rapid results, even during the measurement session. Electrical resistive logging is usually one of the first methods used in a new borehole. Comparing the logging data with measured amplitude data can simply reveal the situations where a nearby and relatively limited conductive formation can mostly be responsible

for the high attenuations levels between boreholes and can hence be taken into account in the interpretation. The transient electromagnetic method (TEM) functions in the time domain. TEM is also a short-range method and can very reliably reveal nearby conductors. Comparisons of RIM and TEM data from the ore district coincide well. These issues are considered in detail in Publication I.

The functioning of the antenna is highly dependent on the environment in which the antenna is placed. The primary task of the antenna is to radiate and receive electromagnetic energy, or the antenna is a transducer between the generator and the environment. A simple bare wire can serve as a diagnostic probe to detect conductors in the borehole vicinity. However, borehole antennas are generally highly insulated to prevent the leakage of current into the borehole, and at the same time the insulation reduces the sensitivity of the antenna current to the ambient medium, especially as the electric properties of the insulation and surrounding material differ significantly. However, monitoring of the input impedance of the antenna could help in estimating its effectiveness in the borehole. This property is lacking in the present device. The scattering parameter defines the relationship between the reflected and incident voltage or it provides information on the impedance matching chain. The behaviour of impedance of the insulated antennas in the different borehole conditions were estimated using simple analytical methods, such as the models of Wu, King and Giri (WKG) and Chen and Warne (CHEN), and highly sophisticated numerical software such as FEKO from EM Software & Systems (Altair). According to the results, our antennas maintain their effectiveness and feasibility in the whole frequency band (312.5–2500 kHz) utilized by the device. However, the highest frequency (2500 kHz) may suffer from different ambient conditions. The resolution is closely related to the frequency, whereby higher frequencies result in better resolution but at the expense of the range. These issues are clarified in Publication II.

Electromagnetic methods are based on the fact that earth materials may have large contrasts in their electrical properties. A geotomographic RIM survey can have several benefits over ground-level EM sounding methods. When the transmitter is in the borehole, boundary effects due to the ground surface and the strong attenuation emerging from soils are easily eliminated. A borehole survey also brings the survey closer to the targets, and higher frequencies can be used, which means better resolution. Viewing of the target from different angles and directions also means better reconstruction results. The fundamental principles of the electromagnetic fields are explained to distinguish diffusive movement (strongly attenuating propagation) from wave propagation and to give a good conception of the possible transillumination depths of RIM. The transillumination depths of up to 1000 m are possible in a highly resistive environment using the lowest measurement frequency (312.5 kHz). In this context, one interesting and challenging case study is also presented from the area for a repository of spent nuclear fuel in Finland. The task was to examine the usefulness of RIM in the area and to determine how well the apparent resistivity could be associated with the structural integrity of the rock. The measurements were successful and the results convinced us of the potential of RIM. Publication III is related to these issues.

In Finland, active use of RIM started in 2005 when Russian RIM experts jointly with GTK carried out RIM measurements at Olkiluoto. The results are presented in Publication IV. In this pioneering work, extensive background information (e.g. versatile geophysical borehole logging, optical imaging, 3D vertical seismic profile (VSP) and single-hole radar reflection measurements) was available from the site. The comparability of the results was good, e.g. low resistive or highly attenuating areas near boreholes from the RIM measurements coincided well with resistive logging and radar results. Electric mise-á-la-masse and high frequency electromagnetic RIM displayed even better comparability. The comparability of the surface electromagnetic sounding data and the RIM data was good. However, the tomographic reconstruction is much more detailed. In overall conclusion, the attenuation measurements were

well suited to the recording of subsurface resistivity properties and continuity information between boreholes at Olkiluoto. To date, we have utilized RIM in two quite different environments. Olkiluoto is a spent nuclear fuel area in Finland with solid crystalline bedrock and Pyhäsalmi is an ore district with massive sulphide deposit. Despite Pyhäsalmi being an ideal research target for RIM, the utilization of the method has proven successful in both cases.

Keywords (GeoRef Thesaurus, AGI): bedrock, boreholes, crosshole methods, radio imaging method, radio-wave methods, resistivity, conductivity, tomography, geophysical methods, electromagnetic methods, Olkiluoto, Pyhäsalmi, Finland

Keywords: ART, SIRT, EMRE, RIM

Arto Korpisalo
Geological Survey of Finland
P.O. Box 96
FI-02151 Espoo, Finland

E-mail: arto.korpisalo@gtk.fi

ISBN 978-952-217-358-4 (paperback)
ISBN 978-952-217-359-1 (PDF version without articles)

Layout: Elvi Turtiainen Oy
Printing house: Lönnberg Print & Promo, Finland

CONTENTS

PREFACE

The research described in this thesis was carried out at the Geological Survey of Finland, in the Bedrock Geology and Resources unit of the Southern Finland office (ESY), and at the Department of Physics of the University of Helsinki during 2000–2016.

I wish to thank the Head of the Department of Physics, Professor Juhani Keinonen, for providing me with an opportunity to pursue postgraduate studies. I especially want to thank Professor Emeritus Folke Stenman and Dr Heikki Soininen, who helped me greatly in taking the first steps and gave me the freedom to do things in my own way. I am grateful to Professor Ilmo Kukkonen for leading me to the goal by guiding me to finish this research.

Special thanks to RF specialist Mika Niemelä (Bandercom Oy), who was the key person in maintaining the proper functioning of the old CW device. Mika carefully guided me in understanding the functioning of the device and helped me to understand and interpret the real-time signals in the field. Geophysicist Eero Heikkinen is acknowledged as the co-author of the fourth publication. Geophysicists Kimmo Korhonen and Tapio Ruotoistenmäki greatly aided me in the construction of the published papers. Geophysicists Dr Meri-Liisa Airo and Dr Suvi Heinonen gave me valuable advice throughout this synopsis. Personal discussions with Dr Declan Vogt from the Council for Scientific and Industrial Research in South Africa (CSIR) have been very rewarding.

The preliminary examiners of the thesis, Dosent V. Viikari and Dr D. Vogt, are thanked for their effort.

And last but not least, I want to thank my beloved and so temperamental wife, Venera, for her support during this enormously interesting time. Sometimes, the path was messy but she always helped me to find the right direction as she has done during all of our common wonderful moments. Let this thesis also be an example to my grandchildren, Emre and Arda, that with Finnish "sisu", one can even plough through granite and grey stone. And remind them that whatever you start you must also finish. I love all of you very much!

So, thanks again to all of you!
Arto Korpisalo

LIST OF ORIGINAL PUBLICATIONS

This thesis consists of a synopsis and the following publications, which are referred to in the text by their Roman numerals:

Paper I: Korpisalo, A. 2014. Geotomographic studies for ore explorations with the EMRE system. Measurement, Vol. 48, 232–247. DOI: 10.1016/j.measurement.2013.11.016.

Paper II: Korpisalo, A. 2013. Borehole antenna considerations in the EMRE system: Frequency band 312.5–2500 kHz. The Open Geology Journal, Vol. 7, 63–79. DOI: 10.2174/1874262901307010063.

Paper III: Korpisalo, A. 2014. Characterization of geotomographic studies with the EMRE system. International Journal of Geophysics, Vol. 2014. Article ID 401654. 18 p. DOI: 10.1155/2014/401654.

Paper IV: Korpisalo, A. & Heikkinen, E. 2014. Radiowave imaging (RIM) for determining the electrical conductivity of the rock in borehole section OL-KR4–OL-KR10 at Olkiluoto, Finland. Exploration Geophysics, Vol. 46. Published online: 14 May 2014. DOI: 10.1071/EG13057.

LIST OF ABBREVIATIONS AND UNITS

AC	Alternating current
AD	Anno Domini
AMT	Audio-magnetotellurics
ART	Algebraic reconstruction technique
$\vec{B}$	Magnetic flux density
BC	Before Christ
C, C_L, C_H, C_1	Capacitances
Cal	The c.g.s. unit of acceleration
CGLS	Conjugated gradient least square
c.g.s.	centimetre-gram-second system of units
CT	Computed tomography
CW	Continuous wave
D	Directivity
$\vec{D}$	Displacement current
dB	Decibel
DC	Direct current
$\vec{E}$	Electric field vector
$\vec{E}_0$	Source field strength
$\vec{E}_\theta$	Electric tangential component
$\vec{E}_r$	Electric radial component
EM	Electromagnetic
EMRE	Electromagnetic radiofrequency echoing
XRD	X-ray diffraction
XRF	X-ray fluorescence
f	Frequency
f_k	Frequency in kHz
FMCW	Frequency modulated continuous wave radar
G	Gravitational constant, Gain
g	Acceleration
G_f	Geometric factor
G_t, G_r	The gains of transmitter and receiver antennas
GPR	Ground penetrating radar
GTK	Geological Survey of Finland
$\vec{H}$	Magnetizing field
HED	Horizontal electric dipole
HIRE	High-resolution reflection vibroseismic survey
HMD	Horizontal magnetic dipole
Hz	Hertz
I	Current
i	Imaginary unit (=sqrt(-1)
IF	Intermediate frequency
IP	Induced polarization
k	Bulk modulus, wave number
LSQR	The iterative least square method
$\vec{M}$	Magnetization
M, m	Masses
$\vec{M}_i$	Induced magnetization
$\vec{M}_r$	Remanent magnetization
MOM	Multi-offset measurement
MT	Magnetotellurics
Mt	Megatonne
Nepers	A natural logarithmic unit for ratios
p	Loss tangent
P_{DC}	The DC ($\omega=0$) conductivity path
P_t, P_r	The transmitted and received power
P-waves	Compressional, primary waves
PRF	Pulse repetition frequency
PRI	Pulse repetition interval
R, R'	Distance
RADAR	Radio detection and ranging
RIM	Radio imaging method
RX	Receiver
T	Tesla
TEM	Transient electromagnetic method
Tr1, Tr2	Filters
TX	Transmitter
S	Siemens
SI	The International System of Units
SIRT	Simultaneous iterative reconstruction technique
S-waves	Shear, secondary waves
VETEM	Very early time EM
VMD	Vertical magnetic dipole
X	Reactance
ZOM	Zero-offset measurement
Z_L	Impedance

LIST OF SYMBOLS

α	Attenuation constant
β	Phase constant
δ	Skin depth
ε	Dielectric permittivity
ε_r	Relative dielectric permittivity
χ_m	Magnetic susceptibility
λ	Wave length
π	pi
η	Wave impedance
ρ	Resistivity or Density
σ	Conductivity
τ	Relaxation time
μ	The magnetic permeability or the rigidity or shear strength of a material
μ_o	Permeability of free space value
μ_r	Relative permeability
ω	Angular frequency
Ω	Ohm

1 INTRODUCTION

1.1 Milestones in geosciences

Human interest in the earth's geology dates back at least ~2.6 million years, when early humans perhaps accidently discovered that sharp stone flakes make it easier to cut the flesh from around bones. The development of tools was not rapid, and it took hundreds of thousands of years until the first handaxes were taken into use. The Stone Age (9300–3300 BC) brought along more practical tools. Even these simple tools provided deeper knowledge of the properties of different stones. The Bronze Age (3300–1200 BC) is the time period when people made tools from an alloy (copper and tin) called bronze. In the Iron Age (1200 BC–700 AD), more durable and practical items were made from iron and steel. New material-related discoveries are continuously being made, such as that of graphene in 2004. Graphene is strong, light, nearly transparent and a good electrical and thermal conductor, thus having all the properties that will be needed in many fields in the future. New transistors with much higher frequencies would make computers much powerful needed, for instance, in complicated geophysical studies where more realistic models of the subsurface can be introduced.

In 1800, Alessandro Volta invented the voltaic pile (battery), and a continuous current of electricity could be established. Hans Ørsted discovered in 1820 that an electric current produces a magnetic field. The next questions to be addressed were whether magnets could produce electric currents, and whether the relationship could be reversed. Subsequently, Michael Faraday discovered electromagnetic induction, diamagnetism and electrolysis. At this stage, a huge journey had been made and humans had all the necessary means to start examining the earth's subsurface. The development has been rapid, resulting in numerous methods (e.g. magnetic, gravimetric, electric and electromagnetic, and seismic) and techniques to resolve the earth's treasures. Oliver Heaviside established the appropriate mathematics when he expressed Ampere's and Faraday's laws in the forms that we know today. James Maxwell continued the work of other scientists and grouped the most important laws on electric and magnetic phenomena. He also added the displacement current to Ampere's law and formulated a complete set of equations governing the behaviour of macroscopic electromagnetic phenomena in 1863. This set of equations is usually known as Maxwell's equations. They describe the behaviour of the electromagnetic field in any material. All possible electromagnetic problems can be solved with the Maxwell's equations when the material equations are introduced. These equations describe the interaction of the electromagnetic field with the material. However, in practical situations where the material can be highly inhomogeneous, the determination of material properties and field quantities cannot be calculated simply from the Maxwell's equations but they must be measured, for instance, with a linear antenna system. Some of the randomly selected milestones in geosciences are illustrated in Figure 1.

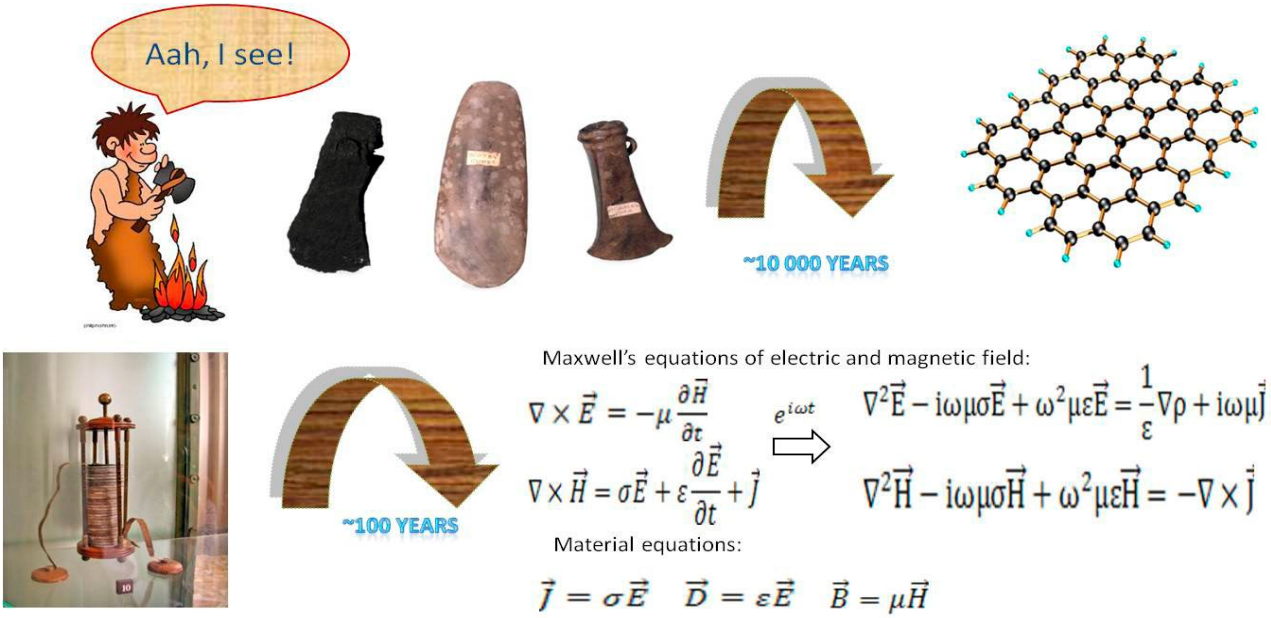

Fig. 1. Milestones in geosciences. The development from simple stone flakes to recent discoveries took millions of years. On the contrary, during an intensive period of ~100 years many sophisticated devices were constructed and the necessary mathematical backgrounds had been established. Handaxes from the Stone, Bronze and Iron Age (the British Museum, above left), graphene (a one-atom thick layer of graphite, ~1 Å (~10^{-10}m, above right, the voltaic pair (bottom left), the frequency-domain complex equations for $\vec{E}$ and $\vec{H}$ and the material equations ($\vec{j}$ electric current $\vec{D}$ electric flux density, $\vec{B}$ magnetic flux density) (bottom right). According to recent findings, the development of primitive tools may have played a decisive role in the development of the human brain and speech.

1.2 Geophysical surveys

Our knowledge of the earth's subsurface systems and structures is still quite limited, and thus new methods and interpretation techniques are continuously developed to better understand geological systems. Geophysical surveys have an important role in providing new data. The electromagnetic frequency spectrum of different geophysical surveys spans ~12 orders of magnitude, at least. Even higher frequencies are utilized in laboratories.

Different geophysical methods can be utilized, for instance, to determine magnetic susceptibility, gravimetric densities, seismic velocities and electrical conductivity. The most important electrical properties of geological materials are the electrical conductivity, electric permittivity and magnetic permeability. Exact knowledge of these parameters is important when the gathered data are interpreted or when new instruments are planned. All the mentioned methods have their own limitations, advantages and disadvantages, and reasonable combination of several methods may therefore provide the best results. The decision on which methods should be utilized in an exploration project must be based on exact planning, in which all available geological, mineralogical and topographical data from the research area should carefully be gathered. In addition, laboratory measurements from core samples should be conducted if possible. These kinds of preliminary preparations ensure which geophysical methods can even be utilized in the research area (Parasnis 1973).

An issue that is common for all the above-mentioned methods is that certain physical properties of rocks (magnetic susceptibility, electrical conductivity, density and velocity) are not merely essential, but the detection of the target depends on the difference between the appropriate property of the target and that of the host rock. However, the estimation of electrical conductivity, with a huge range of over 20 orders of magnitude, is more challenging and subject to larger uncertainties than the others. Conversely, increased electrical conductivity is often associated with deformation of the rock mass (clay and water-bearing fractures, sulphide- and graphite-bearing zones), and the combined data from

different methods could be more informative than using data from one source alone. Thus, although the sensitivity of these methods to various parameters is different, their combined use is complementary. This novel approach is referred to as joint inversion, where different types of data are inverted simultaneously. In general, a common factor for both data sets is needed or the methods used should be sensitive to the same physical property.

The highest part of the spectrum is closely related to laboratory measurements in which, for instance, X-rays are utilized to examine the crystal structures of compounds and identify certain minerals in chemical compounds.

1.3 The radio imaging method (RIM)

The radio imaging method (RIM) is an active geophysical method (e.g. man-made electric dipole sources are utilized), and it is generally used in the transmission mode (bistatic system), when the radio waves are highly attenuated due to the electrical properties of the material between two deep boreholes (cross-borehole survey). A transmitter is fixed in one borehole while a mobile receiver takes readings in another borehole. The transmitter is moved between sets of receiver positions. The survey is completed by interchanging the transmitter and receiver in the boreholes. The technique is known as a full tomographic survey (a two-way measurement). RIM can be used, for instance, to scan subsurface faults and geological contacts, to delineate conductive mineralizations, in mine planning, and in determining the structural integrity of the rock. Greater conductivities mean higher attenuation rates, and both the range and resolution are frequency dependent.

For most cross-borehole survey geometries, the angular coverage is highly limited, and the method is also referred to as a limited angle method. Due to the low frequency band (100–5000 kHz) generally used in RIM, the method is not sensitive to thin discontinuities. Conversely, a massive sulphide deposit could appear as an excellent target. The target would be clearly visible in the signal strengths, but the situation would be paradoxical, because no information would be obtained from inside the target due to the high attenuation rates. We have carried out electromagnetic cross-borehole surveys in two quite different environments, in crystalline bedrock and in an ore district where a massive sulphide target exists. Both of the field cases were successfully accomplished, convincing us that the method can also be utilized in an environment where a potential ore deposit is lacking.

The first studies concerning electromagnetic wave propagation through the earth date back to the beginning of the 20th century. Sommerfeld and Weyl performed rigorous theoretical studies with vertical antennas, and their formulations are useful even today. Eve and Keys conducted measurements in which the propagation of electromagnetic waves through earth materials was also established. The Russian scientist Petrowsky used buried antennas and managed to receive fields in the earth. He calculated the attenuation constants of porphyry and sedimentary rocks at several frequencies (Wait 1969). The work was continued by Lager & Lytle (1977), Lytle et al. (1979) and Somerstein et al. (1984). Stolarczyk & Fry (1986) used RIM to detect faults in the continuity of coal seams, and this can be considered as the starting point of RIM. Russian experts carried out intensive studies using RIM with good results during the late 2000s (Buselli 1980). They measured the decayed or attenuated field and compared it to the theoretically calculated field decay in a homogeneous medium to estimate the conductivity. The Miningtek Pluto-6 system was developed by the Division of Mining Technology of the CSIR (Vogt 2000). The frequency synthesis ranged from 1 MHz up to 30 MHz, and the gain was effectively adjusted to maintain the power at 1 W. The JW-4 system was developed by the Chinese Institute of Geophysical and Geochemical Exploration (IGGE). The group used a technique where the cross-sectional image was reconstructed from the ratio of decayed fields at two frequencies (Cao et al. 2003). In 2010, the Geological Survey of Finland (GTK) took into productive use a RIM system known as the EMRE system (I).

1.4 The main achievements

This dissertation is based on four independent publications provided in the Appendix, and it presents the essential issues concerning the radio imaging method. Although most of the issues discussed in this thesis are in no sense novel, the thesis provides a thorough overview of the fundamental aspects of the borehole imaging method (RIM) and presents novel results from the combination of RIM with other borehole methods. Theoretical clarification of the suitability of the utilized antennas in the rock environment is obtained. The results from the pioneering research in Finland are thoroughly discussed. The main achievements inferred from this empirical research are represented below.

The physical behaviour of an electromagnetic field is governed by the Maxwell's equations, which describe the relationship between electric and magnetic fields in a medium and quantify the material's physical properties. In publication I, Maxwell's equations are solved for the electric and magnetic field. The solution of the equations results in all of the quantities that describe the propagation of an electromagnetic wave in the wave number k. When the observation point is in the far-field region of the antenna, a simple plane wave assumption can be assumed and the waves propagate in a direction that is perpendicular to the wave front (equi-potential plane). After through treatment, two important parameters of the plane waves are conducted, namely the attenuation and phase constant. When amplitude data on an electric field are collected, the attenuation distribution of the section can directly be determined. The derivation is performed in the first paper (I). In addition, the main properties of our present RIM device are explained in some detail. The work was carried out using the back-forward technique without electronic layouts. Thus, the meaning of some electronic solutions remained unsolvable, and this is especially the case with the receiver. Although the weakness of the present device is its complicated construction, the device has proven very reliable. Perhaps the lack of modern Western electric components in the former Soviet Union in the 1980s was the main reason for the unwise solutions. Furthermore, when the results of the RIM measurements were compared with geophysical data obtain using the transient electromagnetic method (TDEM) and electric resistivity logging method, the data sets coincided well. From this very first point, the RIM device operated reliably and the method successfully revealed attenuating (conductive) material distributions between the boreholes, and most importantly, the constructed tomographic images also revealed new features in the borehole sections.

In publication II, I focus on theoretical studies on a half-wave dipole in a dissipative environment (antenna placed in water-filled boreholes). Because direct measurements of the current distribution and the radiative characteristics of the antenna are impossible in these difficult conditions, numerical methods must be utilized. A generalized transmission line model of an insulated antenna is a good and simple starting point. Two different analytical solutions of the transmission line model were implemented in Matlab (an interactive program for numerical computation and simulation from MathWorks): the Wu-King-Giri model (WKG) and Chen and Warne's model (CHEN). However, the water layer must be extracted from both of the above-mentioned models, because it is further required that $\left|k_4^2\right| > \left|k_2^2\right|$ but the wave number of water k_2 is always much larger than that of ambient rock k_4. Thus, the outer conductor of the model corresponds to the ambient rock. The WKG model especially suffers from the conditions due to a low wave number ratio between the rock and antenna insulation. The results from the analytical solutions (WKG, CHEN) were also confirmed with FEKO (an electromagnetic simulation package developed by EM Software and Systems, Altair). The results from FEKO and the analytical methods coincided well, especially when the resistivity and relative permittivity of the ambient rock were high. In less resistive conditions (<200 Ωm), the behaviour of the WKG model differs from that of the other models. However, according to these simple calculations, the antenna appears to operate effectively at the EMRE frequencies. The same calculations were performed with FEKO when the water layer was included in the borehole model. The effect of the water layer was insignificant at the three lowest EMRE frequencies (312.5-1250 kHz), resulting in high scattering parameter s_{11} values, but the highest

frequency (2500 kHz) would seem to suffer from the actual borehole conditions.

Depending on the electrical properties of the medium and the frequency range used, the electromagnetic field may either diffuse or propagate as waves in the medium. Because diffusion is normally related to a random movement (e.g. thermal energy transfer), a more descriptive term could be highly attenuating propagation due to the highly controlled sources utilized. The fundamental principles of the waves in different environments are thoroughly explained to give the reader a good conception of the transillumination depths of RIM. These important issues are covered in publication III. It is necessary to understand the interaction of the fields and the medium when a tomographic reconstruction of a borehole section is being carried out. The third paper also consists of one interesting field case conducted in the proposed area for a repository of spent nuclear fuel at Olkiluoto in Finland. The repository will be constructed deep in the crystalline bedrock of Olkiluoto island in Eurajoki, and knowledge of the integrity of the subsurface is fundamental. The measurement geometry was conic (collars of the boreholes were only separated by few metres), and thus the electric coupling between transmitter and receiver antenna was not optimal. Although the measurements were conducted in conditions that were far from the most favourable ones, the detected low and high resistivity zones, their shapes and orientations were in fair agreement with geological and other geophysical results. As a conclusion, the method could also be utilized, for example, in assessing the integrity of the rock mass, as increased electrical conductivity is often associated with rock mass deformation (clay and water bearing fractures, sulphide and graphite bearing zones).

RIM was utilized as a full tomographic survey (the transmitter and receiver are interchanged in the boreholes; cross-borehole measurement) for the first time in 2005 in Finland when the Geological Survey of Finland (GTK) co-operated with Russian specialists from FGUNPP 'Geologorazvedka' (St. Petersburg, Russia). The results of this significant measurement are gathered in publication IV. In Olkiluoto, the bedrock is granitic, despite the resistivity in the bedrock varying widely due to sulphide bearings. Often, increased conductivity can be associated with deformations in the rock mass, and thus the obtained information can be used when estimating the integrity of the rock mass. A considerable amount of background data was available from the environment. Electrical resistivity logging of boreholes is a widely used prospecting technique for identifying mineralised zones near the boreholes. The registered low resistivity sections in both of the boreholes coincided well with the low resistivity regions in the RIM reconstruction. However, one has to keep in mind that electric logging only senses the close vicinity of boreholes, while in RIM the whole space between the boreholes is scanned. In addition, the sensitivity of the borehole antennas is highest for features near the boreholes. This may generate artifacts in the reconstruction and should be taken into account in the interpretation. A borehole radar of 20 and 60 MHz was also utilized in the reflection mode (transmitter and receiver in the same borehole). The radar measurements produced reflection images of 20–30 m in radius around the boreholes at the best possible resolution. The low resistivity regions coincided well with high attenuation of the radar signal. The mise-a-la-masse method was applied in the cross-borehole mode, and one current electrode was directly connected to the conductor in each borehole. Potential electrodes were moved in the other borehole. Both RIM and mise-a-la-masse successfully delineated the conductive zones between the boreholes. Geophysical methods other than electric and electromagnetic methods were also conducted, and one of them was a seismic cross-borehole survey. The seismic method is based on the fact that elastic waves propagate with different velocities in different rocks. Because the total velocity variation was limited, some low velocity zones associated with thin brittle fault zones dipping only gently between the boreholes were detected. Despite the orientation of the gently dipping zones not being optimal for RIM, the resemblance between the seismic velocity tomogram and RIM was fairly good.

The four published papers and conclusions presented in this synopsis convinced us of the potential of RIM, and future plans have been made to further develop the RIM system.

2 PHYSICS OF GEOPHYSICAL METHODS

New electronic solutions make it possible to use geophysical devices with sufficient accuracy to determine the electrical properties of rocks that reflect the local subsurface geology. Geophysics is an applied discipline of physics of the earth. Prospecting geophysics uses measurements at or near the earth's surface to measure the physical properties of the earth's subsurface, recognizing anomalies in these properties in order to delineate, for instance, the presence and position of ore minerals and geological structures. A geophysical anomaly is defined as the difference between the measured geophysical value and the value that would be observed in uniform earth at the same location. Many different methods exist, such as the seismic method for determining the velocity of seismic waves, the gravity method for measuring density contrasts, the magnetic method for revealing high or low susceptibility mineral deposits, and electric and electromagnetic methods for measuring the apparent resistivity or conductivity of the subsurface.

Geophysical methods can be divided into two categories: passive and active. Passive or natural field methods utilize, for instance, the gravity and magnetic fields of the earth. Passive methods, magnetotellurics (MT) (Chave & Jones 2012, Naidu 2012, Ward 1987) and audio-frequency magnetotellurics (AMT) (Parasnis 1986, Ward 1987), are especially used in deep studies (fields are due to the interactions of fields and particles from the sun with the earth's magnetic field (<1 Hz) and thunderstorms (>1 Hz)). Active or artificial source methods involve local human-made seismic, electrical and electromagnetic fields, which are used analogously to natural fields. Active sources are generally limited to shallow targets and are most often used in near surface applications or in boreholes. Generally, natural field techniques can improve our knowledge of the earth's properties to much greater depths and they are also simpler to carry out than active methods. Thus, one significant difference between passive and active methods is that the depth of prospecting can be controlled using active methods, which is not possible with passive methods. By comparison, active methods are able to produce much more detailed information on subsurface geology. Inherent ambiguity can especially be a serious problem in the passive method data, since a shallow object can generate the same field anomaly as a deeper object. Geophysical methods can also be divided into contacting or non-contacting methods, depending on whether the source or receiver is in contact with the ground. Contacting methods have the advantage that the power input can be greater and the reception more sensitive. Conversely, non-contacting methods are more rapid and can be cheaper. When using active methods, higher frequencies mean better image resolution and shorter depths of penetration into the ground.

Investigations of subsurface geology can also be performed in boreholes, but the high drilling costs set limits for establishing new boreholes. In addition, the limited available space in boreholes for the electronics makes it highly demanding to design borehole devices. However, borehole surveys have several benefits over ground-level methods. Applying a borehole transmitter brings the survey closer to the target and allows the use of higher frequencies, thus enabling a higher spatial resolution. Another benefit is the possibility to view the target from different angles and directions, not only in the vertical direction from the earth's surface. Having the transmitter in a borehole eliminates the boundary effects related to the ground surface and the strong attenuation emerging from soil deposits. A drawback is the suboptimal availability and location of boreholes and limited transmission power of borehole probes.

2.1 Frequency spectrum

Electromagnetic waves can be described, for example, by their frequency f and wavelength λ. The wavelength is inversely proportional to the wave frequency. The frequency range utilized in geophysical prospecting, e.g. magnetotellurics (MT, frequency band: 0.0001–1 Hz, inferred property: resistivity distribution) (Chave & Jones 2012, Naidu 2012, Ward 1987) the radio imaging method (RIM, frequency band: 100–5000 kHz, inferred property: attenuation distribution)

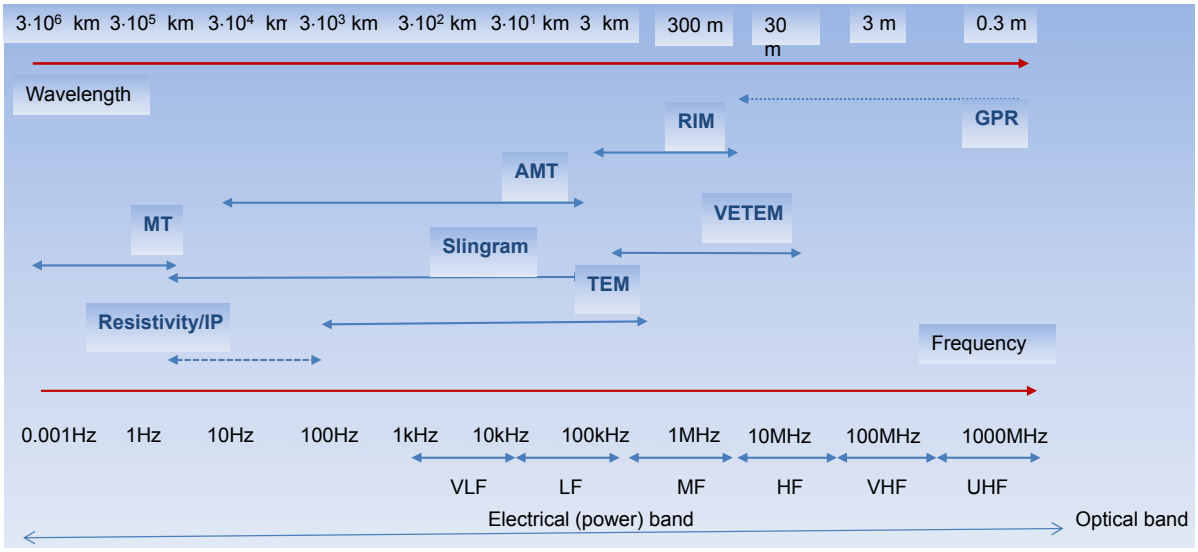

Fig. 2. Common EM geophysical methods in the frequency range of 10^{-3} Hz–1000 MHz. The radio imaging method (RIM; 100kHz–5MHz), audio-frequency magnetotellurics (AMT; 10Hz–100kHz) and magnetotellurics (MT; 10^{-3}–1 Hz). GPR is ground penetrating radar, VETEM is very early time EM, IP is induced polarization, resistivity is galvanic and TEM is the transient EM method (Parasnis 1986, Pellerin & Wannamaker 2005). Bands of radio frequencies: VLF (very low frequency), LF (low frequency), MF (medium frequency), HF (high frequency), VHF (very high frequency), UHF (ultra high frequency). The lower optical bands are infrared, visible and ultraviolet bands. Frequency bands according to IEEE standard 521–2002.

(I, III), (Stolarczyk & Fry 1986) and mineralogical surveys, e.g. X-ray diffraction (XRD, frequency band: 10^{14}–10^{16} Hz, inferred property: e.g. structural information of material (Buhrke et al. 1998, Geological Survey of Finland 2013, Gill 1997, Harrison et al. 1991, Kittel 1976) and X-ray fluorescence (XRF, frequency band: 10^{14}–10^{16} Hz inferred property: elements in geological material (Buhrke et al. 1998, Gill 1997, Harrison et al. 1991), spans over 20 decades. The generally used electromagnetic methods (e.g. Slingram) are utilized in the frequency range of <100 kHz, the shortest vacuum wavelengths being <3000 m (Parasnis 1986). Ground penetrating radar (GPR) can operate from 10 MHz to a few GHz, and the wavelengths can thus be as short as a few centimetres (Daniels 1996). However, when electromagnetic waves exist in a lossy medium, the characteristic electrical properties (relative electric permittivity ε_r, electrical conductivity σ and relative magnetic permeability μ_r) differ prominently from the vacuum values, and their wavelengths are decreased and the waves are effectively attenuated. The attenuation is the main factor that limits the use of frequencies in geophysics (I, III) (Mahrer 1995).

The ultimate goal of different electromagnetic methods is to determine conductivity, permittivity or variations in the solid earth, and the electrical properties of a target should therefore differ sufficiently from that of host rock. Rocks are aggregates of different minerals. Minerals are chemical compounds or pure elements possessing a different chemical composition, internal structure and electrical properties (Parkhomenko 1967). Most rock-forming minerals are highly resistive, but, for instance, even small amounts of sulphide minerals, graphite or pore water can markedly increase the bulk conductivity. When active sources are situated beneath the ground surface, as in borehole electromagnetic surveys (e.g. RIM), the measurement configuration has several clear benefits over ground-level electromagnetic methods (Fig. 4). Applying a borehole source and receiver brings the survey closer to the target and allows the use of higher frequencies, thus enabling a higher resolution. Placing the source in a borehole also enables the elimination of boundary effects related to the ground surface and strong attenuation emerging from soil deposits. In addition, the vertical resolution is the same from the starting point to the lowest measurement point. The aforementioned methods have different advantages and disadvantages. The best results are often achieved by combining many complementary methods.

2.2 Magnetic loop and electric dipole

Electromagnetic fields can be transmitted and received by magnetic loops or electric dipole antennas, and thus the main function of the antenna is to radiate and receive electromagnetic energy. The antennas serve as the transducers between the device and environment, so together they form a signal path. A magnetic loop consists of a conducting loop, and when oscillating current is passed through it electromagnetic waves are produced. This is referred to as an oscillating magnetic loop. The loop is small when its circumference is much shorter than the wavelength, which is generally the situation with ground surface geophysical applications. Small loops are also non-resonant antennas. The radiation resistance of a small single loop is much smaller than that of a short electric dipole, and the loss resistance of a small loop antenna can even be larger than the radiation resistance. The radiation resistance is the resistive component of the antenna impedance. It is not an actual resistance in the antenna, but it is created by the radiation from the antenna (resistance of the signal path) (Collin & Zucker 1969, King et al. 1980, Moore 1963, Seybold 2005). Therefore, a small single-loop antenna is not effective when used as a transmitting antenna at low frequencies. A simple way to increase the radiation resistance of a loop by a factor of N^2 is to increase the turns (N), but an increase in the turn number also increases ohmic losses as ~N. However, a loop antenna is more useful as a receiving antenna, since the signal-to-noise ratio is the most important factor, not the efficiency of the receiving antenna, and the impedance mismatch loss can be tolerated. In its simplest form, an electric dipole is made up of an oscillating (accelerated or decelerated) positive and negative charge pair.

In our present RIM device, the transmitter and receiver antennas are insulated electric dipoles (linear wire antennas). The conductive wires are insulated from the borehole environment, and when the antennas are in different boreholes, the system is referred to as bistatic. The antennas in our system can be considered as electric half-wave dipoles. The insulation layer alters the functioning of the antenna, preventing the current, for instance, from using the conductive borehole water as a complementary current path (II) (King et al. 1980). In general, wire antennas have a good ability to maintain their performance and have an excellent range capacity. In addition, they have the best isotropic radiation pattern. The continuous wave device (CW) was the first radio transmission system that had some commercial importance. For the first time, data could be sent without wiring as on-off clicks (Morse coding) that a recipient could easily understand (Fig. 3) (Holloway 1998).

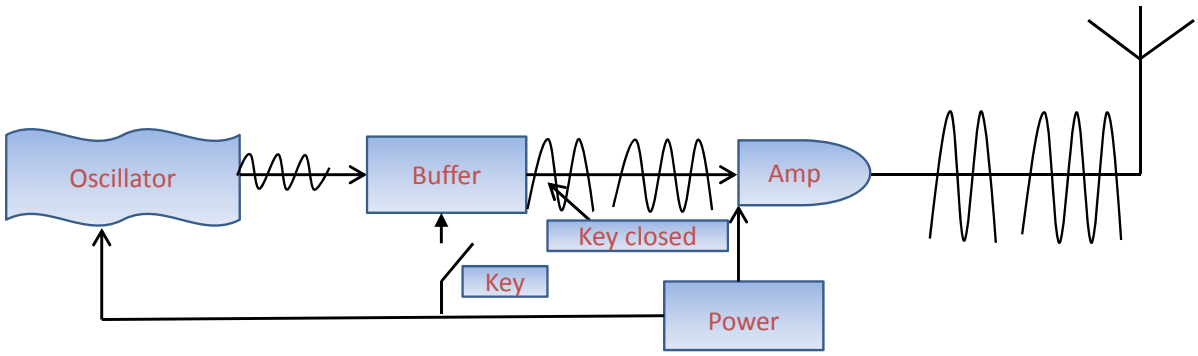

Fig. 3. The CW transmitter. The key is opened and closed to separate the continuous wave into dots and dashes. The oscillator generates the base frequency signal. The buffer is the pre-amplifier stage and it effectively isolates the oscillator from the power stage. The oscillator signal is weak and the voltage must be amplified before it is fed to the power amplifier. Modified after Holloway (1998).

2.3 Magnetic method

The main part of the earth's magnetic field is assumed to be generated by the huge magnetic dynamo in the earth's outer core in the convection process of liquid iron. The field is dipolar and it resembles the field of a large bar magnet aligned approximately along the earth's axis of rotation (at an angle of about 10 degrees). The magnetic flux density $\vec{B}$ is nearly vertical near the poles, but elsewhere is non-vertical. The magnitude of the field falls between ~20 000 nT (equator) and ~70 000 (poles) everywhere on the earth, having local variations of several hundred nT (1 nT = 10^{-9} Tesla). The fields are extremely weak, as a domestic refrigerator can generate fields as large as 0.01 T. The flux density $\mathbb{B}$ can be defined in terms of the magnetizing field $\vec{H}$. The ratio of the flux density $\vec{B}$ to the magnetizing field strength $\vec{H}$ is a constant called the magnetic permeability μ. The interaction of the magnetizing field with the rocks of the earth's crust produces the magnetic anomalies recorded in magnetic surveys at or near the earth's surface. The ultimate goal of magnetic interpretation is to deduce the geometry of magnetic bodies. However, the results are always inherently ambiguous because we do not precisely know the internal structure or physical properties of the earth, resulting in an infinite number of solutions (Kearey et al. 2002).

The variations in the magnetic field depend on the contrasts in the magnetic properties of rocks. The magnetic response of rocks is mainly due to the presence of magnetic minerals such as magnetite and pyrrhotite, and the content of magnetite almost entirely determines the properties when present. When a magnetic material is situated in a magnetic field, the material becomes magnetized (Eq. 1). Magnetization $\vec{M}$ consists of induced $\vec{M}_i$ and remanent $\vec{M}_r$ components. The induced component is a function of the magnetic susceptibility of the medium and the magnitude and direction of the ambient field, whereas the remanent magnetization reflects the geological history of the material (inherited property) (Airo & Säävuori 2013, Kearey et al. 2002, Lowrie 2007, Parasnis 1986)

$$\vec{H} = \frac{\vec{B}}{\mu} - \vec{M} \tag{1}$$

where $\vec{H}$ is the magnetic field strength, $\vec{B}$ the magnetic flux density, $\vec{M}$ the magnetization and μ the magnetic permeability of the medium defined as $\mu = \mu_o\mu_r = \mu_o(1+\chi_m)$; μ_o is the free space value, μ_r the relative permeability and χ_m is the magnetic susceptibility, or χ_m determines how easily a body can be magnetized. When measuring the magnetic field, magnetization due to both the main and induced fields ($\vec{M}_i$, $\vec{M}_r$) is recorded (Eq. 2)

$$\vec{M} = \vec{M}_i + \vec{M}_r \tag{2}$$

The induced field $\vec{M}_i$ relates to magnetic susceptibility and is produced by induction of the main field. In a normal measurement, the remanent component $\vec{M}_r$ cannot be distinguished from $\vec{M}_i$, but in the laboratory the magnetic susceptibility can be determined when the inducing field is known at the original site. The first devices were mechanical magnetometers (e.g. compass) and the direction of the earth's magnetic field could be measured. During the Second World War, new magnetometers called fluxgates were designed to detect submarines. The development of magnetometers has continued and new inventions have been taken into use to detect the low magnetic fields of the earth. In Figure 4, some of the most commonly used vector and scalar magnetometers are presented. An induction coil is also referred to as a search coil magnetometer. It is a vector sensor and it measures changes in the magnetic field, and according to Faraday's Law, the induced voltage is proportional to the changing magnetic field. Thus, it is a transducer that converts the magnetic field into an electric voltage. Fluxgate magnetometers are modern and frequently utilized devices in which a ferromagnetic core is surrounded by two coils: primary and secondary coil (fluxgate). An alternating current is fed to the primary coil, producing an alternating magnetic field that induces an alternating current in the secondary coil. As the external magnetic field changes, so does the total magnetic field in the secondary coil. The intensity and phase of the alternating current in the secondary coil are constantly measured to determine the intensity and phase of the external magnetic field. The superconducting quantum interference device (SQUID) is the most sensitive device to measure extremely weak magnetic fields (e.g. living organs and

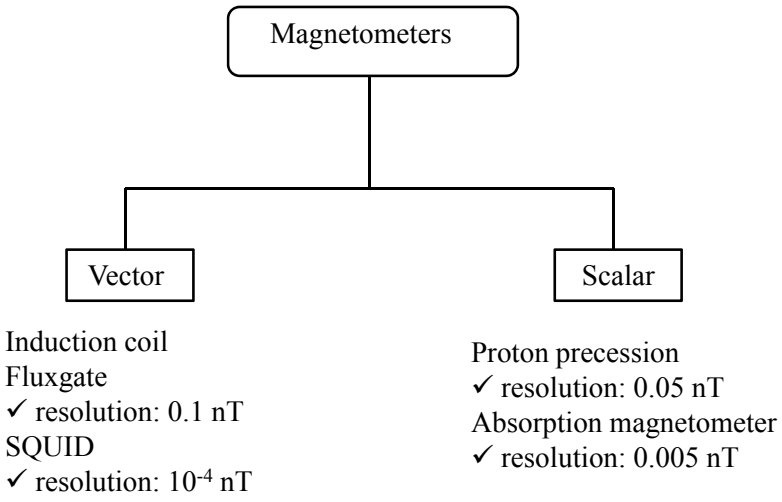

Fig. 4. Magnetic field devices. Modified after Macintury (1999).

remanent magnetization of rocks). A proton precession magnetometer is based on fact that protons have an internal magnetic field. When protons are placed in an external magnetic field, the internal field starts to precess, and the frequency of precession is proportional to the strength of the external field. In absorption magnetometers, the magnetic moments of outer shell electrons are aligned with the external magnetic field. The energy difference due to changing the orientation of the moments is proportional to the external magnetic field. Magnetometers can be used in pairs to measure either horizontal or vertical magnetic field gradients (magnetic gradiometers) in shallow magnetic surveys, and thus regional and temporal variations in the geomagnetic field are automatically removed (Airo & Säävuori 2013, Kearey et al. 2002, Lowrie 2007, Parasnis 1986)

The earth's magnetic field has been observed for several hundreds of years. Even today, magnetic methods are among the most commonly used geophysical survey techniques and are most often performed as aeromagnetic surveys. They are inexpensive and both straightforward and rapid to perform, the applicability is wide. The field can be used to delineate and characterize the geometry and source of magnetization.

In Figures 5a-c, the magnetic responses of theoretical block models (*sides aligned with coordinate axis*) with properties corresponding to massive sulphide ore bodies at different depths are presented to clarify the difficulties in delineating ore bodies: a 1 Mt ore body (x = 100, y = 125, z = 50 m, density 4000 kgm^{-3}, host rock susceptibility $3 \cdot 10^{-3}$, in 10^{-6} SI, Q=0) (Fig. 5a), a 27 Mt ore body (x = 300, y = 375, z = 60 m) (Fig. 5b) and a 135 Mt ore body (x = 520, y = 650, z = 100 m, world class ore) (Fig. 5c). The calculations were performed by geophysicist A. Ruotsalainen (GTK) with ModelVision software. The remanence magnetization is not included in the model Q = 0. Q is the Koenigsberger ratio, defined as $Q = M_r/M_i$.

When an ore body is outcropping (z = 0 m), the ore is easily detectable. Increasing the depth, both the 1 Mt and 27 Mt ore body are not detectable after the level of 500 m. The 135 Mt ore is still detectable (z > 500 m), but the response is weak and flattened. As a conclusion, the recognition of a world-class ore is very demanding, even at quite reasonable depths, using only magnetic data. The requirement for and combination with other possible data types (electric methods, seismic, boreholes, borehole electromagnetic methods) may help in the research. The magnetic field is especially sensitive to ferromagnetic bearing deposits, but being the cheapest, easiest and fastest method, it is normally included in all geophysical research. This is because magnetic distortions, for instance generated by faults, fractures and contact zones, may occasionally be indirectly connected with more economic ore deposits.

a)

b)

c)

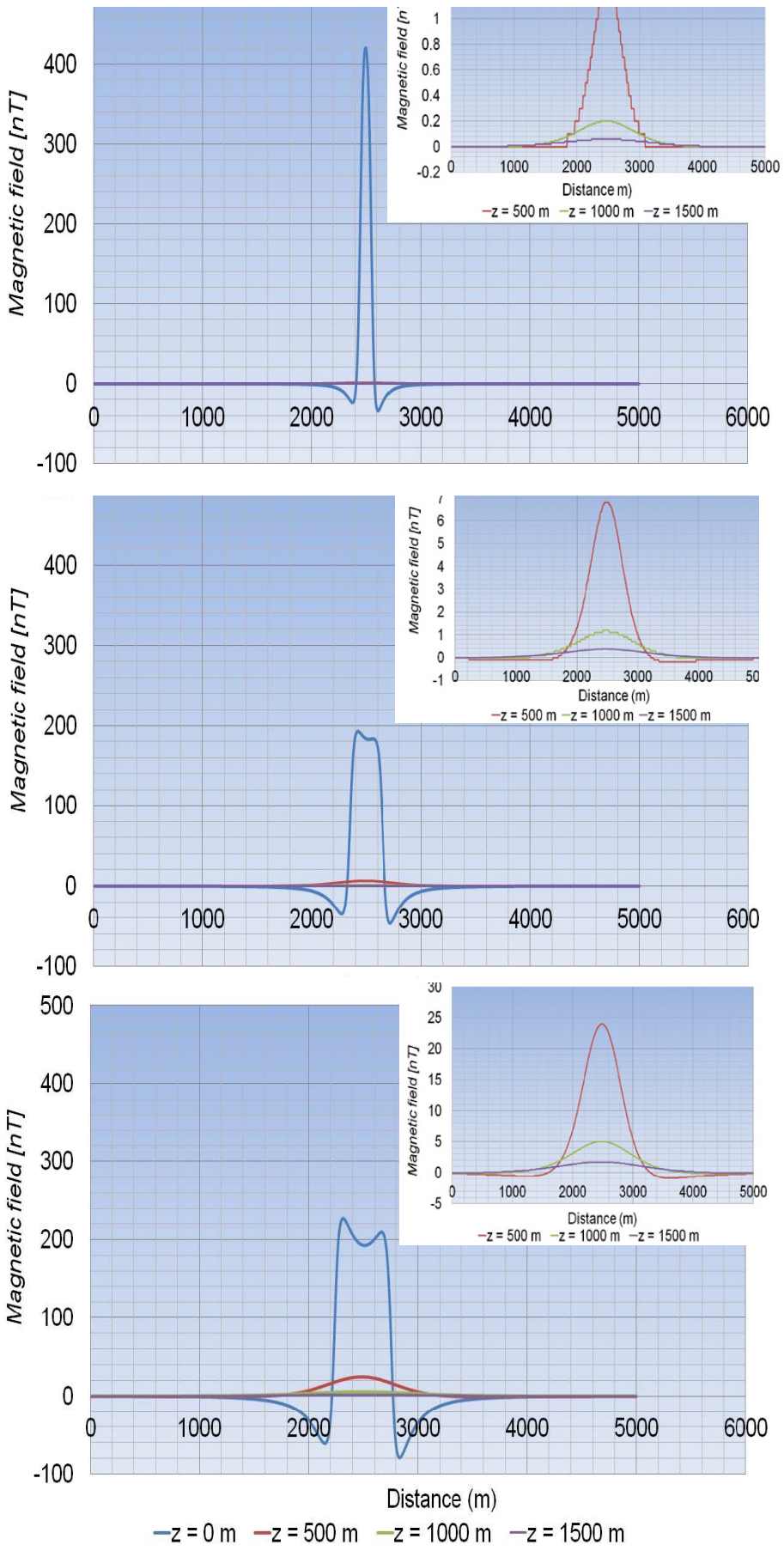

Fig. 5. Magnetic responses of three ore bodies at different depths. a) a 1 Mt ore body, b) a 27 Mt ore body and c) a 135 Mt ore body. The outcrops are removed in the small figures.

2.4 Gravity method

Gravity is also a potential field for exploring the earth's subsurface: the same work is needed to move a mass from one point to another, regardless of the path taken between the two points (conservative field). The gravity method measures differences in the earth's gravitational field (acceleration of gravity) at specific locations caused by the density contrast between a body and its host rock. The densities of rocks and soils vary little from place to place near the surface of the earth. The highest densities we typically observe are about 3200 kgm^{-3}, with values generally being in the range 2600–2900 kgm^{-3}. Soils have low densities of about 1000 kgm^{-3} (Fig. 6) (Kearey et al. 2002, Lowrie 2007, Parasnis 1986).

The physical basis of the gravity method depends on the universal law of gravitation and the second law of motion. According to the first law, the force of attraction between two bodies of known mass (M, m) is directly proportional to the product of the two masses and inversely proportional to the square of the distance (R) between their mass centres. Thus, the greater the distance, the smaller the force of attraction:

$$\vec{F} = G \cdot \frac{Mm}{R^2}\vec{r}\,, \tag{3}$$

where G is the gravitational constant, G = 6.67·10^{-11} Nm^{2}kg^{-2}, $\vec{r}$ is a unit vector directed from M to m. The second law of motion states that a force ($\vec{F}$) is equal to mass (m) times acceleration ($\vec{g}$) due to gravity:

$$\vec{F} = m\vec{g} \tag{4}$$

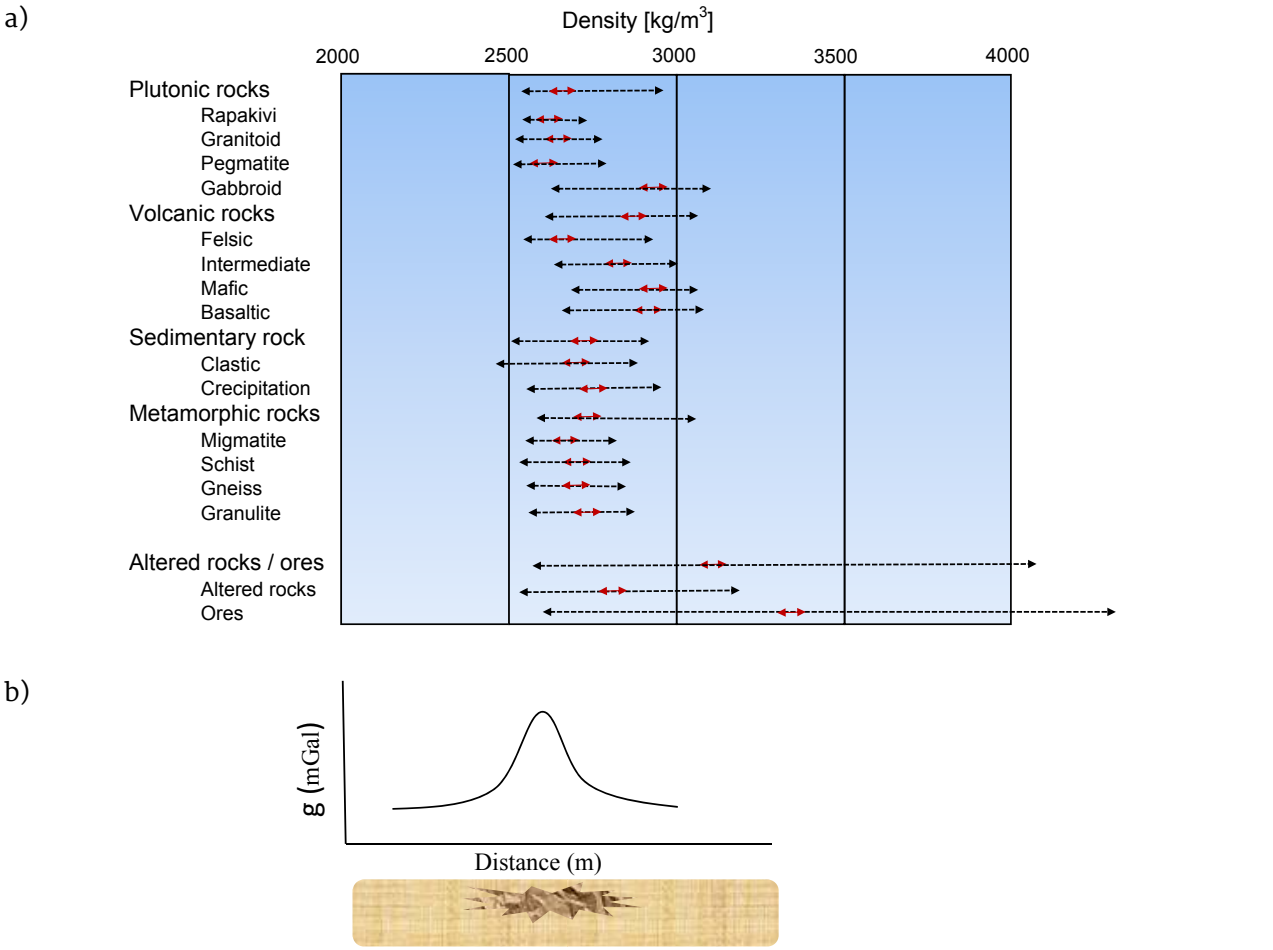

Fig. 6. a) Densities for different rock types (kgm^{-3}). The red arrows indicate the most probable densities. Black arrows mean the whole variability in density in a specified rock type; for instance, the whole number of samples of plutonic rocks is 64442 and that of pegmatite samples 1801. Modified after Airo & Säävuori (2013). b) The response of a material body along the measurement line. The dark object in the middle is denser material than the background.

Combining the equations, we obtain a simple relationship:

$$\vec{g} = \frac{GM}{R^2}\vec{r} \quad (5)$$

Thus, the magnitude of acceleration due to gravity ($\vec{g}$) is directly proportional to the earth's mass (M) and inversely proportional to the square of the earth's radius (R). Due to the earth's slightly ellipsoidal shape (flattened sphere), rotational movement, surface topography and variable mass distribution, gravity varies from place to place at the earth's surface. In addition, the polar radius is shorter than the equatorial radius, and thus the points at the poles are closer to the earth's mass centre, and the value of gravity at the poles is therefore greater than that at the equator. The centrifugal acceleration due to the earth's rotation is greatest at the equator and decreases to zero at the poles. The normal approximate value of g is 9.80 ms^{-2} ($9.8 \cdot 10^5$ mGal) at the Earth's surface (Kearey et al. 2002, Lowrie 2007, Parasnis 1986).

Two types of gravimeters exist. An absolute gravimeter measures the actual value of $\vec{g}$. Precisions to within a few μGals can be achieved when distance and time can be determined with high precision. The second type of gravimeter measures the relative changes in $\vec{g}$ with a precision of a few μGal at best. Normally, the conventional devices have precision of ~0.02 mGal. Instead of utilizing gravimeters, one can measure the gradient of the gravitational field using gradiometers. The unit of gravity gradient is $1/s^2$ and 1 nano/s^2 is defined as 1 Eötvös (E). Normally, the accuracy of gradiometers is in the order of 1 E (Erkan 2008, Kearey et al. 2002, Lowrie 2007).

As a rule, relatively dense and heavy materials generate additional gravitational attraction downwards and create positive gravity anomalies. By comparison, for light materials, the gravitational pull is diminished and the anomalies are negative. The same theoretical block models as with the magnetic method were used to determine the practical limits for gravimetric studies by geophysicist A. Ruotsalainen (GTK). The same conclusions (Figs. 7a-c) can be drawn and the delineation of an ore body at greater depths is a difficult task. For instance, the recognition of a world-class ore is very demanding at a depth of z > 500 m due to the small gravity anomalies, which can be easily masked, for instance, by topographic irregularities. Thus, as with the magnetic method, all other possible means (electric methods, seismic, boreholes, borehole electromagnetic methods) are needed to reliably delineate the body. In addition, deep ore prospecting should establish the location of favourable host rock for ore, for utilization of the host rock structures or even for the indicator mineral method. Normally, the gravitational method is seldom used only for reconnaissance purposes of ore prospecting due to being quite expensive and the weak anomalies can be effectively masked, for instance, by topographic irregularities, but it is often used as an auxiliary method to distinguish, for instance, non-economic graphite zones from massive ore deposits. As with the magnetic method, the inherent ambiguities makes the interpretation very challenging, and gravimetric measurements can seldom uniquely determine the anomalous target alone, even if the measurements have been made with the highest possible accuracy.

a)

b)

c)

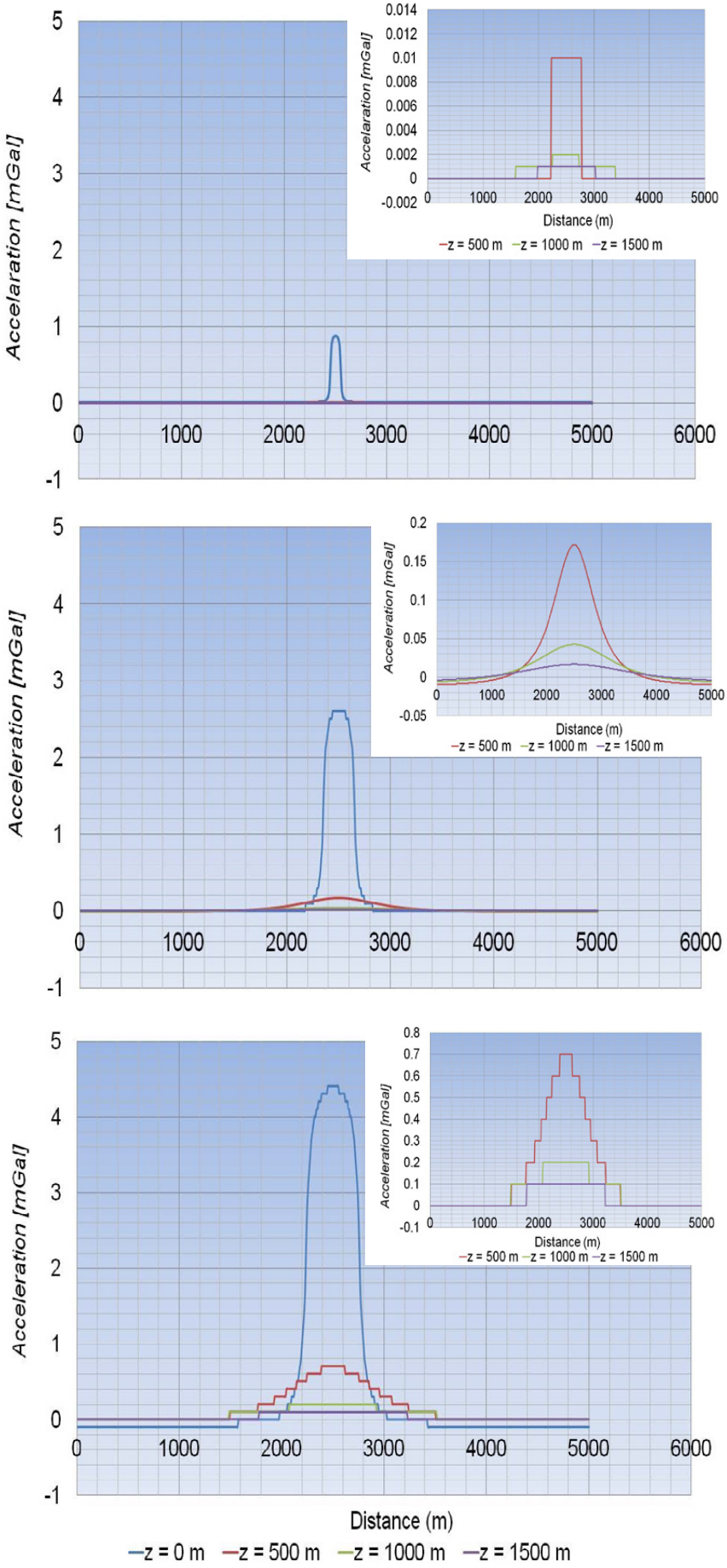

Fig. 7. Gravimetric responses of three ore bodies at different depths. a) a 1 Mt ore body, b) a 27 Mt ore body and c) a 135 Mt ore body. The outcrops are removed in the small figures.

2.5 Electric and electromagnetic method

Electric and electromagnetic methods are utilized in determining the electrical conductivity, (resistivity) (σ, ρ) and dielectric properties (ε) of subsurface rocks. The current can be directly injected into the ground with electrodes using DC (static or contacting method) or low frequency currents to avoid polarization effects between the electrodes and ground. At higher frequencies, the current flow is induced in the ground by time-varying electromagnetic fields (Faraday's law, Fig. 1). The primary sources (loop or wire antenna) do not even need any contact with the ground (non-contacting method). Electromagnetic methods can be divided into two categories depending on the magnitude of energy loss (conductivity) relative to energy storage (permittivity, permeability): diffusive (quasi-stationary) or wave propagation (I, III) (Jol 2009, Zhang & Li 2007). Diffusive fields are low-frequency fields and penetration into rock is restricted by the dissipation of energy as heat due to the electrical conductivity of rocks. In quasi-static conditions, the fields diffuse over the boundaries with different electrical properties such as heat. When the fields propagate as waves, much higher frequencies must be utilized. For instance, in ground penetrating radar (GPR), frequencies larger than 10 MHz are used due to the better resolution (Daniels 1996, Jol 2009). Reflection, diffraction and scattering occur when the wave strikes different obstructions in its way through a material, and refraction occurs at boundaries with different electric properties. Reflection occurs when an electromagnetic wave impinges on a reflective object that has very large dimensions as compared to the wavelength of the wave. In the reflection, the wave changes its direction. In diffraction, a wave can propagate, for instance, into the shadow of a sharp obstacle with dimensions comparable to the wavelength of the wave. Scattering occurs when the dimensions of objects are much smaller than the wavelength of the wave. In all these phenomena, some of the transmitted power is lost. Dispersion is closely related the phenomena where the velocity of the wave depends on the frequency. Colours (having different wavelengths) are produced when white light enters and passes through, for instance, a prism. Different wavelengths (colours) are separated due to the different refracted indices and a spectrum of colours is generated (Orfanidis 2004, Seybold 2005, Zhang & Li 2007). In addition, the penetration depths are highly limited by the electrical conductivity and permittivity of the non-magnetic rocks (I, III). GPR is more generally used in the reflection mode, and thus the transmitter and receiver are, for instance, in the same borehole. The radio imaging method (RIM) is normally utilized at frequencies lower than 5 MHz and the data are gathered in the transmission mode (cross-borehole geometry; the transmitter and receiver are in different boreholes).

The transmitter antenna is a radiating element in which the input voltage (current) is converted to a radiating field or $U \rightarrow \vec{E}(\vec{r})$. The opposite occurs in the receiver antenna, in which a received field induces a voltage at the terminals of the antenna or $\vec{E}(\vec{r}) \rightarrow U$. Antennas are typical reciprocal, that is, their properties are the same in transmission and reception (same frequency and impedance). In transmitters with high powers, the losses should be minimized due to the high development of heat. Conversely, the signal-to-noise ratio of the receiver is not an important property if the signal levels are high enough and above the noise level. One important property of the antennas is the radiation pattern, which is a mathematical description of the spatial variations in the electric and magnetic field, or it determines the directional property of the radiation from the antenna. The directivity of the antenna in a given direction is the ratio of the radiation intensity (P_r) normalized by the corresponding intensity of the isotropic antenna. It is a measure of the ability of the antenna to direct its power towards a given direction. The gain is defined in the same way as the directivity, but it is normalized by the total power (P_t) fed to the antenna (Jol 2009, Orfanidis 2004, Seybold 2005) and therefore incorporates losses in the antenna. It is normally expressed in dBi units: dBi stands for the antenna gain over an isotropic antenna (a lossless half-wave dipole has a gain of 2.15 dBi or 1.64) (Smith 1977). These parameters are defined in the far-field domain $\left\|\vec{k} \cdot \vec{r} >> 1\right\| \; or \; 2\pi r >> \lambda$, where r is the distance from the antenna and λ is the wavelength, but when used in a dissipative environment, the distance from the antenna should be taken into account in the definitions. Generally, the gain is

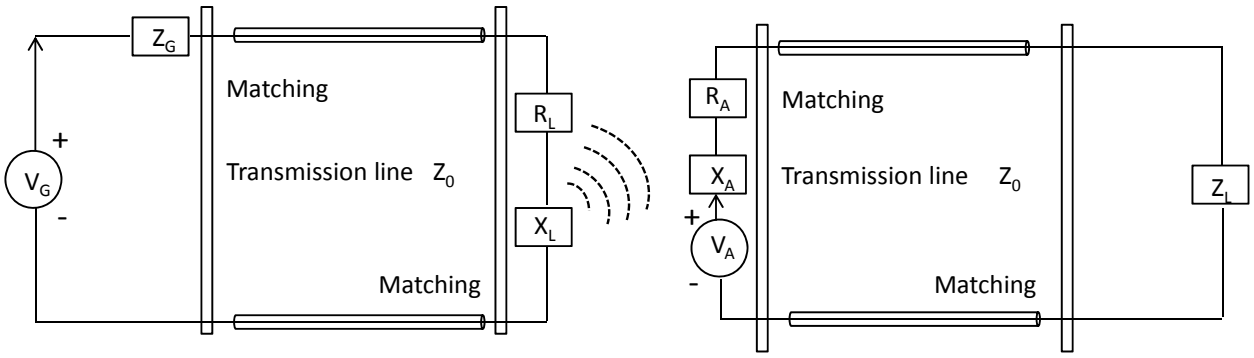

Fig. 8. Schematic representations of transmitting (left) and receiving (right) antennas. V_G is the generator and Z_G the impedance related to the generator. R_L and X_L are the resistances and reactance of the load (antenna). Z_0 is the impedance of the transmission line. Thus, a transmitting antenna appears as a load (Z_L) to a generator. Respectively, a receiver appears as a load to a receiving antenna. Matching can be carried out at one or both ends of the transmission line. When the generator and load are well-matched or $Z_G = Z_L = Z_0$, the maximum power is fed to the antenna. V_A, R_A and X_A are the corresponding parameters of the receiving antenna. Modified after Orfanidis (2004).

smaller than the directivity. When an alternating current is used, the impedance is an important electrical concept. It is the complex ratio of the voltage to the current. The input impedance Z_L of the antenna is the impedance presented at its terminals (Collin & Zucker 1969, King et al. 1981, Moore 1963, Seybold 2005):

$$Z_L = R_L + i \cdot X_L \tag{6}$$

where R_L is the total resistance of the antenna ($R_L = R_r + R_h$, R_r is the radiation resistance, R_h is the ohmic loss resistances) and X_L the reactance, which is proportional to the energy stored in the near field. The reactance X_L determines the power accepted from the generator. In Figure 8, the schematic presentations of the transmitting and receiving antenna are presented (Orfanidis 2004).

While the energy lost by ohmic resistance is converted to heat, the energy lost by radiation resistance is converted to electromagnetic radiation. Defining the efficiency of the antenna as $\eta = R_r/(R_r+R_h)$ or $\eta = P_r/P_t$, the gain can expressed as $G = \eta \cdot D$. The antennas can be resonant or non-resonant. In a resonant antenna, the power fed to the antenna is almost entirely radiated and $Z_L \approx R_L$ or the impedance is a pure resistance. The physical length of the antenna is generally different from the electrical length due to the end effect when an icrease in capacitance near the end of the rectilinear conductor occurs. Making the antenna resonant means either lengthening or shortening it. This can be done mechanically or electrically. When changing the electrical length of a dipole wire antenna without changing its physical length, an inductor is used if the antenna is too short (X_L is capacitive reactance), whereas a capacitor is used when the antenna is too long (X_L is inductive reactance) (Gustrau & Manteuffel 2006, King et al. 1981, Ludwig & Bretchko 2009, Seybold 2005). The current distribution of an antenna is a function of the antenna dimensions, the frequency used and the electrical parameters of the surrounding environment. Thus, analysis of the current could serve as a means to estimate the electrical parameters of the surrounding rock. In a bare metal antenna, this could be done by measuring the input impedance, because it is highly sensitive to the electrical properties of the surrounding materials. However, general antennas are highly insulated and the properties of the insulation layer differ significantly from those of the surrounding material and alter the effect of the surrounding material. Thus, insulated antennas are not useful for estimating the electrical properties of the surrounding rocks (King et al. 1981). In addition, the current distribution should be known along the whole length of the antenna, which is not possible in practical situations. The behaviour of input impedance of the insulated antennas utilized in the EMRE system in different kinds of environments is thoroughly presented in publication II.

In the low frequency domain, when considering the physics of a time-varying electromagnetic

field in a conductor, two main effects may occur, induction and the galvanic effect, depending on the geometric coupling of the conductor with the primary field and the primary current. The vortex currents induced according to Faraday's Law in the conductor have different geometries and spectral behaviour, and the secondary field generated by these currents is very characteristic for each effect. The vortex effect is present in any conductor having sufficient coupling with the primary field. The maximum coupling occurs when the magnetic flux impinges perpendicularly on the surface of a conductor. The electric currents (eddy or vortex) circulating in closed loops within the conductor are the sources of the secondary fields. The electromagnetic field generated is approximately equivalent to the field of a closed electrical circuit and resembles the field of a horizontal magnetic dipole (HMD, Fig. 9a) at a larger distance. In Figure 9, a schematic representation of inductive and galvanic effects is presented due to a rectangular vertical magnetic dipole (VMD) at the earth's surface. High frequency waves suffer from strong attenuation between the boreholes (amplitude-depth). The galvanic effect is referred to as a current gathering or channelling effect. For a finite-sized target embedded in a conductive host rock having electrical contact with the host, the target itself can be either more conductive or less conductive than the host. The galvanic effect does not exist in very resistive host rocks because the effect is due the interaction between the target and currents produced by the primary field induction circulating in the host rocks. The currents are gathered into the target when it is more conductive than the host and diverted away from the target when it is less conductive than the host. For an elongated conductive target aligned favourably with the primary current, the gathered current can be several times the primary current. The electromagnetic field generated by this effect outside the target is equivalent to the field of an open segment of current. At a large distance, it is equivalent to the field of a horizontal electric dipole (HED, Fig. 9b) (Nabighian 1987). A 3-component receiver measures the total magnetic field (primary + secondary) at the earth's surface (Fig. 9). Secondary currents are induced in all conductors, but when a conductor also has sufficiently high magnetic permeability, an additional component adds the total field received in addition to the induced secondary magnetic field. A magnetic material becomes magnetized when placed in the magnetic field (Eqs. 1-2), and induced oscillating magnetization $\vec{M}_i$ is also induced in the conductor. The vortex currents depend on the frequency and the strength of the primary field strength, but $\vec{M}_i$ is only proportional to the primary field strength, and thus at low frequencies the induced magnetization $\vec{M}_i$ may dominate over the vortex currents. The

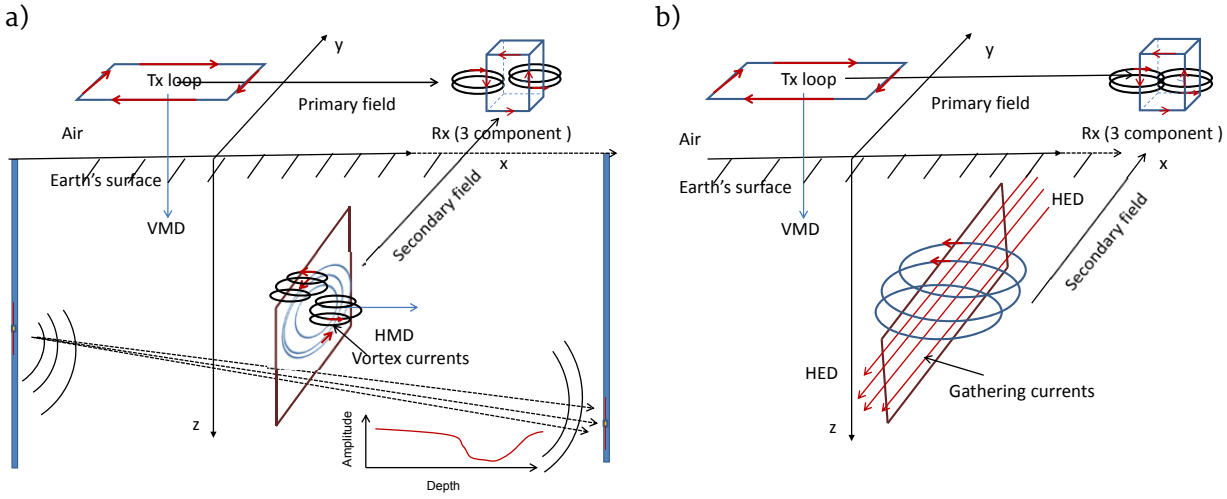

Fig. 9. a) Vortex currents are induced in a conductor by the time-varying electromagnetic field, and when the antenna system between the boreholes (water-filled boreholes) is operating, the amplitude of the field is highly attenuated due to conductive material. b) Galvanic currents generated by the induction in a conductive host where the vortex currents gather into a more conductive target. VMD is the vertical magnetic dipole, HDM the horizontal magnetic dipole, and HED the horizontal electric dipole. (Not to scale).

maximum coupling occurs when the magnetizing primary field is, for instance, in the plane of an elongated conductor (Parasnis 1973). The measurements should thus be conducted at least at two frequencies, because when increasing the frequency, the magnetization component does not increase but can even decrease due to the skin depth effect. The skin depth determines the depth to which the electric field, current and magnetic field can penetrate into a conductor. The skin depth is inversely proportional to the square root of the product of electric conductivity and frequency, which means that field penetration is more difficult in better conductors and at higher frequencies (Smith 1977). On the contrary, the vortex currents increase at the higher frequencies and start to dominate due to the increase in conductivity as frequency increases (Parasnis 1973).

In the previous paragraph, Faraday's law was the basis for the secondary fields generated by both the vortex and galvanic currents using either passive or active sources. In the high frequency domain, the electromagnetic field in a vacuum or in an isotropic medium propagates as waves in the particular direction specified by its Poynting vector (Smith 1977). The waves cause the charges to oscillate, and thus generate additional waves travelling in any direction. The additional waves (scattered waves) have the same frequency as the incident wave. If the emitted waves are out of phase with the incident wave (phase difference ~ $\pm\pi$ radians), then the scattered and incident wave interfere (combine together through superposition) destructively and the new wave is attenuated. In certain directions, the scattered and incident wave can interfere constructively, forming beams that may furthermore undergo reflections/refractions at the interfaces due to different electrical properties and continue propagation in the medium (transmitted waves) at the angle that satisfies Snell's law (Zhang & Li 2007). Energy losses are related to all of these phenomena (Jol 2009, Seybold 2005).

The principle of surface electrical resistivity surveying assumes that the electrical potential in the ground depends on the electrical resistivities of the underlying soils and rocks. The current used is either direct current or low frequency (<20 Hz). When two electrodes, one feeding the current into the ground and the other for collecting the current, are placed on the ground surface, the resulting potential V_p can be used to estimate the electrical resistivity of the subsurface. Several different electrode configurations exist (e.g. Wenner, Schlumberger) (Parasnis 1986), resulting, however, in different resistivity distributions in inhomogeneous conditions (Fig. 10). In the Schlumberger configuration, the spacing of potential electrodes 2*l* is much shorter than the current electrode spacing 2*L* (Parasnis 1973, Parasnis 1986).

The resistivity distribution is closely related to the geometry of the electrode system, and the measurement unit is usually referred to as apparent resistivity. Resistivity measurement is one of the electrical methods. In the mise-a-la-masse method (excitation of the mass), one current electrode is directly connected to the conductor, and the second one is placed on the ground at a great distance. Potential electrodes are moved over the surface. Thus, a part of conductor (e.g. outcrop) must be accessible to ensure electrical earthing. The method can be used to estimate whether an outcrop is part of a large continuous conductor (Fig. 11) (Parasnis 1973, Parasnis 1986).

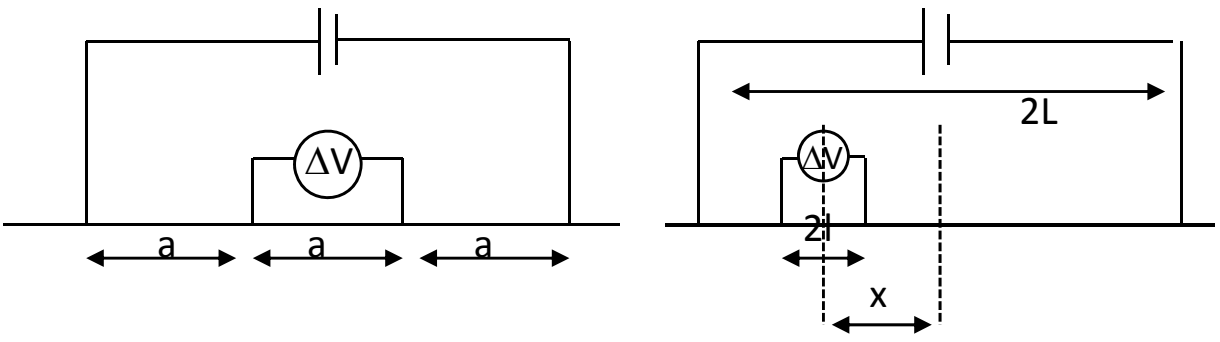

Fig. 10. The Wenner and Schlumberger configurations. Figure modified after Parasnis (1973).

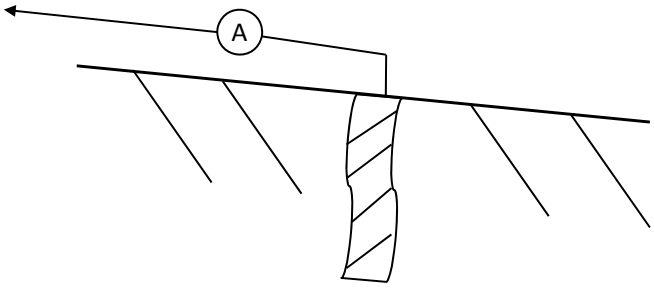

Fig. 11. The mise-a-la-masse configuration. Figure modified after Parasnis (1973).

IP method (induced polarization) is based on the fact that the ionic current flow is impeded, for instance, by metallic (electrode polarization) or clay (membrane polarization) particles. Polarization occurs at the surfaces, and thus a disseminated deposit with a large effective surface of particles is an ideal target for IP prospecting. Both of the methods are widely used electric methods (Kearey et al. 2002, Lowrie 2007, Parasnis 1986).

2.6 Seismic methods

Seismic methods can be divided into two categories based on refractive and reflective properties of the rays. In the refraction method, the internal physical properties of the subsurface materials can be estimated. On the other hand, the goal of the reflection method is to detect the reflected signals from the subsurface discontinuities. Thus, the reflection method can be regarded as an imaging method for subsurface structures, and the internal properties are not resolved. The seismic method is based on the fact that elastic waves propagate with different velocities in different rocks. When a force is applied to a material, particles of the material are displaced from their original positions. When the displacement is reversible, the particles return to their original positions when the force is removed. This is referred to as elastic behaviour. The main elastic waves are longitudinal (compressional, primary waves) or P-waves (V_p) when the movement of material particles occurs in the direction of wave propagation (compressed ↔ dilated), and transverse (shear, secondary waves) or S-waves (V_s) when particle movement occurs perpendicular to the direction of wave propagation. The frequency of seismic wave ranges between ~15 and ~100 Hz. P- and S-waves are often referred to as body waves and they propagate in all directions from the source. Rayleigh (R) and Love (L) waves are surface waves propagating along an interface between two media. They are slower than body waves or have lower frequencies (Erkan 2008, Kearey et al. 2002, Lowrie 2007, Parasnis 1986). The velocities of seismic waves for an isotropic material (material properties independent of direction) can be calculated from

$$V_p = \left(\frac{k + 4\mu/3}{\rho}\right)^{1/2} > \mathrm{V_s} = \left(\frac{\mu}{\rho}\right)^{1/2} \quad (7)$$

where k is incompressibility or the ability of a material to resist compression (bulk modulus), μ is the rigidity or it describes the shape distortion (shear modulus), and ρ is the density of the material. P-waves travel through any material, whereas S-waves do not travel through liquids or gas because $\mu = o$.

According to Eq. 7, waves propagate faster in more rigid materials. Generally, the velocities increase with increasing densities due to the greater increase in the bulk and shear modulus. The mean density of the earth's crust is ~2800 kgm^{-3}. The crust is solid, consisting of continental and oceanic crust. Oceanic crust has an average thickness of 6 km, whereas continental crust has an average thickness of ~35 km. Typical values for V_p in the earth's crust are ~5–7 kms^{-1}; compared to ~1.5 kms^{-1} in water and ~0.3 kms^{-1} in air. P-waves are most often used in seismic surveys because they have higher velocities, ensuring that they always reach a detector before S-waves. Conversely, due to the lower velocities of S-waves, the wavelengths are shorter, meaning better resolution. The corresponding value in typical crust for V_s is ~3–4 kms^{-1} (Kearey et al. 2002, Lowrie 2007, Parasnis 1986, Sheriff & Geldart 1995, Touloukian et al. 1981).

The waves return to the surface devices after refraction or reflection at geological boundaries within the subsurface. A set of devices detects the motion in the ground caused by these waves and hence measures the arrival times of the waves. The travel times may be converted into depth values and, the distribution of sub-

a) b)

Fig. 12. Schematic figure showing the principle of a reflection survey. a) Seismic waves are generated by the truck are transmitted and are transmitted to the rock. b) Waves reflected from a contact of different rock types are detected with geophones on the surface. Figures by Prof. Ilmo Kukkonen, University of Helsinki.

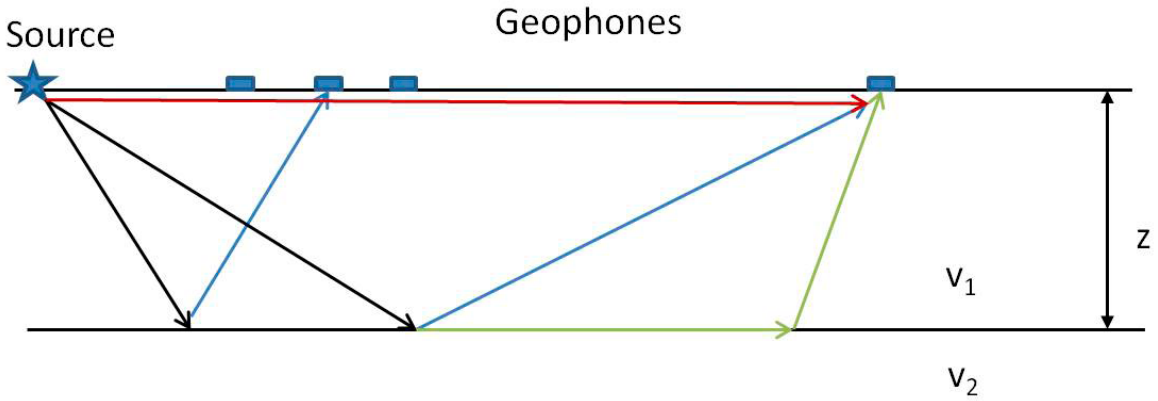

Fig. 13. Direct (red), reflected (blue) and refracted (green) ray paths from a source to a surface geophone (two-layer model). Figure modified after Keary et al. (2002).

surface geological interfaces may be delineated (at al. 12–14).

In seismic surveys, basically three types of seismic arrivals are measured with the surface geophones (Fig. 13). Direct rays travel along the top layer from the source to the detector at velocity v_1. Subsurface changes cause reflection and refraction of seismic waves. Rays incident on the interface (v_1,v_2) are reflected to the detector with velocity v_1. A certain incidence angle causes so-called critical refraction, where refracted waves travel along the interface at a higher velocity v_2, before bouncing off up through the upper layer at v_1 (Kearey et al. 2002, Lowrie 2007).

Nowadays, seismic reflection studies used in hydrocarbon prospecting for decades have also become more popular in the hardrock environment. The reflection seismic method is a high-resolution technique with a great depth extent without any essential decrease in resolution with depth. The method can be used to directly detect deposits and trace structures related to deposits, because many ore types have a strong acoustic impedance contrast with their host rocks (Kearey et al. 2002, Lowrie 2007, Salisbury et al. 2000). The interfaces serve as strong reflectors like electromagnetic waves impinging on the interface with different wave impedances. However, ore targets can occur, for instance, as elongated thin veins, and despite being highly economic they can be very difficult to determine seismically because their influence on the propagation of seismic waves is insignificant.

Posiva Oy has carried out research and development on a spent nuclear fuel disposal site in Finland. The repository will be constructed deep in the crystalline bedrock of Olkiluoto island in Eurajoki. Construction of the underground characterization facility ONKALO started in 2004. Posiva Oy has actively examined methods for

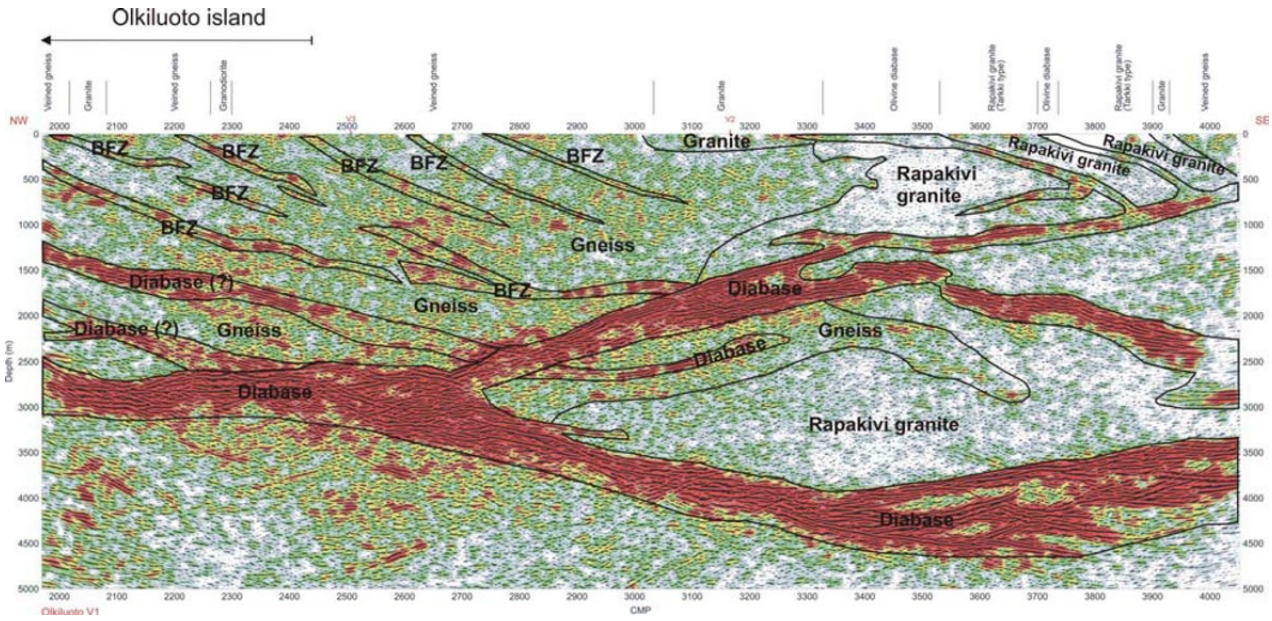

Fig. 14. Processed reflection profile section from the Olkiluoto area showing strong reflectors interpreted to be diabase dykes in an otherwise granitic environment. The figure shows wiggle traces representing subsurface reflectivity underneath each surface point with an amplitude envelope in the background. The amplitude envelope represents the smoothed absolute value of reflection amplitudes and automatically enhances strong reflections (red) (Kukkonen et al. 2010). Figure by Kukkonen et al. (2010).

revealing the properties of granitic, i.e. crystalline bedrock. One of the considered methods was a seismic reflection survey as a part of the project HIRE (High Resolution Reflection Seismics for Ore Exploration 2007–2010). The survey was carried out in the Olkiluoto area of western Finland in July 2008. The promising HIRE results revealed numerous previously unknown structures in the upper crust of the area (Fig. 14) (Kukkonen et al. 2010, Kukkonen et al. 2012).

The main principles of four very important geophysical methods have been explained above: magnetic, gravity, electromagnetic and seismic methods. Magnetic and gravity methods are static methods, and thus the measured fields do not vary with time. They are also referred to as natural field methods, because no artificial man-made sources are needed. Electromagnetic and seismic methods are dynamic methods and the measured fields change with time. They can also be utilized in both a natural and an artificial manner. All the mentioned methods have limitations, advantages and disadvantages, and reasonably combining several methods may thus provide the best results. The decision on which method or methods should be utilized in a prospecting project must be based on careful planning in which all available geological, mineralogical and topographical data from the research area should carefully be gathered. In addition, laboratory measurements from core samples should be conducted every time if possible. Preliminary preparations of this kind ensure which geophysical method or methods can even be utilized in the research area. An issue that is common for all the above-mentioned methods is that certain physical properties of the rock (magnetic susceptibility, electrical conductivity, density and velocity) are not merely essential, but the detection of the target depends on the difference between the appropriate property of the target and that of the host rock (Parasnis 1973).

Deep ore prospecting should also confirm the location of favourable host rock for ore and for the utilization of the rock structures (e.g. faults, fractures and fissures), because certain kinds of mineral deposit are only found in specific types of rocks or are associated with certain geological structures. For instance, massive sulphide deposits almost always occur in volcanic rocks, and chromite is most often found in ultrabasic igneous rocks (Dixon 1979). These structures are not economically interesting, but when they bear conductive brines, they can cause electromagnetic anomalies that, on the other hand, can have an indirect connection with the ore. When

conductive mineral such as pyrite, pyrrhotite and magnetite is essential in the deposit, it is also a suitable object for electromagnetic prospecting. The abovementioned minerals do not have such a large economic value, but they are often associated with sulphide ores and can then help to delineate sulphide formations. Zinc-bearing ores and chromite are economically interesting, but they are poorly conducting ore minerals, and thus they are difficult targets for electromagnetic methods. However, when the deposits contain, for instance, disseminated pyrite minerals in the resistive matrix, zinc ores can often also be delineated. The indicator mineral method has lately been developed and vastly expanded to prospecting for different types of deposits, for instance, kimberlites (e.g. pyroxene, chromium spinels) or volcanogenic massive sulphides (e.g. sphalerite, Zn-spinel) (McClenaghan 2005, Parasnis 1973). The appearance of an indicator mineral, even a few grains, may indicate the presence of a specific type of mineralization.

3 LOSSY ENVIRONMENT

Geophysical surveys have an important role in improving our knowledge of geological systems of the Earth. In particular, knowledge of the *in situ* properties of rocks is valuable when interpreting these surveys and developing new geophysical devices. This thesis is focused on RIM surveys, in which insulated dipole antennas are used as sources and receivers for electromagnetic energy at medium radio frequencies. When an antenna is situated in air, calculation of the antenna parameters (Gustrau & Manteuffel 2006, Ludwig & Bretchko 2009, Orfanidis 2004, Seybold 2005) and wave propagation is quite straightforward, but when situated in a dissipative medium, the situation is much more complicated. However, even then, the same approach as within non-conducting media can be used, although the constituent electric and magnetic properties must now be regarded as complex values (Moore 1963). The radiated field intensity at any point is a function of the distance from the source, the frequency used and the electrical parameters of the subsurface. In the far-field domain, the transmitter-receiver distance is great ($r >> \lambda$; r is the distance and λ is the wavelength). Spherical spreading is a valid assumption and the amplitude decays as $1/r$. Higher frequencies mean shorter ranges but better resolution. When an external field exists in a medium, some of the energy is dissipated as heat (intrinsic attenuation). Attenuation is a function of electric conductivity and permittivity, magnetic permeability and frequency, and it is the most important factor when amplitude data are considered in a low resistive environment.

The physical behaviour of an electromagnetic field is governed mathematically by Maxwell's equations, which describe the relationship between electric and magnetic fields in a medium and quantify the material properties (Jol 2009, Lafleche 1985, Smith 1977, Zhang & Li 2007). The form of an electromagnetic wave is dependent on the nature of the material in which the wave is propagating. The simplest waves in a homogeneous medium are uniform plane waves that exist at a large distance from the source. Plane waves can be regarded as an asymptotic form of the wave front of a spherical wave at large distances from the source, having negligible curvature over a limited area (infinite planar surface), and are called transverse electromagnetic waves (TEM waves). TEM waves have only transverse electric and magnetic field components and no longitudinal component in the direction of propagation or in the direction of power flow. Plane waves are the simplest way to apply the necessary equations. The four electromagnetic equations that explain the field characteristics are (Jol 2009, Smith 1977, Zhang & Li 2007):

$$\nabla \cdot \vec{D} = \rho \quad \text{(Gauss' law, electricity)} \quad (8)$$

$$\nabla \cdot \vec{B} = o \quad \text{(Gauss' law, magnetism)} \quad (9)$$

$$\nabla \times \vec{E} = -\partial \vec{B} / \partial t \quad \text{(Faraday's law)} \quad (10)$$

$$\nabla \times \vec{H} = \vec{J} + \partial \vec{D} / \partial t \quad \text{(Ampere's law)} \quad (11)$$

The expressions for an electromagnetic wave propagating in a linear, isotropic and homogeneous medium can be derived from these four equations. The notation used in the above equations is: D = electric displacement [C/m^2],

E = electric field intensity [V/m], B = magnetic induction [T], H = magnetic field intensity [A/m], J = electric current density [A/m^2], ρ = free charge density [C/m^3]. Thus, the sources of the electric displacement are electric charges with density ρ (Eq. 8). The magnetic field is solenoidal (divergence free vector field) or no magnetic charges exist (Eq. 9). The vortices of the electric field are generated by temporal variations in the magnetic induction (Eq. 10). The vortices of the magnetic field are generated either by an electric current with density J or by temporal variations of the electric displacement (Eq. 11). The material properties determine the relationships between vector fields in Maxwell's equations, and the material equations can be written in a linear, homogeneous and isotropic medium as

$$\vec{D} = \varepsilon\vec{E} \qquad \vec{H} = {}^{\vec{B}}/_{\mu} \qquad \vec{J} = \sigma\vec{E}\,, \tag{12}$$

where ε is electrical permittivity, determining the ability of the medium to store and release electromagnetic energy (the storage ability of a capacitor), or it can be described as the degree of polarization in the medium; μ is magnetic permeability and describes how atomic and molecular magnetic moments respond to the magnetic field; and $\sigma$is electrical conductivity, which describes the medium's ability to transmit free electric charges (electrons in metals or ions in electrolytes) (Jol 2009, Smith 1977, Zhang & Li 2007). All these parameters are scalar constants under the conditions stated above. Using Eq. 12, taking the curl of Eq. 11 and substituting the results in Eq. 10, the inhomogeneous generalized time-domain wave equations for $\vec{\mathrm{E}}$ and $\vec{\mathrm{H}}$ are derived:

$$\nabla^2\vec{E} - \mu\sigma\frac{\partial\vec{E}}{\partial t} - \mu\varepsilon\frac{\partial^2\vec{E}}{\partial t^2} = \frac{1}{\varepsilon}\nabla\rho + \mu\frac{\partial\vec{J}}{\partial t} \tag{13}$$

$$\nabla^2\vec{H} - \mu\sigma\frac{\partial\vec{H}}{\partial t} - \mu\varepsilon\frac{\partial^2\vec{H}}{\partial t^2} = -\nabla\times\vec{J}\,. \tag{14}$$

The sources of the fields are on the right-hand side. On the left-hand side, the second-order time-derivative term is the wave term (oscillating term) with an energy storage factor ($\mu\varepsilon$) and the first-order time-derivative term is the damping term with an energy dissipation factor ($\mu\sigma$). For sinusoidal time-harmonic fields ($\mathrm{e}^{\mathrm{i}\omega t}$), these equations (in a source-free region, σ = 0 and $\vec{\mathrm{J}} = 0$) become frequency-domain Helmholtz's equations. Using the following substitutions; ${}^{\partial}/_{\mathrm{dt}} \to \mathrm{i}\omega$ and ${}^{\partial^2}/_{\partial \mathrm{t}^2} \to -\omega^2$, Eq. 13 and Eq. 14 can be written as

$$\nabla^2\vec{E} - i\omega\mu\sigma\vec{E} + \omega^2\mu\varepsilon\vec{E} = 0 \to \nabla^2\vec{\mathrm{E}} + \mathrm{k}^2\vec{\mathrm{E}} = 0 \tag{15}$$

$$\nabla^2\vec{H} - i\omega\mu\sigma\vec{H} + \omega^2\mu\varepsilon\vec{H} = 0 \to \nabla^2\vec{\mathrm{H}} + \mathrm{k}^2\vec{\mathrm{H}} = 0 \tag{16}$$

$k^2 = \omega^2\mu\sigma - i\omega\mu\sigma$ is the complex wave number and $\mathrm{i} = \sqrt{-1}$ an imaginary unit.

The Q factor defined by $\mathrm{Q} = \dfrac{\omega\varepsilon}{\sigma}$ (inverse loss tangent) is an important constant that describes the characteristics of field behaviour. When Q >> 1, energy storage effects associated with permittivity (ε) and permeability (μ) are dominant (fields are propagating). When Q << 1, energy loss effects associated with conductivity (σ) are dominant (fields are diffusing). In a plane wave, the fields propagate in a direction that is perpendicular to the plane of the wave. This is also known as the wave front, in which the front is an equi-amplitude plane, meaning that the field strength is constant on the plane. For a linearly x-polarized wave propagating in the positive z-direction (E directed along the x-axis), the solutions to Eq. 15 and Eq. 16 are

$$\vec{E}_x = \vec{E}_0 exp(-\gamma z)\vec{x} \tag{17}$$

$$\vec{H}_y = \vec{H}_0 exp(-\gamma z)\vec{y}, \tag{18}$$

where γ is the propagation constant as $\gamma = \alpha + i\beta = i\cdot k$ and $\vec{E}_0$, $\vec{H}_0$ are constant vectors. Thus, Eqs. 17 and 18 can then be written as

$$\vec{E}_x = \vec{E}_0 exp(-i\beta z - \alpha z)\vec{x} = \vec{E}_0 exp(-i\beta z)exp(-\alpha z)\vec{x} \tag{19}$$

$$\vec{H}_y = \vec{H}_0 exp(-i\beta z - \alpha z)\vec{y} = \vec{H}_0 exp(-i\beta z)exp(-\alpha z)\vec{y} \tag{20}$$

$$\vec{H}_y = \frac{\vec{E}_0}{\eta} exp(-i\beta z - \alpha z)\vec{y}\,, \tag{21}$$

where η is the wave impedance. In a dissipative medium, the wave impedance is a complex quantity and the electric and magnetic fields are no longer in phase (Zhang & Li 2007). As can

be seen from Eqs. 19-20, the amplitudes and phases of the fields are controlled by the terms αz and βz. The first exponential function is the phase term and the second is the attenuation (damping) term.

In the EMRE system, the electromagnetic fields are transmitted/received using insulated electric dipole antennas that are aligned parallel to the borehole axis. The electromagnetic field of an electric dipole has three effective components: a magnetic component ($\vec{B}_\varphi$), an electric tangential component ($\vec{E}_\theta$) and a radial component ($\vec{E}_r$). The tangential component dominates in the far-field domain, which is generally assumed in radio imaging measurements (RIM). When an electromagnetic field exists in a homogeneous and isotropic medium, three properties of the medium are important: electric permittivity and conductivity and magnetic permeability, and the magnetic permeability when attenuation rates are estimated.

3.1 The attenuation and phase constant

In the high frequency domain, the electromagnetic field in a vacuum or in an isotropic medium propagates as waves in the particular direction specified by its Poynting vector until (Smith 1977) it impinges on the interface with different electrical properties. Then, some of the energy is reflected and some is refracted (transmitted), depending on the angle of the incident wave and the wave impedances across the interface. The wave impedance η in a material is defined as the ratio of the amplitude of electric and magnetic fields (Seybold 2005, Smith 1977, Zhang & Li 2007).

$$\eta \approx \sqrt{\frac{\mu_{eff}}{\varepsilon_{eff}}}\ , tan\,\delta \ll 1;$$

$$\eta = \sqrt{\frac{i\omega\mu_{eff}}{\sigma_{eff} + i\omega\varepsilon_{eff}}}, tan\delta \approx 1;$$

$$\eta \approx \sqrt{\frac{i\omega\mu_{eff}}{\sigma_{eff}}} \approx \sqrt{\frac{\omega\mu_{eff}}{\sigma_{eff}}} e^{i\frac{\pi}{4}}, tan\delta \gg 1 \qquad (22)$$

The last expression in Eq. 22 is valid for good conductors, and thus the phase difference between the electric and magnetic field is $\pi/4$, and the magnetic field dominates in the wave. In a vacuum, $\eta = \eta_o \sim 377$ Ohm (Smith 1977, Zhang & Li 2007). Thus, one possible definition of an antenna is that it converts the output impedance of a transmitter into the corresponding impedance of the surrounding medium. In free space, the conversion is: antenna impedance in Ohms $\rightarrow$377 Ohm.

The solution of Maxwell's equations yields quantities that describe the propagation of electromagnetic waves in the wave number k:

$$k^2 = \omega^2\mu\varepsilon \pm i\omega\mu\sigma = \mu\omega(\omega\varepsilon \pm i\sigma) = \beta \pm i\alpha\,, \qquad (23)$$

where the sign of ±i is determined by the direction of the wave ($e^{-i\omega t}$ or $e^{+i\omega t}$ dependence). ω is the angular frequency, ε, σ and μ are the permittivity, conductivity and permeability, which may be complex quantities, and β is the phase and α the attenuation constant (Knoll 1996, Lafleche 1985, Zhang & Li 2007). The field depends on the distance r from the source and the wave number $\vec{k}$ multiplied by the distance $\vec{r}$ defines the behaviour (III). Certain characteristics of an electromagnetic field dominate at one particular distance from the antenna, while a completely different behaviour can dominate at another location. The simplest waves in a homogeneous medium are uniform plane waves that exist at a large distance from the source, having negligible curvature over a limited area (the far-field domain $\|\vec{k}\,\vec{r}\| >> 1$). The field strength in a homogeneous and isotropic medium can be written as:

$$E(z) = E_0 e^{-i\vec{k}\cdot\vec{r}} = E_0 e^{-i\beta z} e^{-\alpha z}\,, \qquad (24)$$

where E_o is the source strength and z the distance from the source. As can be seen from Eq. 24, the amplitudes and phases of the fields are determined by the terms αz and βz. The first exponential function is the phase term and the second is the attenuation (damping) term. The general expressions for β and α can be written as (deBettencourt & Surcliffe 1962, Jackson & Tweeton 1996, King et al. 1981, Lafleche 1985, Vogt 2000, Zhang & Li 2007)

$$\beta = \omega\sqrt{\frac{\mu\varepsilon}{2}}\left(\sqrt{1+\left(\frac{\sigma}{\omega\varepsilon}\right)^2}+1\right)^{\frac{1}{2}} = \omega\sqrt{\frac{\mu\varepsilon}{2}}\left(\sqrt{1+p^2}+1\right)^{\frac{1}{2}}(rad/m) \quad (25)$$

$$\alpha = 8.686\omega\sqrt{\frac{\mu\varepsilon}{2}}\left(\sqrt{1+\left(\frac{\sigma}{\omega\varepsilon}\right)^2}-1\right)^{1/2} = 8.686\omega\sqrt{\frac{\mu\varepsilon}{2}}\left(\sqrt{1+p^2}-1\right)^{1/2}(dB/m), \quad (26)$$

where p is referred to as a loss tangent.

In weakly lossy dielectrics (high frequencies, $p \ll 1$ or the conduction currents are much smaller than the displacement currents), Eqs. 23, 25–26 can be simplified as $k^2 = \omega^2\mu\varepsilon$ and $\beta \approx \omega\sqrt{\mu\varepsilon}$ or $\beta \approx \beta_o\sqrt{\varepsilon_r}$, where $\beta_0 = \frac{2\pi}{\lambda_0} = \omega\sqrt{\mu_0\varepsilon_0}$ and λ_o is the free space wavelength in metres. The relationship between the wavelengths can be written as $\frac{\lambda}{\lambda_0} = \frac{1}{\sqrt{\varepsilon_r}}$. The attenuation can now be expressed as $\alpha \approx \frac{\sigma}{2}\sqrt{\frac{\mu}{\varepsilon}} = \beta_0\sqrt{\varepsilon_r}\frac{p}{2}$ (Np/m) or $\alpha \approx 1.637\cdot 10^3\frac{\sigma}{\sqrt{\varepsilon_r}}$ (dB/m). In most solids, $\beta > \alpha$ (deBettencourt & Surcliffe 1962, Jackson & Tweeton 1996, King et al. 1981, Lafleche 1985, Zhang & Li 2007).

In good conductors (low frequencies, $p \gg 1$), $k^2 = \pm i\omega\mu\sigma$ and the attenuation rate is equal to the phase constant or $\alpha = \beta \approx \sqrt{\omega\mu\sigma/2}$ or $\alpha \approx \beta_o\sqrt{\varepsilon_r}\sqrt{\frac{p}{2}}$ (Np/m or rad/m). The attenuation can be simplified to $0.5458\cdot\sqrt{f_k\sigma}$ (dB/m), where f_k is the frequency in kHz and the wavelength $\lambda \approx 2\pi\sqrt{\frac{2}{\omega\mu_o\sigma}}$ (metres) (deBettencourt & Surcliffe 1962, Jackson & Tweeton 1996, King et al. 1981, Lafleche 1985, Zhang & Li 2007).

At distance $\delta = 1/\alpha = \sqrt{\frac{2}{\omega\mu_o\sigma}}$, when the wave number becomes $k \approx \frac{1-i}{\delta}$ the field has attenuated to a fraction e^{-1} of the initial field strength. The distance is known as the skin depth (deBettencourt & Surcliffe 1962, Jackson & Tweeton 1996, King et al. 1981, Lafleche 1985, Zhang & Li 2007) and it can also be written as $\delta \approx \frac{15.92}{\sqrt{f_k\sigma}}$ (m). Table 1 presents the skin depths (δ) and attenuation constants (dB/m) with different material properties at the EMRE frequencies. The relationships between the exact skin depth and the high and low frequency approximations are presented in Figs. 15a–b. It is theoretically possible to use the whole frequency band of the EMRE system so that the conductivity and permittivity can both be determined from the measured amplitudes. Namely, when using the low frequency of 312.5 kHz and having high p conditions, the attenuation is proportional to $\sqrt{\sigma}$ and the conductivity can thus be determined from the decayed amplitudes. On the contrary, using the high frequency of 2500 kHz and having low p conditions, the attenuation is also proportional to $\left(\sqrt{\varepsilon}\right)^{-1}$, and the relative permittivity (ε_r) can thus be determined using the conductivity from the low frequency measurement (deBettencourt & Surcliffe 1962).

Traditionally, electromagnetic field propagation is referred to as diffusion and wave propagation depending on the conductivity of the medium and the used frequency. Because diffusion is closely related to a random movement (e.g. thermal energy transfer (Kittel 1976), a more descriptive term could be highly attenuating propagation due to the highly controlled sources utilized. In a low resistive medium (ρ = 100 Ωm, ε_r = 10), the quasi-static conditions (displacement current negligible or high p conditions) are valid up to ~1000 kHz. By comparison, in a highly resistive environment (ρ = 10 000 Ωm), the quasi-static conditions are valid up to ~10 kHz (Fig. 15c). Increasing the relative permittivity of the medium, the cut-off frequencies decrease (ε_r = 20) and the quasi-static conditions are valid almost up to ~600 kHz, while in a highly resistive environment (ρ = 10 000 Ωm), the quasi-static conditions are valid up to ~5 kHz (Fig. 15d).

Table 1. The skin depths (δ) and attenuations (dB/m) with different material properties.

Resistivity	**2500 Ωm**				**7500 Ωm**				**15 000 Ωm**			
kHz	312.5	625	1250	2500	312.5	625	2500	2500	312.5	625	1250	2500
δ (m)												
ε_r = 10	55	44	42	42	133	126	126	126	256	252	252	252
ε_r = 40	87	84	84	84	252	252	252	252	504	504	504	504
dB/m												
ε_r = 10	0.16	0.20	0.20	0.20	0.065	0.068	0.068	0.068	0.034	0.034	0.034	0.034
ε_r = 40	0.10	0.10	0.10	0.10	0.034	0.034	0.034	0.034	0.017	0.017	0.017	0.017

a)

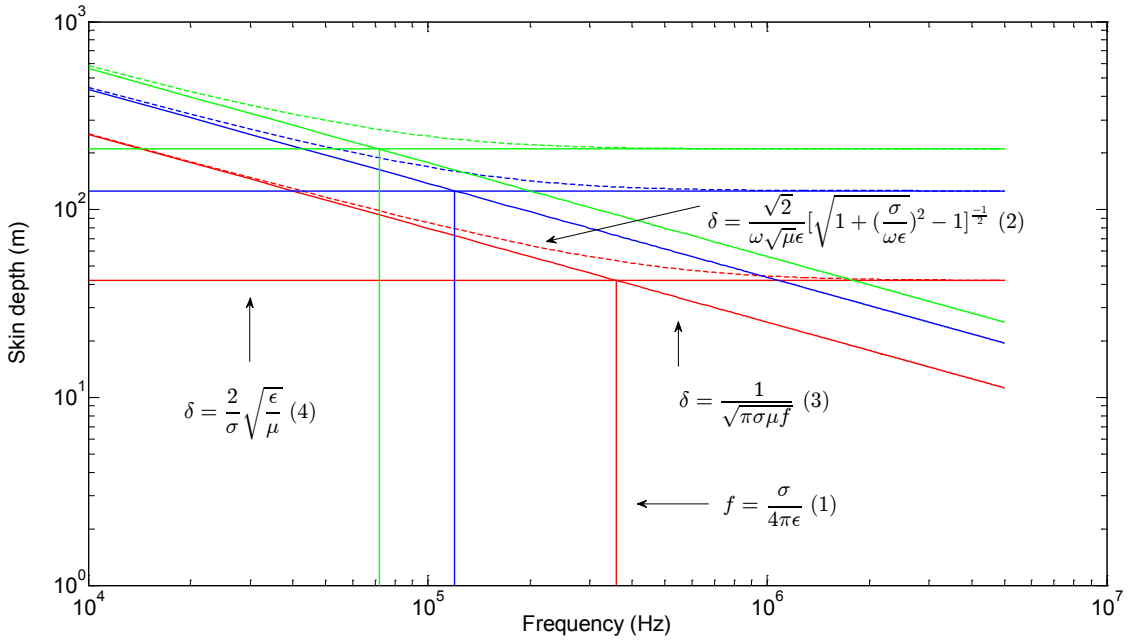

Fig. 15. a) The relationship between the exact skin depth (expression 2, dashed lines) and low-loss (expression 4, vertical bold lines) and high-loss material (expression 3, bold lines) approximations. The intersection frequency (expression 1, vertical lines) where the high and low approximations intersect is also presented. The resistivities are ρ = 12500 Ωm (green lines), ρ = 7500 Ωm (blue lines), ρ = 2500 Ωm (red lines) and the relative permittivity ε_r = 10.

b)

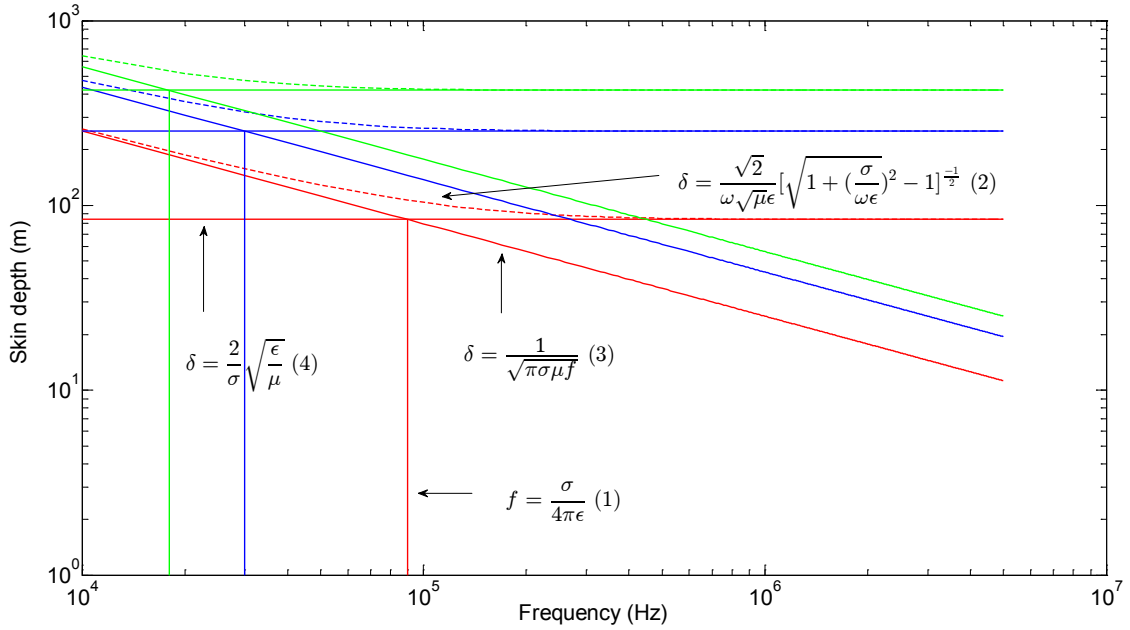

Fig. 15. b) The corresponding presentation with ε_r = 40.

c)

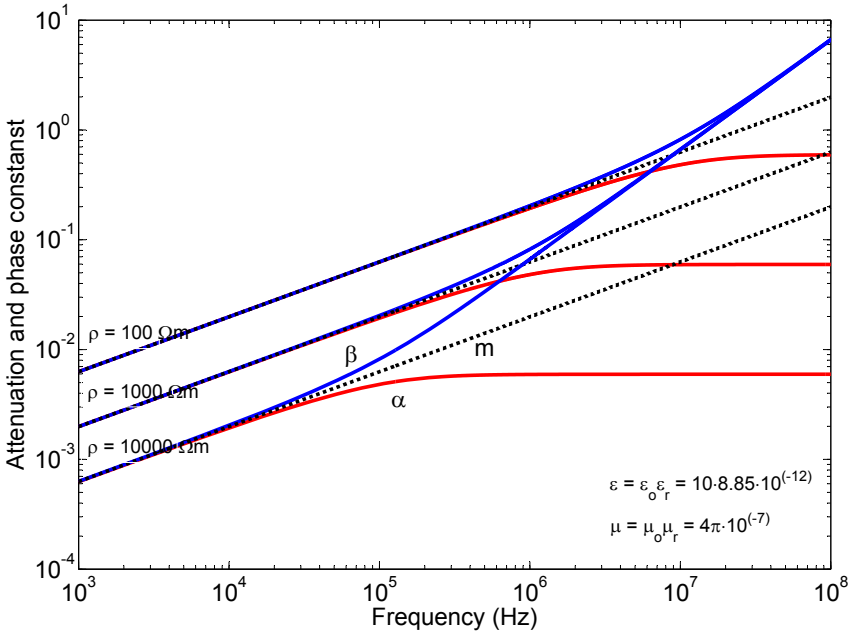

Fig. 15. c) The attenuation (α) and phase (β) constants in a dissipative medium with ε_r = 10 and ρ = 100, 1000 and 10 000 Ωm. α is the attenuation (red lines) as Nepers/m and β is the phase constant (blue lines) as rad/m. The m curve is valid when the attenuation constant equals the phase constant or $\alpha \approx \beta$ (black curves).

d)

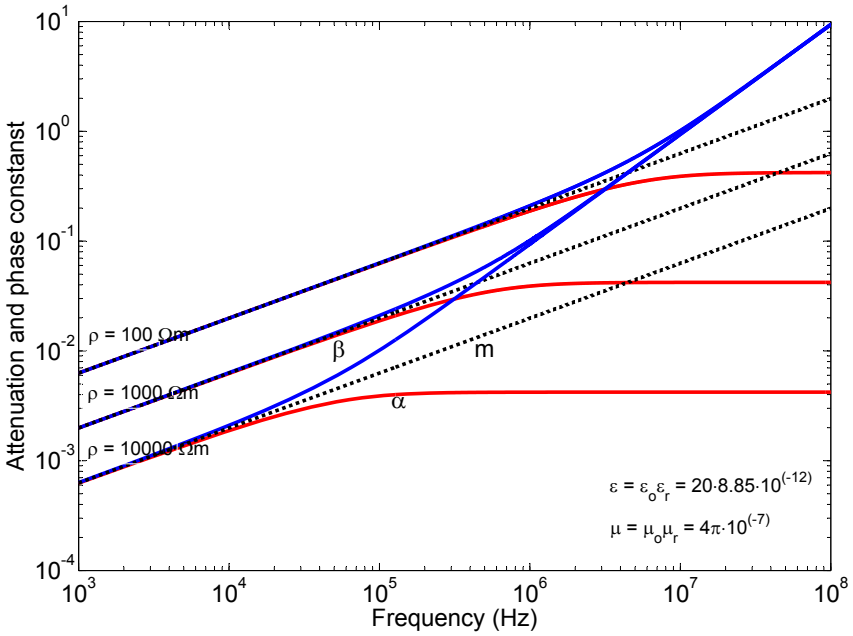

Fig. 15. d) The phase and attenuation constants in a dissipative medium with ε_r = 20. α is the attenuation (red lines) as Nepers/m and β is the phase constant (blue lines) as rad/m. The m curve is valid when the attenuation constant equals the phase constant or $\alpha \approx \beta$ (black curves).

The main factor that limits the use of radio frequencies in geophysics is the strong absorption of energy in most earth materials, or that the penetration is highly frequency dependent. When amplitude data are collected, the attenuation can be directly estimated from the decayed amplitudes. Using the plane wave assumption, which is valid in the far field, the measured amplitudes can be converted to the attenuation distribution in a simple way (Fullagar et al. 2000, Holliger & Maurer 2004, Holliger et al. 2004, Jackson & Tweeton 1996, Pears & Fullagar 1998, Thompson & Hinde 1993). Lee et al. (2002) used a technique where the vertical components of

frequency domain magnetic fields were transformed to the wave field to obtain the first arrival time of the wave field. Pralat and Zdunek (2005) utilized a Bayesian framework for determining the attenuation distribution. Russian scientists carried out intensive work using RIM with good results during the late 1900s (Buselli 1980), and they have also developed their own philosophy when interpreting RIM measurements (Redko et al. 2000a, Redko et al. 2000b, Stevens et al. 1998). The obtained information can be used, for instance, in mine planning, ore prospecting and assessing the integrity of the rock mass, as increased electrical conductivity is often associated with rock mass deformation (clay and water bearing fractures, sulphide and graphite bearing zones), and thus with higher attenuation values. Another approach is to use mathematical means, and the electrical properties must therefore be known. The attenuation and phase rate of electromagnetic wave propagating in the material with known electrical properties is governed by Eqs. 25–26. Both values are functions of magnetic permeability (μ), electric permittivity (ε), conductivity (σ) and frequency (ω).

Figure 16a presents log-log plots of attenuation rates versus conductivities for several permittivities in the EMRE band ($\mu_r = 1$). At the lower conductivities, the permittivity curves are parallel and the attenuation rate is lower for higher values of permittivity. When the critical conductivity is encountered, the permittivity curves

a)

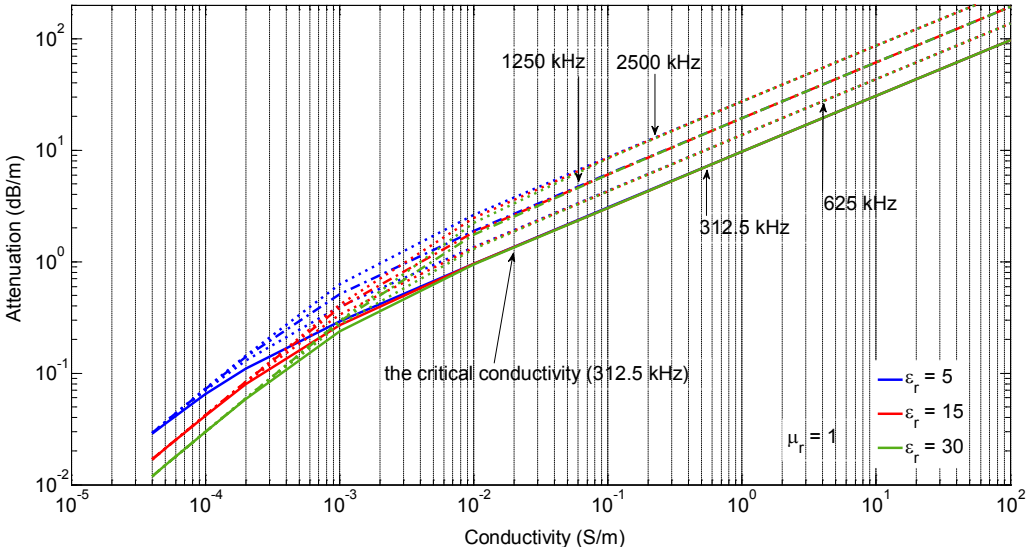

Fig. 16. a) The attenuation rates versus conductivity for several permittivities in the EMRE frequencies ($\mu_r = 1$). The permittivity curves merge together at the critical conductivity when $\alpha \approx \sqrt{\omega\mu\sigma}$.

b)

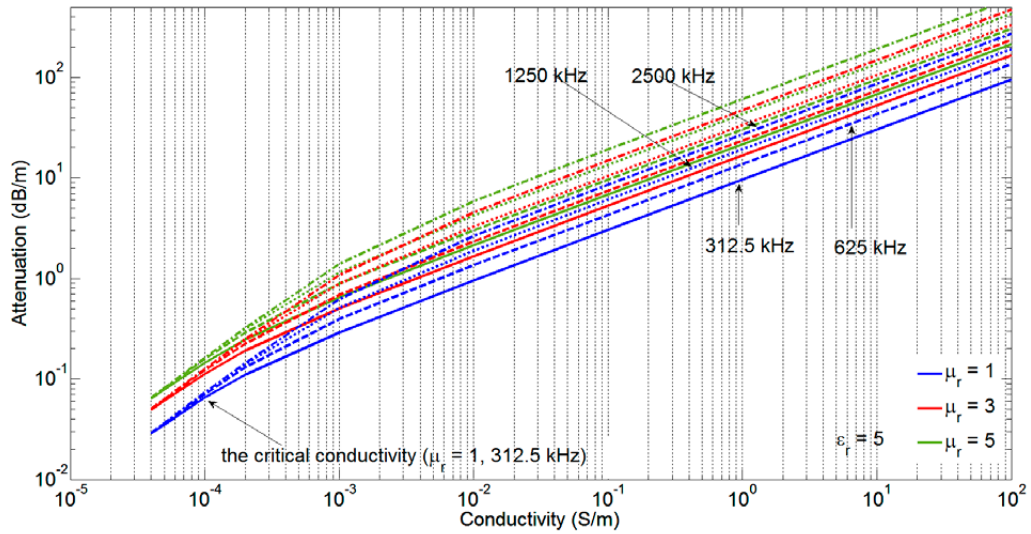

Fig. 16. b) The attenuation rates versus conductivity for several permeabilities in the EMRE frequencies ($\varepsilon_r = 5$). The bending of the permeability curves occur when the loss tangent is equal to unity.

merge together and become identical at higher conductivities when $\alpha \approx \sqrt{\omega\mu\sigma}$. Figure 16b presents log-log plots of attenuation rates versus conductivity for several magnetic permeabilities in the EMRE band (ε_r = 5). The attenuation rate increases with increasing permeability. The permeability curves are parallel until the critical conductivity is reached, when the curves bend and furthermore increase linearly but the slopes decrease. This occurs when the loss tangent is equal to unity (Lafleche 1985). However, the permeability is generally accepted to be that of free space (μ_0) for most common geological materials (non-magnetic).

As a summary, the increase in conductivity (σ) increases attenuation, but the increase in relative permittivity (ε_r) has an opposite influence and attenuation decreases. The relative permeability (μ_r) also has an increasing effect on attenuation rates. Thus, both conductivity and permeability increase attenuation rates. The magnetic permeability appears as a product with the conductivity ($\mu\sigma$) in the general complex wave equations (Jol 2009). Because the electric conductivity σ varies over a much larger range than the magnetic permeability, the conductivity overweights, and the permeability has a minor effect on the propagation of the electromagnetic field in the EMRE band. Naprstek (2014) has examined the basic issues concerning the behaviour of radiofrequency electromagnetic fields in a homogeneous whole space utilizing a simple model of a vertical electric dipole (Naprstek & Smith 2016). He followed the same strategy as the Russian experts and fitted theoretical data with measured data sets to clarify how radiated fields change due to the electrical parameters (Redko et al. 2000a, Redko et al. 2000b, Stevens et al. 1998). Furthermore, according to his studies, the geometric effects (borehole angles) can have a very complex effect on the measured signals (shifting data, increasing or decreasing amplitudes) and should be taken into account in the interpretation. However, true 3D numerical modelling techniques with a full waveform are needed to obtain more precise reconstructions of borehole sections when realistic antenna losses, as well as electric and magnetic losses in the earth's subsurface could be taken into account.

Laboratory measurements of electrical properties of rocks are performed on core samples, and sample selection can therefore be carried out with a high degree of control. However, laboratory conditions differ from the conditions in which the core samples were taken. Thus, the electrical properties determined in the laboratory can only be good estimates of *in situ* properties. In boreholes, the temperature and pressure increase with depth. The content of water in rock depends on the porosity of the rock, and the conductivity of the aqueous solution itself depends, for instance, on the dissolved salts. The conductivity increases with temperature and the water content in rocks decreases with pressure, resulting in decreased conductivity. The water content may also vary from place to place in boreholes, and the water in samples may even be destroyed during transport to the laboratory, thus significantly changing the electrical properties of the samples. An *in situ* measurement using a cross-borehole geometry is the most accurate method for estimating attenuation rates. As in measuring electrical properties, *in situ* attenuation rates can deviate significantly from laboratory values. The reasons for this problem are various. For instance, samples may suffer alteration during transport and scale dependence. *In situ* attenuation represents a value over a much larger rock volume than laboratory measurements performed on small samples and perhaps resulting in the loss of small-scale variations. In addition, the results from small-scale measurement are not easily converted to large-scale values.

4 MAGNETIC AND ELECTRICAL PROPERTIES OF ROCKS

4.1 The classification of rock types and their properties

Rocks are very complex compounds of different minerals and generally have a crystal structure. Their properties are determined to a large extent by the properties of the existing constituent minerals. Crystalline rock is comprised of individual mineral grains, and the grains are clearly visible. Minerals can be classified according to their chemical composition. Feldspar is

the most common mineral group, and hundreds of different feldspar minerals exist. Feldspar is followed by quartz as the second most common mineral (the main component of quartzite and sandstone; also exists e.g. in granite, gneiss). It is also possible that the properties of accessory minerals (magnetite, pyrrhotite, graphite) mainly determine the electrical and magnetic properties of the rock. Rocks may be classified into three main genetic groups (based on origin): igneous, sedimentary and metamorphic (Parkhomenko 1967).

Igneous rocks are formed by the cooling of magma or molten rock, and when the process happens at great depths, the rock is intrusive (plutonic, e.g. granitoids). Extrusive rock (volcanic rock) is formed at the surface or at shallow depths (e.g. basalt). Plutonic and volcanic rocks are also referred to as magma rocks. Igneous rocks have the lowest conductivities, and the conductivity is greatly dependent on the degree of fracturing and the amount of water in the fractures, from $\sigma \sim 10^{-9}$–10^{-16} S/m for granite (acid) and from $\sigma \sim 10^{-4}$–10^{-10} S/m for diabase (basic), depending on whether it is wet or dry. The relative dielectric permittivities are generally low, $\varepsilon_r \sim 4$–7 for granite (acid) and $\varepsilon_r \sim 10$–12 for diabase (basic) (Lytle 1973, Parkhomenko 1967). Thus, dielectric permittivities are greater for basic rocks than for acid rocks. The susceptibilities χ_m are in a range of <120 000 (10^{-6} SI units), resulting in relative permeabilities very close to μ_o (Fig. 17) (Airo & Säävuori 2013, Hunt et al. 1995).

Sedimentary rocks are deposited and layered at the earth's surface due to different exogenetic processes (erosion, transport, sorting, deposition). Sedimentary rocks are generally stratified (e.g. metamorphosed black shales) (Airo & Hyvönen 2008), usually porous and have a higher water content, and thus have higher conductivity values than igneous rocks. The conductivity values are largely dependent on the porosity of the rocks, and the salinity of the contained water. The relative permittivities can be variable, for instance, $\varepsilon_r \sim 10$ for dolomite and $\varepsilon_r < 45$ for shale (Lytle 1973, Parkhomenko 1967). The general values of susceptibilities of sedimentary rocks are low and can range up to hundreds of thousands (10^{-6} SI units) (Fig. 17) (Airo & Säävuori 2013, Hunt et al. 1995). Thus, the relative permeabilities μ_r remain very close to μ_o (Fig. 17).

Metamorphic rocks are formed by changes in pre-existing rocks under the influence of high temperature, pressure, and chemically active solutions. Thus, metamorphic rocks are formed as a product of igneous, sedimentary or other metamorphic rocks. They have intermediate conductivities. The relative permittivities are in the range of <4–10 (e.g. quartzite, granite gneiss) (Lytle, Parkhomenko 1967). The common values of susceptibility are low, and the relative permeabilities remain thus very close to μ_o (Fig. 17) (Airo & Säävuori 2013, Hunt et al. 1995).

Variations in the magnetic and electrical properties not only exist between different rock types, but considerable variations also occur within a given rock type. The magnetic susceptibility of the rocks is mainly governed by the quantity of ferrimagnetic minerals. Most rock-forming minerals have low conductivities and low susceptibilities, but small amounts of iron sulphide minerals with high susceptibilities (e.g. pyrrhotites) and iron oxides (e.g. magnetite) can significantly increase the volume susceptibilities. Magnetite is the most important ferrimagnetic mineral, with a susceptibility of as much as $\sim 15 \cdot 10^7$ (10^{-6} SI units). In rocks with more than 1% magnetite, the susceptibility is directly related to the magnetite content, and vice versa (Parasnis 1986). The same behaviour can also occur in resistivities and relative permittivities. For instance, when small amounts of pyrite ($\sigma \sim 0.01$ S/m$_{<1\ \mathrm{MHz}}$; $\varepsilon_r \sim 50_{<1\ \mathrm{MHz}}$) are involved, decreased values for both properties are possible. In addition, resistivities of typical rock types (e.g. granite, quartzite) decrease with increasing frequency, while the relative permittivities remain at constant values (Vogt 2000).

The two most important electrical material parameters with respect to radio wave propagation in non-magnetic rock ($\mu \approx \mu_o$) are electric conductivity (σ) and dielectric permittivity (ε). These relate the free current density vector and electric polarization vector to the electric field in the material equations (Eq. 12). If the material is linear (properties independent of the field), isotropic (properties independent of direction) and non-dispersive (properties independent of frequency), μ_r and ε_r are scalar values and ≥1. In addition, the ratio of the conduction current to the displacement current, referred to as a loss tangent p, is an important factor. If $p >> 1$, the

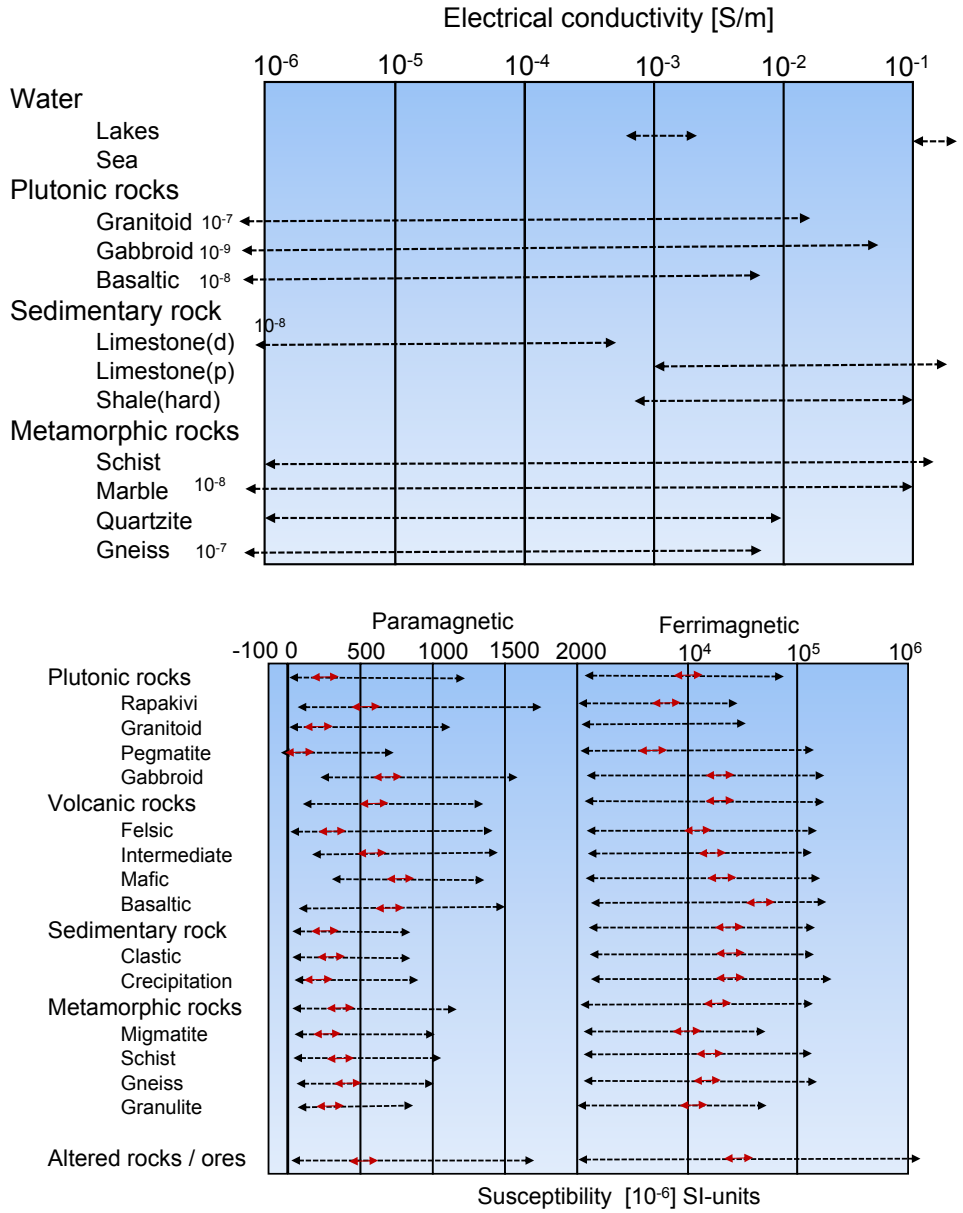

Fig. 17. Conductivities (S/m) (upper) after deBettencourt & Surcliff (1962) and magnetic susceptibilities χ_m (10^{-6} SI units) (lower) for different rock types after Airo & Säävuori (2013). The red arrows indicate typical values. Black arrows mean the whole variability in density in a specified rock type, for instance, the whole number of samples of volcanic rocks is 5266 and that of felsic volcanite 364.

fields obey the diffusion equation; if $p << 1$, the fields propagate as waves with minor losses in dielectrics (I, III) (deBettencourt & Surcliffe 1962, King et al. 1981, Zhang & Li 2007). Both conductivity and permittivity are dependent on the frequency, temperature and water content, and are possibly enhanced by some measure of salinity (Daniels 1996, Parkhomenko 1967). When the amount of water is significant, the electric properties of a rock may be primarily determined by the properties of the water and only secondarily by the material that forms the rock. Even small amounts of water can have an increasing effect on the permittivity of rock due to the large relative permittivity of water (ε_r ~ 81). Most rock-forming minerals are highly resistive but, for instance, small amounts of sulphide minerals, porous water or graphite can increase the bulk conductivity (Buttler 2005, Parkhomenko 1967). At low frequencies, both the conductivity (free charges) and polarization (bounded charges) current vary in-phase with the external electric field. However, at higher frequencies, both conductivity and polarization current lag behind

in the external field due to inertial and frictional forces, and thus the conductivity and permittivity can be regarded as complex quantities with conductivity in the form of $\sigma = \sigma' + i\sigma''$ and permittivity $\varepsilon = \varepsilon' - i\varepsilon''$ (King et al. 1981, Knoll 1996, Murphy & Morgan 1937, Murphy & Morgan 1938, Murphy & Morgan 1939). σ' (ohmic conduction) and ε' (energy storage or release term) are in-phase components; at low frequencies, the currents vary in phase with the applied field. In contrast, σ'' (frequency dependent loss-term due to bounded charges) and ε'' (energy loss-term due to polarization lag) are out-of-phase components. The response times of free charges and polarization to the changing field can be significant, and the currents lag behind the applied field and out-of-phase components (Knoll 1996) are generated (King et al. 1981). For non-magnetic materials, the magnetic permeability μ has the value of free space ($\mu_o = 4\pi \cdot 10^{-7}$ Henry/m) and is real-valued. The solution of Maxwell equations (Eqs. 8–11) yields the quantities that describe the propagation of an EM wave in the complex wave number $k^2 = \mu\omega(\omega\epsilon - i\sigma)$ ($e^{i\omega t}$ time dependence) (King et al. 1981, Zhang & Li 2007). Substituting the complex conductivity and permittivity in the parenthetical part of k, the effective conductivity, permittivity, loss tangent and dielectric constant can be determined as (Hunt et al. 1979, Knoll 1996, Ruffet et al. 1991, Turner & Siggins 1994, Vogt 2000)

$$\sigma_{eff} = \sigma' + \omega\varepsilon'' \qquad \tan\delta = \frac{\sigma_{eff}}{\omega\varepsilon_{eff}}$$

$$\varepsilon_{eff} = \epsilon' + {}^{\sigma''}/_{\omega} \qquad \varepsilon_r = \frac{\varepsilon_{eff}}{\varepsilon_0} = \frac{\epsilon'}{\varepsilon_0} + \frac{\sigma''}{\omega\varepsilon_0} \qquad (27)$$

Equations 27 define the effective conductivity and permittivity, loss tangent and dielectric constant (the relative dielectric permittivity). The second terms in the effective conductivity and permittivity are referred to as dielectric conductivity (out-of-phase polarization current) and conductive permittivity (out-of-phase conduction current) (Lafleche 1985). The effective parameters are the directly measurable quantities. They imply that both the measured conductivity and permittivity consist of two components.

However, neither of the out-of-phase components can be distinguished from the corresponding true currents σ' and ε' (King et al. 1981, Knoll 1996). Strictly speaking, the dielectric constant does not imply that ε_r is constant, but it varies with materials and frequencies. When $tan\delta \gg 1$, the conduction currents are dominant, and the fields are diffusive whereas when $\tan\delta \ll 1$, the displacement currents are dominating, and the fields are propagating. The laboratory measurements of effective conductivity and permittivity can be performed using different techniques depending on the frequency band used (Iskander & DuBow 1983). At low frequencies, a capacitive method can be utilized (Murphy & Morgan 1937, Murphy & Morgan 1938, Murphy & Morgan 1939, Vogt 2000), while at intermediate frequencies, the transmission line technique and at high frequencies a time-domain reflection technique can be applied (King et al. 1981).

According to King (1981), the real and imaginary component of complex conductivity $\sigma = \sigma' + i\sigma''$ can written as:

$$\sigma' = \frac{e^2 Z_e^2 n_e \nu_{ce}}{m_e(\omega^2 + \nu_{ne}^2)}, \quad \sigma'' = \frac{e^2 Z_e^2 n_e \omega}{m_e(\omega^2 + \nu_{ne}^2)}, \qquad (28)$$

where it is assumed that the contribution of positive ions is negligible compared to electrons, and the corresponding terms are removed, $Z = 1$ is the charge number of electron, e is the electron charge, n_e is the density of electrons, ω is the frequency of the external field, ν_{ce} is the collision rate of electrons, and m_e is the mass of the electron. In conductors, where the density of free charges is high ($\nu_{ce} >> \omega$) or bounded charges are sufficiently screened by free charges, then

$$\sigma' = \frac{e^2 n_e}{m_e \nu_{ce}}, \quad \sigma'' = \frac{e^2 n_e \omega}{m_e \nu_{ce}^2} << \sigma'. \qquad (29)$$

Thus, $\sigma = \sigma' + i\sigma'' \approx \sigma'$ because σ'' is negligible compared with σ' and is independent of the frequency. It corresponds to the stationary value of conductivity and it is also referred to as the d.c. conductivity.

The complex permittivity ε could be expressed as $\varepsilon = \varepsilon' - i\varepsilon''$ and it can be modelled by an electric circuit with a single relaxation time such as in Figure 18 by Olhoeft (1976).

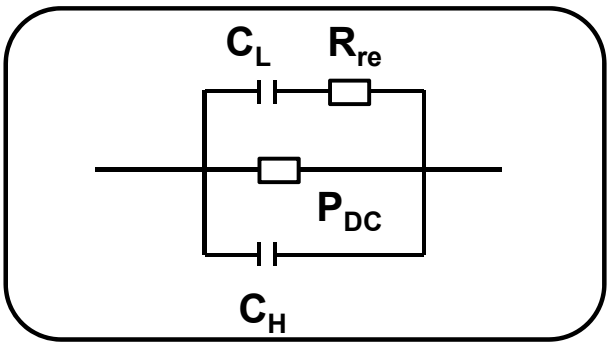

Fig. 18. Schematic representation of relative permittivity. Figure modified after Olhoeft (1973).

In Figure 18, P_{DC} represents the DC (ω = 0) conductivity path. The capacitance C_L determines the low frequency limit of the dielectric constant and is caused by the accumulation of charge at boundaries. The time constant (τ) of the relaxation is determined by $R_{re}C_L$. The upper limit of the dielectric constant is determined by C_H. According to the model (Fig. 18), the conductivity of rocks should increase when the frequency of the current passing through them increases. Water is one of the major reasons for the increase in conductivity and attenuation, because when the polar water molecules are polarized in the applied electric field, high effective conductivities may be recorded (Olhoeft 1976). Several expressions have been presented to model the electrical properties of rocks across a frequency band. For instance, the generalized Cole–Cole equation with multiple relaxation times is widely used in heterogeneous materials (Daniels 1996, Knoll 1996, Murphy & Morgan 1937, Murphy & Morgan 1938, Murphy & Morgan 1939, Vogt 2000):

$$\varepsilon(\omega) = \varepsilon_\infty + \sum_{m=1}^{n} \frac{\Delta\varepsilon_m}{1 + (j\omega\tau_m)^{1-\alpha_{cc}}} \qquad (30)$$

where $1 - a_{cc}$ is the breadth parameter, τ_m is the relaxation time of the mth pole and is the permittivity increment such that $1 - a_{cc} = 1$ and *m = 1* means the Debye model with a single relaxation time, ε_s is the permittivity at ω = 0, and ε_∞ is the permittivity as $\omega \to \infty$. Using the Debye model (polar molecules) with a single relaxation time, the permittivity and effective conductivity in a polar system can be expressed as (Daniels 1996, Hunt et al. 1979, Knoll 1996, Murphy & Morgan 1937, Murphy & Morgan 1938, Murphy & Morgan 1939, Vogt 2000):

$$\varepsilon(\omega) = \varepsilon' = \varepsilon_\infty + \frac{(\varepsilon_s - \varepsilon_\infty)}{1 + \omega^2\tau^2}$$

$$\varepsilon'' = \omega\tau\frac{(\varepsilon_s - \varepsilon_\infty)}{1 + \omega^2\tau^2}$$

$$\sigma(\omega) = \omega^2\tau\frac{(\varepsilon_s - \varepsilon_\infty)}{1 - \omega^2\tau^2} \qquad (31)$$

Thus, according to the Debye model, the real component of the complex permittivity ε' (blue curve) has a decreasing trend in the range of ε_s–ε_∞ (anomalous dispersion, (Murphy & Morgan 1937, Murphy & Morgan 1938, Murphy & Morgan 1939), and the imaginary component ε'' (green curve) peaks at the relaxation frequency (Fig. 19a). The effective conductivity increases with frequency until the relaxation frequency is reached, when it asymptotically approaches a constant value (Eq. 31) (Fig. 19b), at electrical frequencies. The Debye response is not met in geological materials (Knoll 1996).

Vogt (2000) used a parallel plate method and determined the electrical properties of different rock types from core samples in the frequency range of 1–100 MHz. A core sample is placed between two plates forming a capacitor. The method is based on the measurement of the complex impedance of the sample (magnitude and phase of the impedance). However, although the laboratory measurements can be performed on core samples with a high degree of control through the selection of the sample, the fact that the sample is not measured *in situ* is a disadvantage. The core sample represents only a small volume of rock, whereas the *in situ* measurement integrates a volume of about three orders of magnitude bigger. Thus, *in situ* electric properties may deviate significantly from the laboratory values. The electrical properties may vary over several decades, the results may not even reflect their *in situ* properties and the largest finding of the measurement is perhaps only indicative. The effective electrical properties of the samples as a function of the measured parameters $|Z|$ and *argZ* can be written as:

$$\varepsilon_r = \frac{d}{\pi r^2}\frac{\sin(argZ)}{|Z|\omega\varepsilon_o}$$

$$\sigma = \frac{d}{\pi r^2}\frac{\cos(argZ)}{|Z|} \quad , \qquad (32)$$

where *d* is the distance between the plates of the capacitor, *r* the radius of the plates and *argZ* is an arctan function of the inverse loss tangent. The measurement technique resulted in poor values for permittivities when *argZ* was small and for conductivities when *argZ* was large, respectively.

The behaviour of effective electric properties of different rock types observed by Vogt as a function of frequency is illustrated in Figure 20.

In highly resistive rocks, the effective conductivities increase linearly with increasing frequency due to the polarization currents (dielectric conductivity, $\omega\varepsilon''$) or the effective conductivity increases as the frequency increases when an extra path becomes available to the current. The effective permittivities remain at constant values in the whole frequency scale, because conductive permittivity (σ''/ω) is small taking into account the scaling effect of frequency in the denominator (Jol 2009, Turner & Siggins 1994). Sulphide mineralization can be regarded as a conductor and the dielectric conductivity ($\omega\varepsilon''$) in Eq. 27 is almost negligible or $\sigma_{eff} \cong \sigma'$. Thus, the effective conductivities remain at nearly constant values, but the permittivities decrease, even in the EMRE band, probably due to high values of the out-of-phase conduction component at low frequencies. At higher frequencies, the effect of the out-of-phase component becomes weaker (Jol 2009, Vogt 2000). Ore minerals (pyrite) having, for instance, high iron contents, saline porous water and clay particles

a)

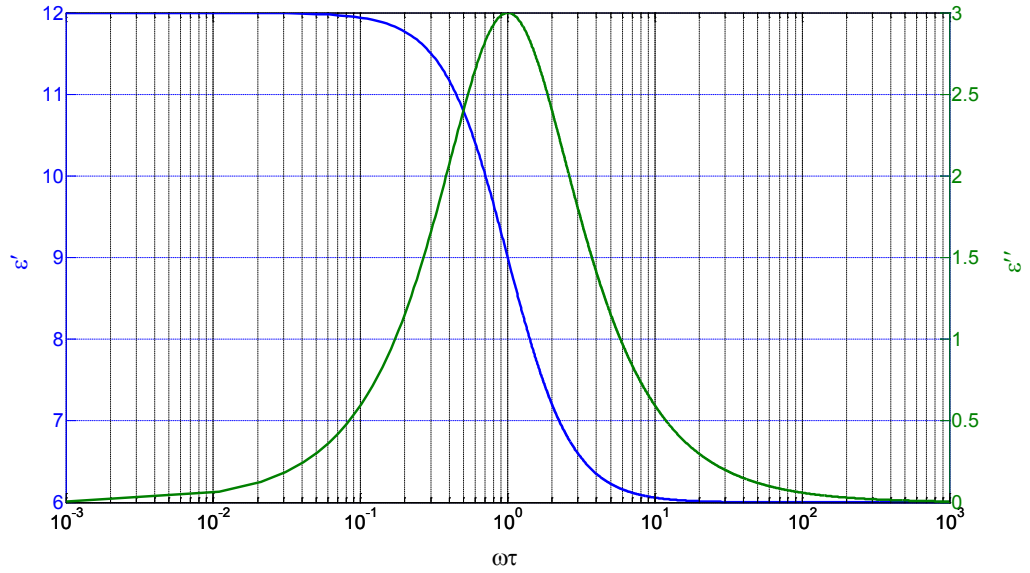

b)

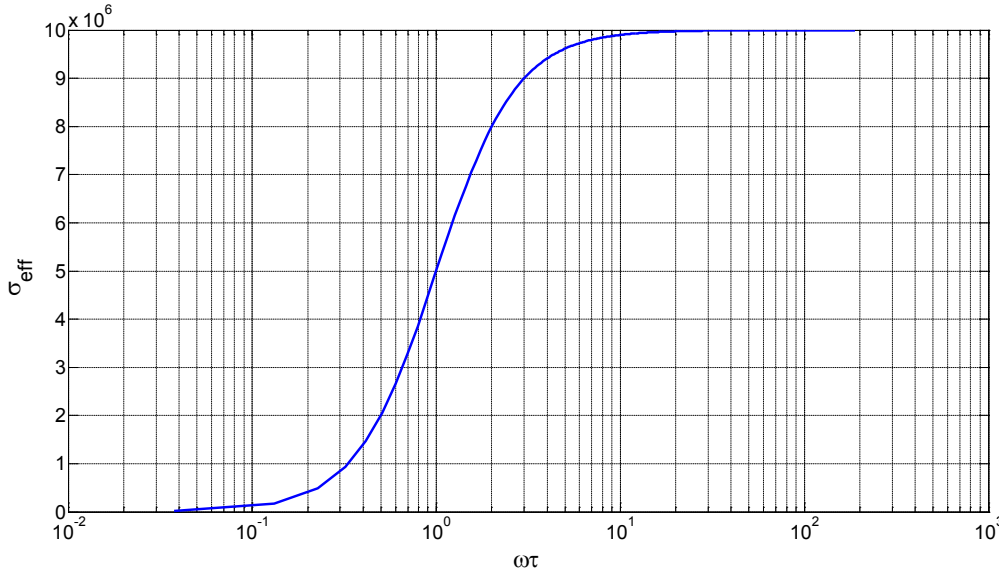

Fig. 19. The electrical properties of the Debye model ($\varepsilon_s = 12$; $\varepsilon_\mu = 6$). Thus, the relative permittivity ε_r has only a real part with direct current ($\omega = 0$) and assumes the extreme value, ε_s. At high frequencies, the relative permittivity is also real, but has a minimum value, ε_∞. a) Complex permittivity. b) Effective conductivity.

have high electrical conductivities. The relative permittivities are high at the low frequencies, but decrease with increasing frequency. In intermediate rocks (lossy dielectrics) (e.g. peridotite, dolerite), the effective conductivity is determined by the real part of the complex conductivity at low frequencies, but at higher frequencies the dielectric conductivity ($\omega\varepsilon''$) starts to dominate and the effective conductivity increases. The effective permittivity decreases as a function of frequency (Vogt 2000).

As a summary, the electric conductivity of major rocks increases as the frequency of the applied field increases at electrical frequencies (below optical frequencies, Fig. 2). Conversely, the relative dielectric permittivity decreases as the frequency increases, because the polarization has insufficient time to form completely (anomalous dispersion).

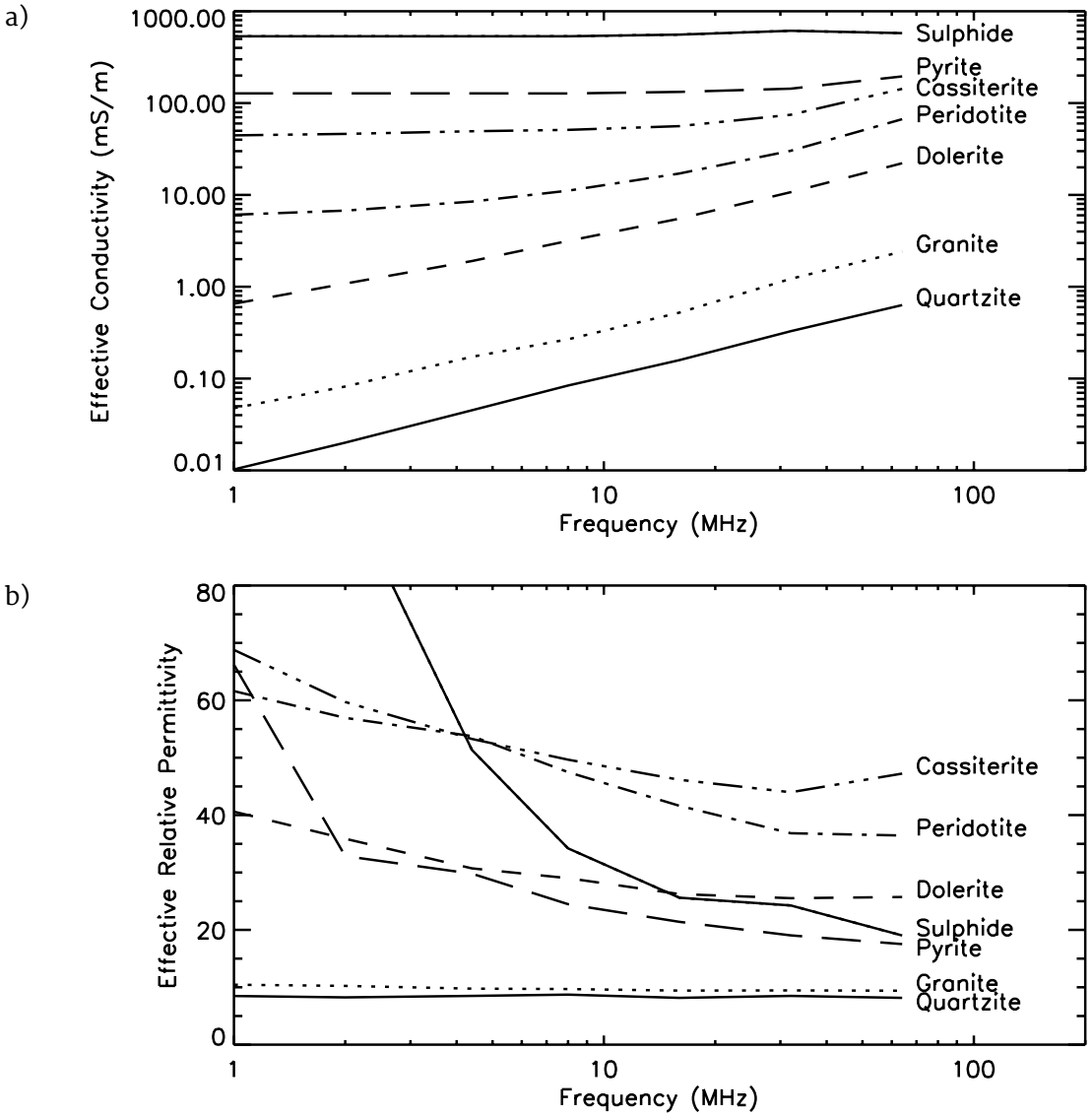

Fig. 20. Behaviour of effective properties as a function of frequency for selected rock types, minerals and sulphide mineralization. a) The effective conductivity. b) The effective permittivity. The sample report follows (Vogt 2000). Quartzite is almost a pure silica sample. Granite is a coarse-grained igneous intrusive rock sample (consisting of quartz,-feldspar and biotite mica). Dolerite is a fine to coarse-grained igneous intrusive rock and represents a more mafic sample. Peridotite is a coarse-grained ultramafic rock sample with a low silica content (has undergone weathering and contains clay). Cassiterite is a tin ore sample. Pyrite is a quartzite-rich pyrite (>25%) mineralization sample. Sulphide is referred to as a massive sulphide mineralization sample (consisting of copper, lead and zinc). Granite and quartzite are dielectrics with low DC conductivities. Figures by Vogt (2000).

4.2 The origin of currents

Electrons occupy discrete energy levels in an atom having quantized energies referred to as bands. Two bands have particular significance in determining the electronic properties of a material: the conduction band and the valence band. Conductors (e.g. metals, sulphide-bearing ore deposits) have no gap between the valence and the conduction band, or the bands overlap, so that numerous electrons can thus move easily and conduct electricity, and conductivity decreases with temperature due to increased interactions. Maximum conductivity is found near to absolute zero. Semiconductors have a small gap (<1 eV) between the valence and the conduction band. At higher temperatures, some electrons can gain enough energy to lift them from the valence band to the conduction band, resulting in holes. Thus, conductivity increases with temperature due to an increased concentration of carriers. At low temperatures, semiconductors are nearly insulators. Both electrons and holes contribute to the conduction, but the conductivity is low due to the fact that only a small number of valence electrons take part in conduction. Many sulphide minerals, some oxides and graphite can be considered as semiconductors. Dielectrics have a large gap (~5 eV) between the valence and the conduction band. A large amount of energy is required to move electrons from the valence to the conduction band, and thus the current carriers are, for instance, bounded charges or weakly bonded ions with much lower mobility. In crystalline dielectric materials, the possible ion conduction can be classified into three groups: normal lattice ions which may be displaced to interstitial positions through dissociation energy, ions generated due to lattice defects at high temperatures and impurity ions. Dielectrics have the same temperature dependence as semiconductors. Dielectrics are weakly conducting materials or insulators, and when exposed to an external field they become polarized (polarization or charging current). The great majority of minerals (pure elements or chemical compounds) are insulators. In an ideal insulator, the density of free charges would be zero, but in general there are always present some free charges determining the d.c. conductivity of the insulator. A material's susceptibility to polarization is related to its dielectric permittivity. Thus, the conductivity of rocks can be widely variable, and depends on the electrical properties of the constituent minerals. The conductivity of rocks covers over 20 orders of magnitude. The electric permittivity varies moderately in rocks, about two orders of magnitude. On the contrary, porous water, clay and graphite, which are usually present, may have a profound effect on the conductivity and permittivity (Kittel 1976, Parkhomenko 1967).

An electrical current can flow in rocks and soils via three main mechanisms. Slow moving of ions in aqueous fluids (electrolyte) in porous rock is characteristic of electrolytic conduction. Common examples of electrolytes are aqueous solutions of inorganic salts, acids and bases. For instance, NaCl (sodium chloride) is an electrolyte in its dissolved state. Electronic conduction (Fig. 21a) occurs in metals, and for example, in some metal oxides and sulphides, by the rapid movement of electrons. Thus, conductivity is the response of free charges to an applied field. Polarization can occur in homogeneous materials in different ways, e.g. as a slight displacement of bound charges, resulting in polarization (charging) currents (Fig. 21b). Electronic polarization occurs in the visible and ultra-violet frequencies in the electronic cloud in all materials. For instance, in crystalline rock, when polarized, the electrons shift slightly relative to positive nuclei. In atomic polarization, atoms in a molecule are displaced from their normal positions. Electronic and atomic polarization occurs at the optical frequencies, and they belong to the group of instantaneous polarizations (induced effects). Orientational polarization occurs at electrical frequencies when, for example, the randomly oriented dipole moments of polar molecules are aligned in the direction of the applied field (rotational effects). For instance, water is a symmetrical molecule and has a permanent dipole moment. When exposed to an electromagnetic field, water molecules are highly susceptible to polarization due to their high relative permittivity value, ε_r ~ 81. Forces due to thermal agitation oppose the external field effects to restore the random orientations of the molecules. The effects of induced polarization must also be taken into account in the total polarization of the polar molecules. In an ideal situation, the d.c. conduc-

tion should be 0 because there are no free charges to establish conduction current. In a heterogeneous material, a polarization mechanism is possible where free charges (ions) are involved (interfacial polarization, Maxwell-Wagner effect). The Maxwell-Wagner effect arises from the contrast in electric properties at an interface between two media of different electrical properties. When an external field is impressed, the charges accumulate at the interface of the two different media. The interfacial polarization can be notable at quite a low frequency level (*>100 kHz*) (Jol 2009, Murphy & Morgan 1937, Murphy & Morgan 1938, Murphy & Morgan 1939, Parkhomenko 1967, Vogt 2000).

When a static electric field is impressed on ideal dielectrics, the polarization (charging) current should be zero after the polarization is completely developed. The state is referred to as maximum polarization at zero frequency. However, actual dielectrics always contain some conduction electrons and ions, and the current does not fall to zero but to the constant value determined by the conductivity due to free charges. In conductors, the static electric field makes the free charges move onto the surface in such a way that the field inside vanishes. On the contrary, a static magnetic field induces no current within the conductor and the magnetic field is the same as without the conductor (Smith 1977). When an alternating electric field is impressed on a conductor, the field is not zero in the conductor but the field is gradually damped (skin depth) and concentrated on the surface of the conductor (Knoll 1996, Smith 1977, Zhang & Li 2007). In dielectrics where free charges are not provided, the polarization current is characterized by limited movements of charged particles or the orientation of polar molecules (sum of different polarization currents). When the frequency increases, the response of individual molecules is not instantaneous due to the inertia of the molecules and, for instance, the orientation of dipole moments lags behind the changes in the external electric field. Energy is dissipated as heat due to friction, but less than an equal current in a conductor, and the amount of heat is dependent on the material (King et al. 1981, Murphy & Morgan 1937, Murphy & Morgan 1938, Murphy & Morgan 1939).

For almost all rocks, the magnetic susceptibility is $\chi_m << 1$ ($\mu_r = 1+\chi_m$), and the magnetic permeability is thus $\mu \cong \mu_o$ or $\mu_r = 1$. Due to the large range of conductivity and permittivity variation in the Earth's materials, the conductivity and permittivity outweigh the permeability changes in non-magnetic materials. Thus, magnetic losses are indistinguishable from conductivity losses. The boundary between conductors and semiconductors, and on the other hand between semiconductors and insulators, is not sharp. The difference between the domains originates more from the conduction mechanism than from the value of conductivity itself (Parkhomenko 1967). In the great majority of rocks, electric conductivity increases as the frequency of the applied field increases. Conversely, the relative dielectric permittivity decreases because the polarization has insufficient time to form completely (anomalous dispersion). Parkhomenko (1967) has listed three general factors that mostly affect the conductivities of rocks, including whether the conductive component is a continuous host material or occurs as disseminated particles

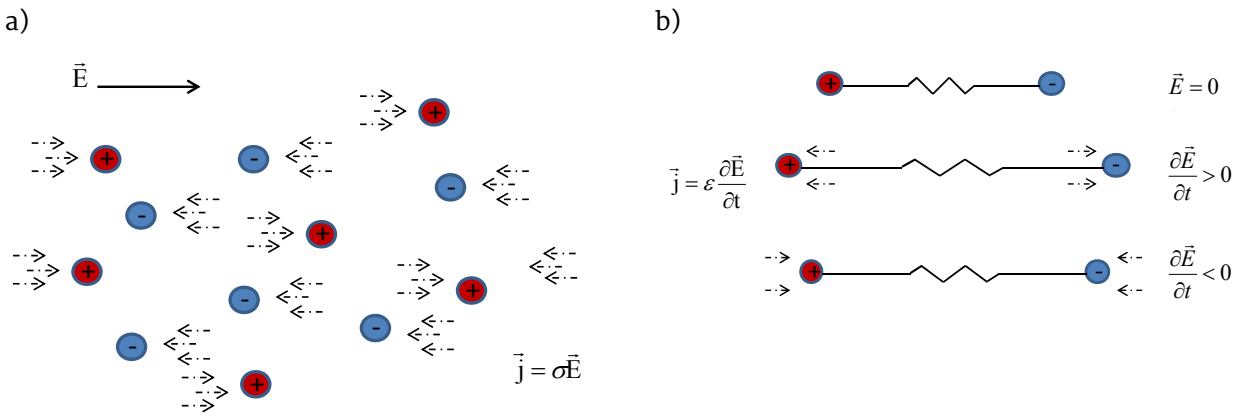

Fig. 21. a) Conduction current, b) polarization current. Figure modified after Jol (2009).

within the host material. In resistive host rock, the volume conductivity increases only moderately with a slightly increasing amount of disseminated particles. However, when the host rock is conductive, the reaction is opposite and a small increase in conductive material generates a large increase in the volume conductivity. When one dimension of the conductive object is emphasized (elongated), the volume conductivity is strongly enhanced due to existing anisotropy and the largest conductivity occurs along the emphasized dimension. Small amounts of conductive cement or clay can serve as an extra conduction path, resulting in increased conductivity values.

5 RADIOFREQUENCY TECHNIQUES

The measurement principle of radar is to transmit electromagnetic waves and receive returning signals, or "echoes", to detect the existing target, and to estimate the range between the radar and the target (Puranen 2009). Radars can be classified into two groups: pulse radars and continuous radars. Several important characteristics must be taken into account when deciding which particular type of radar to use, for instance, the target detection capabilities, dynamic range, bandwidth and power. The German scientist Christian Hülsmeyer invented a device called the telemobiloscope in the early 1900s, which was one of the first radar-like devices for detecting metallic objects. By changing the elevation of the transmitter, the range could also be measured (Hülsmeyer 1904a, Hülsmeyer 1904b). During the Second World War, the development of radars was intensive, and serious work was carried out in many countries to detect, for instance, hostile aircraft and ships. After the war, civilian applications also began to conquer the world. The first radars were simple unmodulated continuous wave (CW) radars. CW radars utilize low continuous power (few watts). They are referred to as moving target radars (target identification based on the Doppler effect (Seybold 2005). When the transmitted signal is imparted a bandwidth, as in a frequency modulated continuous wave radar (FMCW) where the transmitted frequency is varied with time, the range is also available by comparing the frequencies of the transmitted and received signals (Jankiraman 2007). Radar systems can be mono- or bistatic systems depending on whether separate antennas are used for transmission and reception.

The main factor that limits the use of radiofrequencies in geophysics is the strong absorption of energy in most earth materials, or the penetration is highly frequency dependent. Two electromagnetic prospecting methods use radiofrequencies: ground penetrating radar (GPR) and the radio imaging method (RIM). Both methods are referred to as radar techniques, but strictly speaking, only GPR is a radar (radio detection and ranging) technique. This thesis mainly discusses the latter, but a short review of GPR is presented (Annan 2003, Jol 2009, Mukhopadhyay 2005, Saksa et al. 2005).

5.1 Pulsed radar

GPR is better known as a time domain device that is normally used in a reflection mode and is referred to as a pulsed technique. Thus, short pulses are sent to an antenna, which generates electromagnetic waves at the pulse repetition frequency (PRF) or during the pulse repetition interval (PRI), the inverse of the PRF. During the transmit pulse, the receiver is not able to detect signals in a mono-static system. Electromagnetic waves are transmitted into the ground and reflected/scattered waves from the interfaces/objects with different electrical properties are received. The range to the target is determined by measuring the round-trip delay of the pulse. Shorter pulses mean better range precision, because the delay time measurements are more precise, but at the same time higher peak powers must be utilized. Nowadays, GPR devices are used in the frequency band of 10–2000 MHz. Because of the high attenuation properties of the earth's materials, generated by the frequency-dependent electrical and scattering losses, the

frequency must be kept as low as possible to achieve greater penetration into the material. Normally, GPRs are classified according to the centre frequency. Thus, a 50 MHz GPR is referred to as one with a 50 MHz bandwidth centred at 50 MHz (Jol 2009).

GPR has also been applied in borehole conditions, but due to the higher frequency band normally utilized the practical transmission ranges are limited. The ARCOLab borehole radar imaging system has been developed at the Universities of Oxford and Sydney during the past decade (Claassen 1995). The radar consists of two asymmetric dipoles, one transmitting and one receiving, each having one resistively loaded arm and one metallic arm. The antennas are placed in a PVC tube. The operating bandwidth is approximately 20 to 80 MHz at a centre frequency of 50 MHz. It transmits pulses of up to 20 kW.

The most popular commercial borehole radar system is the RAMAC short-pulse borehole radar developed by the Swedish company Malá Geoscience. Both reflection and transmission mode devices are available (MALÅ GPR Resource Center 2014). In transmission mode, the signal is received in a different borehole.

5.2 Continuous wave device

In the radio imaging method (RIM), the system consists of a continuous wave (CW) device and the method is used in the frequency domain when the unmodulated measurement frequencies are transmitted continuously. In addition, a cross-borehole technique (transmission mode) is used. The benefits of CW radars include their high sensitivity due to the narrow bandwidth and low power needed. Stolarczyk and Fry (1986) were the pioneers of RIM in geophysics. In addition, Russian experts carried out intensive studies using RIM with good results during the late 1900s (Buselli 1980). Their device is known as FARA-MCH. The Miningtek Pluto-6 system was developed by the Division of Mining Technology of the CSIR (Vogt 2000). The JW-4 system was developed by the Chinese Institute of Geophysical and Geochemical Exploration (*IGGE*) (Cao et al. 2003). In 2010, the Geological Survey of Finland (GTK) took into productive use a RIM system known as the EMRE system in which the Russian invention is utilized.

5.3 The radio imaging method (RIM)

RIM is generally conducted in the transmission mode when the radio waves are attenuated due to the electrical properties of the medium between deep boreholes. Greater conductivities mean higher attenuation rates, and both the range and resolution are frequency dependent. For most cross-borehole survey geometries, the angular aperture is limited and the horizontal resolution is less than the vertical resolution. Usually, the central sections are best covered and contain the greatest amount of information. The ray coverage is typically low at the top and bottom of the inter-borehole plane, resulting in ghost structures and smearing of anomalies, which reduces the resolution in these areas. Commonly, the smallest structure that can be resolved is estimated by the width of the first Fresnel zone. The Fresnel zones are ellipsoids drawn between the transmitter and receiver. A transmitted wave can alternatively reach the receiver by a direct route, or when the wave is spread out at an angle, the wave may not even reach the receiver at all. On the contrary, when, for instance, the wave strikes an obstruction, the reflected wave may reach the receiver as a reflected wave. The width of the Fresnel zone is spatially variable and is determined by the wavelength and the distance between the boreholes, being smallest near the source and receiver boreholes and largest midway between the boreholes. The first Fresnel zone is a region around a ray that mostly affects the propagation of the wave (Buursink et al. 2008, Seybold 2005, Spetzler & Snieder 2004). Due to the low frequency band (long wavelengths) generally used in RIM, the method is not sensitive to thin discontinuities (e.g. conductive black schists). Conversely, a massive sulphide deposit could appear as an excellent target. The target would be clearly visible in the signal strengths, but the situation would

be paradoxical, because no information would be obtained from inside the target due to high attenuation rates. A disseminated sulphide target with lower attenuation rates is an excellent research object. We have carried out electromagnetic cross-borehole surveys in two different environments, in crystalline bedrock (III, IV) and in an ore district where a massive sulphide target exists (I). Both of the field cases were successfully accomplished. RIM obtained similar but more detailed information than with electric and electromagnetic measurements from the ground surface in the crystalline bedrock area. The conductive sulphide mineralization could be delineated in a more detailed way than using the other geophysical methods.

5.4 The EMRE system

The configuration of RIM consists of two deep boreholes. The section should be roughly in a common plane, and the minimum starting depth is greater than the horizontal separation of the boreholes. Thus, clearly below the air-earth interface to minimize the disturbing effects of reflected rays from the air-earth interface. In addition, the boreholes should be deeper than the distance between the boreholes. On the contrary, when the transmitter is located deeper than the receiver, the measurement is possible to start at even shallower depths. A scanning aperture of 30–50 degrees together with dense receiver stations result in reasonable smooth tomographic reconstructions. The normal measurement is taken as a two-way measurement, where the transmitter and receiver are interchanged in the boreholes to complete a full tomographic survey. Our RIM system is referred to as EMRE. The device itself is a continuous wave (CW) device with a nominal power of 2 W (33 dBm). The power level is low, and thus the batteries will not run out during a normal working day. The transmitter simultaneously radiates unmodulated frequencies

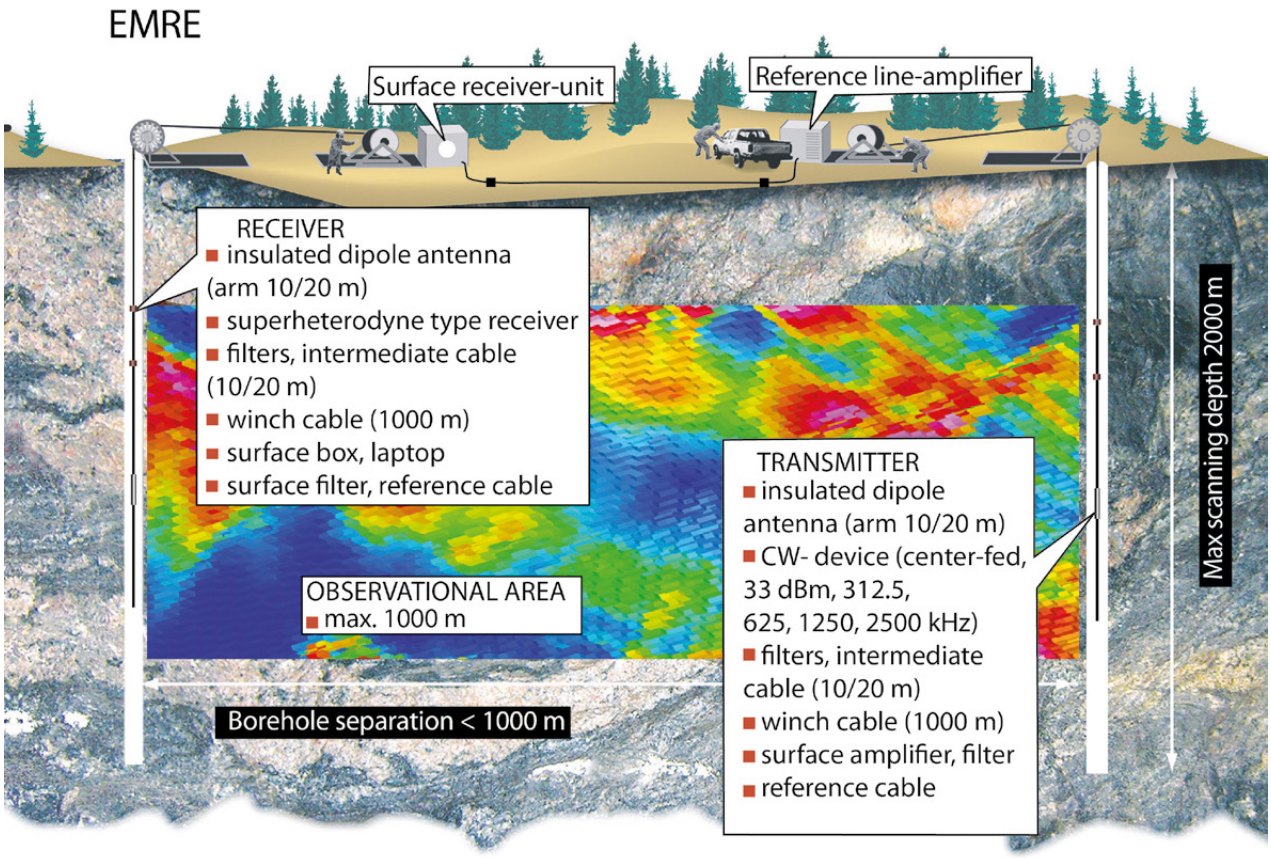

Fig. 22. The radio imaging method (RIM) and a reconstruction of the attenuation distribution of a borehole section (not to scale). The maximum separation between the boreholes can be ~1000 m, and the deepest scanning depth 2000 m or according to the available winch capacity.

(312.5–2500 kHz), and it cannot therefore be used to measure the distance to the target due to the lack of a time mark. Technically, the receiver is established in a manner that does not deviate from a normal radio. It consists of a borehole and surface receiver. In the borehole receiver (the preselector stage), the measurement frequencies (2500–1250–625–312.5 kHz) are heterodyned (mixed) against a local oscillator (2600 kHz) to generate sum and difference (100–50–25–12.5 kHz) frequencies referred to as the intermediate frequencies (IF frequencies) (Henney 1950, Reintjes & Coate 1953). Because the local oscillators are not synchronized, the unknown initial phases of the oscillators make the phase measurement unreliable. The intermediate frequencies are further guided to the surface receiver through the winch cable in which the final detection of the amplitude and relative phase difference is performed. The amplitude of received signal is proportional to that of the input signal, while the phase is equal to the sum of the propagation phase delay between the boreholes and the random unknown initial phase of the receiver oscillator. Thus, only the relative phase differences can be saved. In Figure 22, the measurement geometry of RIM and the reconstruction of the borehole section are represented. In addition, the main parts of the EMRE system are illustrated.

A reliably working device is the most important part of every measurement system. We used a Russian-based FARA-MCH device in our measurements, and it has proven very reliable. The construction and operational principles of the device were presented and discussed in some detail in publication I. Because no electronic layouts were available, we had to use the back-forward engineering technique to inspect the electronic solutions used in the devices. Thus, the meaning of some electronic solutions remained unsolvable or may even have been incorrectly interpreted. In the same paper, the results from the RIM measurements were also compared with other geophysical data. RIM reliably revealed the attenuating or conductive material distributions between the boreholes, and most importantly, the constructed tomographic images also revealed new features in the borehole section. The weakness of present device is in its construction. The core of the system is an un-stabilized crystal oscillator. This determines the accuracy of the whole system. Because the oscillator is connected without any adjustments or compensations, it is very sensitive to changes in the source voltage and temperature. The limited dynamic range of the device (<40 dB) sets limits for its use over short distances, where the saturation of the device can make its

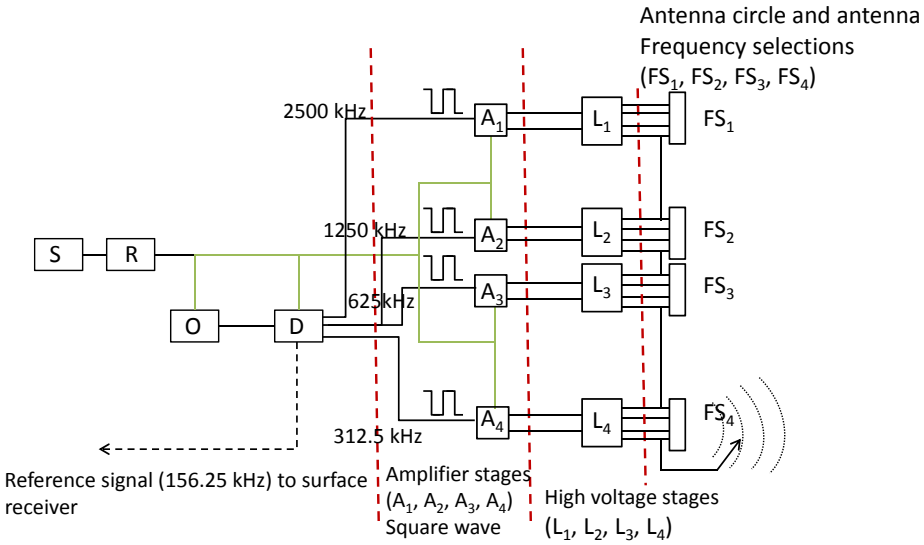

Fig. 23. Schematic representation of the borehole transmitter. The main parts of the transmitter are the accumulator (S), the voltage regulator (R), the un-stabilized oscillator (2500 kHz) (O), and the buffer and frequency division circuit (2500–1250–625–312.5–156.25 kHz) (D). The amplifier stage consists of four amplifiers (transistor-transistor logic (TTL), driven by square wave), one for each measurement frequency (A_1, A_2, A_3, A_4), the high voltage stages (L_1, L_2, L_3, L_4) generate the needed high voltages to feed the power to the antenna, and the frequencies are selected in the FS_n circuits (FS_1, FS_2, FS_3, FS_4). The selected frequencies are collected into one signal. All the selected signals are thus sent simultaneously.

usage impossible. It should be at the level of 60 dB, which could easily be reached by a modern receiver. The proper functioning of the device requires a reference signal strong enough to be generated from the basic frequency of the transmitter oscillator, and when the reference signal is missed by the receiver, the phase information is totally lost, but the noisy amplitude data are still exploitable at some level.

In the author's opinion, the principal of the EMRE device is sound. However, several poor solutions have been utilized in its construction. Many of them have possibly resulted from the lack of good electronic components. The overall electronic construction of the whole device is also very complicated. The borehole transmitter operates simultaneously at four medium radio frequencies (312.5–2500 kHz). The highest frequency is the basic frequency of the local crystal oscillator (2500 kHz), which is the core of the transmitter. When the voltage is supplied, the oscillator outputs the basic frequency. The other measurement frequencies and the vital reference frequency are divided from the basic frequency. In Figure 23, a schematic representation of the transmitter of the EMRE system is illustrated.

Because temperature and voltage compensation are not utilized, the basic frequency may fluctuate (±30 kHz), and possible variations in bandwidth are thus evident (Fig. 24).

The proper functioning of the receiver is based on the reference frequency (156.25 kHz) generated in the borehole transmitter from the local oscillator of 2500 kHz. The reference signal is guided along an intermediate cable to successive borehole transformer circuits. The inductances (L_2) and capacitances (C_3 and C_4) existing between the borehole wires operate as low-pass filters and prevent the propagation of higher RF signals to the winch cable, because the circuits have insignificant impedances only at the reference frequency, but at the lowest measurement frequency (312.5 kHz) the impedance is already high enough to prevent the signal from getting further. The transformer also serves as a galvanic isolation. The winch cable feeds the reference signal to the surface amplifier (Amplifier) at the ground surface, where the signal is amplified and further fed through the surface transformers (L_1) to the surface receiver unit. The inductances L_1 together with the capacitances (C_1 and C_2) also serve as low-pass filters. The noise induced from the environment is effectively cancelled and only the reference frequency reaches the receiver box. In the receiver borehole, the corresponding transformer circuits (L_2) together with capacitances (C_5 and C_6) effectively prevent the

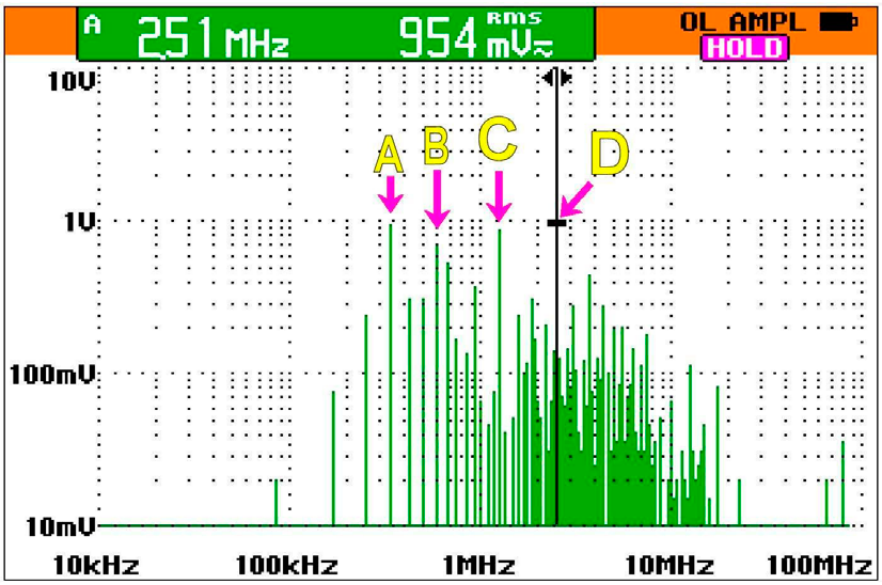

Fig. 24. The spectrum of the present borehole transmitter. A, B, C and D correspond to the measurement frequencies (312.5–625–1250–2500 kHz). In an ideal situation, only the measurement frequencies should be enhanced and the unwanted frequencies rejected. The black arrow points to the 3rd harmonic frequency of 2500 kHz. Above 2500 kHz level, a great part of the power is delivered to unwanted frequencies or the transmitter effectively disturbs itself. The main reason for this is the usage of the square wave technique in the TTL circuits in the amplifier stage (Fig. 23).

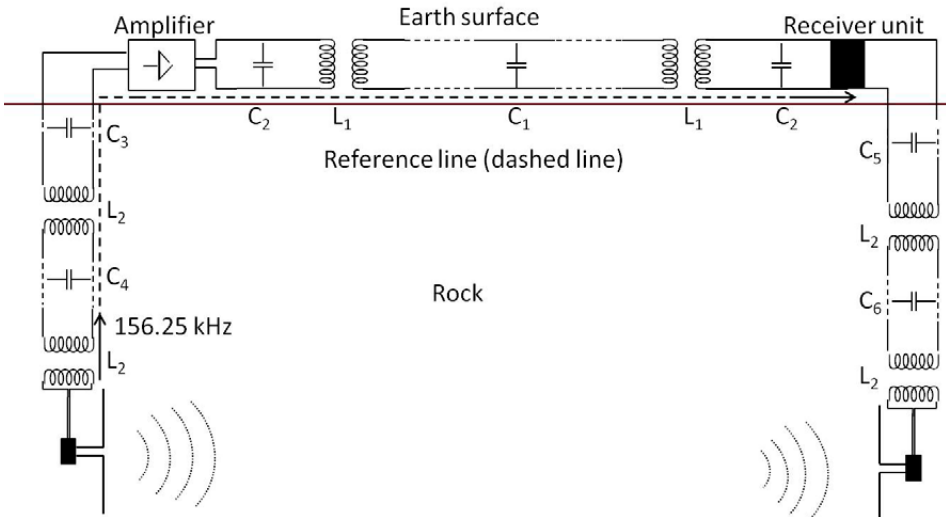

Fig. 25. The reference line (two wire line) between the borehole transmitter and surface receiver (not to scale). The inductances L_2 together with the capacitances (C_3, C_4) serve as low-pass filters and only the reference signal (156.25 kHz) is fed to the surface amplifier (Amplifier). After the amplification, the reference signal is directed to the surface receiver through a similar successive inductance-capacitance circuit (L_1, C_1, C_2). Thus, the surface part of the reference line is also well protected against the eternal RF noise. In the receiver borehole, the corresponding inductances (L_2) and capacitances (C_5, C_6) operate as parallel resonance circuits (low-pass filters) preventing the higher RF frequencies from disturbing the surface receiver.

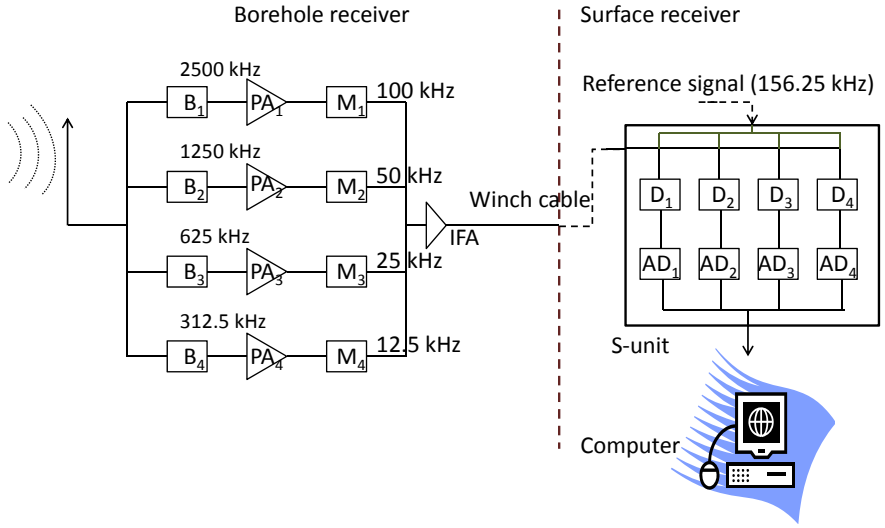

Fig. 26. Diagram of the receiver. The EMRE system consists of two receivers, one in the borehole and the other at the surface. The received signals are fed through band-pass filters (B_1, B_2, B_3, B_4). The amplified signals (PA_1, PA_2, PA_3, PA_4) are further directed to the mixer circuits (M_1, M_2, M_3, M_4) where the received frequencies are heterodyned against a local oscillator (2600 kHz) to generate sum and difference frequencies (100-50-25-12.5 kHz) referred to as the intermediate frequencies (IF frequencies). The intermediate frequencies are amplified (IFA) and fed to the surface receiver (S-unit), where the final detection (demodulation) is produced when a strong enough reference signal (156.25 kHz) is detected. After the detection stages (D_1, D_2, D_3, D_4), the signals are digitized (AD_1, AD_2, AD_3, AD_4) and directed to the computer, where the amplitudes and phases can be monitored in real time.

higher RF signals from reaching the surface receiver unit (Fig. 25).

Technically, the EMRE receiver is set up in a manner that does not deviate from a normal radio. The front end of the receiver (amplifier stage; PA_1, PA_2, PA_3, PA_4) and mixers (M_1, M_2, M_3, M_4) are situated in the borehole unit and the normal components (e.g. detectors; D_1, D_2, D_3, D_4, analog to digital transformers; AD_1, AD_2, AD_3, AD_4) in the surface receiver. The received radiofrequency signals are first filtered (band-pass filters; B_1, B_2, B_3, B_4) and amplified before the mixing stage, where the four intermediate frequencies (IF) are generated. The intermediate

frequencies are further guided to the surface receiver. The cable system consists of the same components as the transmitter system: the antenna, intermediate cable, two low-pass filter circuits and winch cable. The demodulation (detection) of the amplitudes and phases are carried out in the next stage. Thus, the first detection stage is carried out in the borehole unit and the borehole cable system of ~1000 m is used as a guiding path for the modulated signals to the surface. After detection, the signals are digitized and fed to the computer and the measurement can be monitored in real time (Fig. 26).

Normally, any receiver processes signals by performing certain basic functions such as reception, selection and detection, and has some general and important characteristics, namely sensitivity, a low noise level, selectivity and fidelity. The sensitivity of a receiver is the minimum RF signal level that can be detected. The best way to improve the sensitivity of a receiver is to reduce the noise level (e.g. reducing temperature, bandwidth). Selectivity, the receiver's ability to discriminate the wanted signals, is the most important feature for sensing small signals in the presence of strong interferences. Fidelity is a measure of the ability of a receiver to reproduce the original source information. The dynamic range of a receiver is the input power range over which the receiver is useful (Holloway 1998).

5.5 The interpretation of RIM datageotomographic reconstruction

The problem of forming a cross-sectional image or a tomographic reconstruction from its projections arises in a variety of contexts, including medical computed tomography (CT) and radio frequency imaging (RIM) between two deep boreholes. The projections refer to information that is derived from the transmitted electromagnetic waves propagating through the area of interest, for instance using MOM (multi-offset measurement) or ZOM (zero offset measurement) techniques in the RIM measurements (Jol 2009). Mathematically, the problem was solved by Radon (Olaffson & Quinto 2006) in 1917. Radon demonstrated that an object can be exactly reconstructed from a complete set of its projections when the full angle geometry of the measurement is achieved. CT imaging, in which the full angle geometry is not a problem, has become an effective diagnostic tool, and high-quality tomographic images with high accuracy can easily be produced. Conversely, the RIM geometry is highly restricted by the boreholes and is referred to as a limited angle problem. In geotomography, special purpose methods such as the algebraic reconstruction technique (ART) (Kaczmarz 1937, Kak & Slaney 1998, Popa & Zdunek 2004, Tanabe 1971) and the simultaneous iterative reconstruction technique (SIRT) (Jackson & Tweeton 1996, Lakshminarayanan & Lent 1979) are commonly used, even today. In addition to the two algebraic reconstruction methods, the iterative least square method (LSQR) (Paige & Saunders 1982) and the iterative conjugated gradient method (CGLS) (Hansen 1998) are also used. New algorithms that are also effective with limited angle data are available in dentistry. They could perhaps also be used in solving complicated geotomographic problems, resulting in more reliable reconstructions of sections. When working with tomographic reconstruction, it is always important to remember that the reconstruction is a response of the subsurface medium to the existing electromagnetic fields in the range of the used frequency band. Thus, the user must understand the physical meaning of a medium's electrical and magnetic properties, and how these relate to the attenuation of electromagnetic fields. As a high-resolution technique, RIM is a powerful tool to gain a more detailed view of the existing ore body and can efficiently guide new drilling programs and even mine planning (Vogt 2000).

Tomography is widely used in the medical world and it is also gaining ground as a geophysical prospecting technique for determining variations in the physical properties of subsurface targets. Inversions of medical data can provide high-resolution images of body sections, even at a millimetre scale, due to the 2π geometry (360 degrees scanning possibility). In geotomography, the 2π geometry is never met, because the sources and receivers are usually restricted to the earth's surface or a few boreholes, and the insufficient measurement geometry thus leads to sparsely sampled data series. For instance, in the borehole geometry, the lower and upper parts of the boreholes are very critical parts where

image artifacts also exist. In addition, our knowledge of the earth's subsurface structures is limited, and thus the interpretation of the gathered data usually provides ambiguous and not unique results. A typical technique to compensate for limited data is to use additional constraints, e.g. assuming smoothly varying conditions. However, this strategy may result in blurred images and small-scaled features may not be resolved. In addition, the model parameters can be restricted to a narrow range of values. Despite the fact that EM fields and subsurface properties are non-linearly related, RIM data are traditionally interpreted using linear reconstruction algorithms, because practical interpretation methods have not been developed (Musil et al. 2003, Yu et al. 1998). Even today, suitable forward codes for simulation studies are only just becoming available, and are still very computer time intensive (Meles 2011). With increased computer power, a true 3D numerical modelling technique could also be applied for geotomography, resulting in more precise reconstructions of borehole sections when realistic antennas and electric and magnetic losses in the earth's subsurface can be taken into account. The use of a true 3D technique would replace linear inversion with full-waveform nonlinear inversion, but the rapid linear results could still be useful in serving as seeds for these modern methods. Yu et al. (1998) have thoroughly clarified the benefits and weaknesses when one utilizes simple imaging techniques. They also emphasized the fact that modern numerical forward solvers have not been developed for RIM data, and hence one cannot use the linear reconstruction algorithms.

Published papers concerning RIM measurements and interpretation are even today quite scarce, although the method is widely recognized as a potential prospecting method. Medium radiofrequencies are high enough to give much better resolution and sensitivity to conductive targets in the subsurface than the traditional ground-level and borehole methods, but at the same time radiofrequencies are low enough that transillumination depths of even 1000 m long can be reached. In actual situations, RIM is often utilized in the intermediate domain or between highly attenuating and pure wave propagation, and this complicates the interpretation.

The Friis transmission equation in a dissipative medium can be used to convert the projections to attenuation values, but its use requires knowledge of certain equipment properties (Lafleche 1985, Seybold 2005, Vogt 2000):

$$\frac{P_r}{P_t} = \left(\frac{\lambda}{4\pi R}\right)^2 G_r(\phi,\varphi) G_t(\phi,\varphi) e^{2\int_0^R -\alpha \delta r}, \quad (33)$$

where λ is the wavelength, R is the distance between the transmitter and receiver, and G_t and G_r are the gains of the transmitter and receiver antennas. The gains are related to the effective capture area (A_e); $G = {4\pi A_e}/{\lambda^2}$. A_e (especially for receiving antennas) defines the maximum power the antenna can obtain from the incident wave. For thin wire antennas, it is more convenient to use the parameter the effective electric length. It defines the voltage at the terminals of a receiving antenna. P_t and P_r are the transmitted and received powers. The Friis equation holds only in the far field region of the antenna. Taking natural logs of both sides of Eq. 33 gives the total attenuation along the specified path in Nepers/m. Amplitude data are generally expressed in decibels (dB/m), thus taking $10log_{10}$ of both sides of the reduced equation and multiplying by 0.115 $(= ({1}/{20\log(e)}))$, where e is the Euler's number, Eq. 33 can now be written as

$$\int_o^R \alpha(r)\delta r = P_{t_{dB}} + 10log_{10}\left(\frac{1}{4\pi R^2}\right) + 10log_{10}\left(\frac{G_t G_r \lambda^2}{4\pi}\right) - P_{r_{dB}} \quad (34)$$

If the Friis equation (Eq. 34) is used, the wavelength, the gains (G_t, G_r) and the transmitted and receiver powers have to be known accurately, and the attenuation can be determined. The gains are not known in the EMRE system. According to Vogt's (2000) results, G_t can be highly variable in different rock conditions. The transmitted and received powers can be accurately measured. However, the estimation of the wavelength could be problematic. When the exponential term in Eq. 33 is excluded, the remaining part is the Friis free space equation, and the received power is proportional to the inverse square root of the distance R. According to Lafleche (1985), the total attenuation α_{tot} that the electromagnetic

wave suffers in rock between two boreholes can be written as a sum of the material's internal attenuation (α) (Eq. 32) and spreading loss α_{spr} (the power lost due to measurement geometry):

$$\alpha_{tot=}\alpha \cdot R + \alpha_{spr} \quad (35)$$

where $\alpha_{spr} = Gt_{dB} + Gr_{dB} - (20\log_{10}(R) + 20log_{10}(f) + 32.44)$, R is in km and f in MHz. In free space, the wavelength can be written as $\lambda = c/f$. In Figure 27, the total attenuation is presented with different material properties at the EMRE frequencies.

Figure 27 presents the total attenuation (dB) as a function of the transmitter–receiver distance (R). The increase in frequency effectively increases the total attenuation. The trend is more enhanced in more conductive material. Thus, the penetration depths are reduced. On the contrary, when the antenna gains (1→3) and permittivities (10→40) increase, the total attenuation decreases and longer penetration depths are achieved. In the optimal measurement geometry, the borehole depths must not be less than twice the distance between the boreholes to ensure reasonable angle coverage. According to the results presented in Figure 27, the EMRE system can be reliably utilized between boreholes that are separated by 800 m at least, the host resistivity being ρ > 7500 Ωm and permittivity ε_r > 10. The theoretical results presented here coincide well with our first experiences with the EMRE system.

The plane wave assumption is valid in the far-field domain, where the distance between the transmitter and receiver is several wavelengths. In the far-field domain, the relationship between the source amplitude and measured amplitude can be written as:

$$E_f = E_o \frac{e^{-\int \alpha(r)\delta r}}{r}, \quad (36)$$

where $\int \alpha(r)\delta r$ is the attenuation along a ray path (Fullagar et al. 2000, Holliger & Maurer 2004, Holliger et al. 2004, Pears & Fullagar 1998,

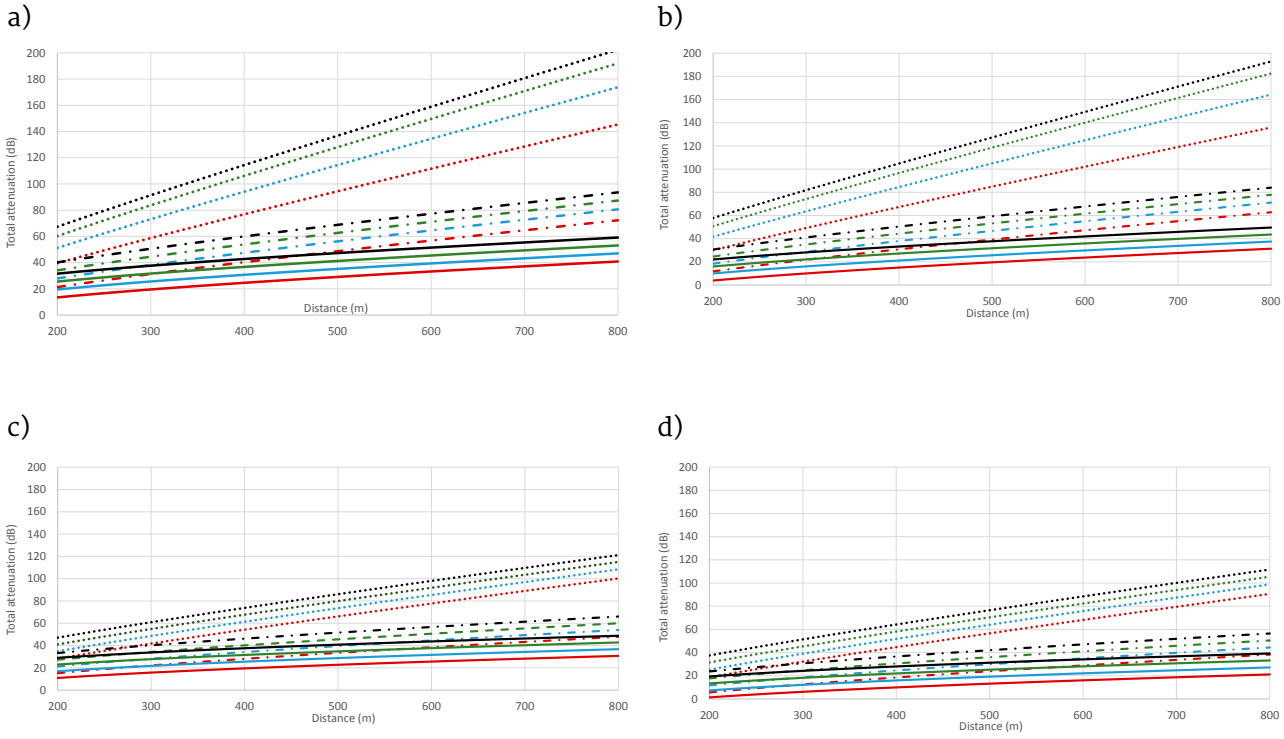

Fig. 27. Total attenuation (dB) with different material properties and antenna gains at the EMRE frequencies (red lines 312.5 kHz, blue lines 625 kHz, green lines 1250 kHz, black lines 2500 kHz). Bold lines (lowest) correspond to the host resistivity of 20 000 Ωm, dashed lines 7500 Ωm and dotted lines 2500 Ωm. a) The electric relative permittivity is ε_r = 10 and the gains $G_t = G_r$ = 1. b) The electric relative permittivity is ε_r = 10 and the gains $G_t = G_r$ = 3. c) The relative electric permittivity is ε_r = 40 and the gains $G_t = G_r$ = 1. d) The relative electric permittivity is ε_r = 40 and the gains $G_t = G_r$ = 3. The loss behaviour presented here is valid only when the maximal coupling between the transmitter and receiver is met.

Thompson & Hinde 1993). E_o is the unknown source strength, which can be estimated by the linear regression of reduced amplitudes in a homogeneous medium (Zhou et al. 1998, Zhou & Fullagar 2001). In geotomography, two basic principles are generally accepted: a far-field condition when the source and receiver are separated by several wavelengths and the straight ray assumption. Thus, the radiated fields from the transmitter antenna can be regarded as plane waves sufficiently far from the antenna. In addition, according to the straight ray assumption, the electromagnetic energy propagates along a ray, and the changes in the electromagnetic field are generated by the changes in the material properties along the ray. When the contrasting electrical properties are moderate, the transmitter-receiver separation distance $>>\lambda$ (far-field domain) and displacement currents predominate, the simple straight ray assumption works well. Curved ray paths should not generally be used in amplitude inversion, because the ray path curvature is determined by the velocity, not the attenuation. However, when the dielectric properties of the medium are insignificant (low-Q domain, the slowness (1/velocity) is proportional to the attenuation and curved ray paths could be used (Jackson & Tweeton 1996).

In Figure 28, the theoretical wavelengths for different material parameters (electric conductivity σ and relative dielectric permittivity ε_r, $\mu = \mu_o$) are presented. A decrease in conductivity from 10^{-3} to 10^{-4} S/m has a slight effect on the wavelengths when $\varepsilon_r \leq 20$, but in a less conductive environment ($<10^{-4}$ S/m) the wavelengths stay at constant values for a fixed permittivity. When permittivity is high enough ($\varepsilon_r > 20$), the wavelengths reach the constant values earlier ($\sigma < 10^{-3}$ S/m).

The EMRE measurements are controlled and information is recorded by a laptop. The operator can monitor the data quality from the laptop's screen at all frequencies in real time. This allows rapid adjustments to the survey depth range and makes the shortening or lengthening of the transmitter step size easy, and thereby enables decisions on rapid re-measurements. An experienced operator can even visualize the continuation of subsurface geological formations during scanning periods. In Figure 29, a) an electric field normalised by the transmitter-receiver distance (2500 kHz), b-c) the relative phase difference between the transmitter and receiver (2500 kHz), d-e) electrical resistivity logging data and electric field data, and f) the tomographic reconstruction of borehole section PYS127-PYS113 (Pyhäsalmi volcanic complex, Ruotanen formation, Kettuperä member, Finland) are plotted.

Plotting the amplitudes and phases of the electric fields of both boreholes in the same figure (Figs. 29a-b) is a simple and rapid way to delineate possible targets in the section. In the bore-

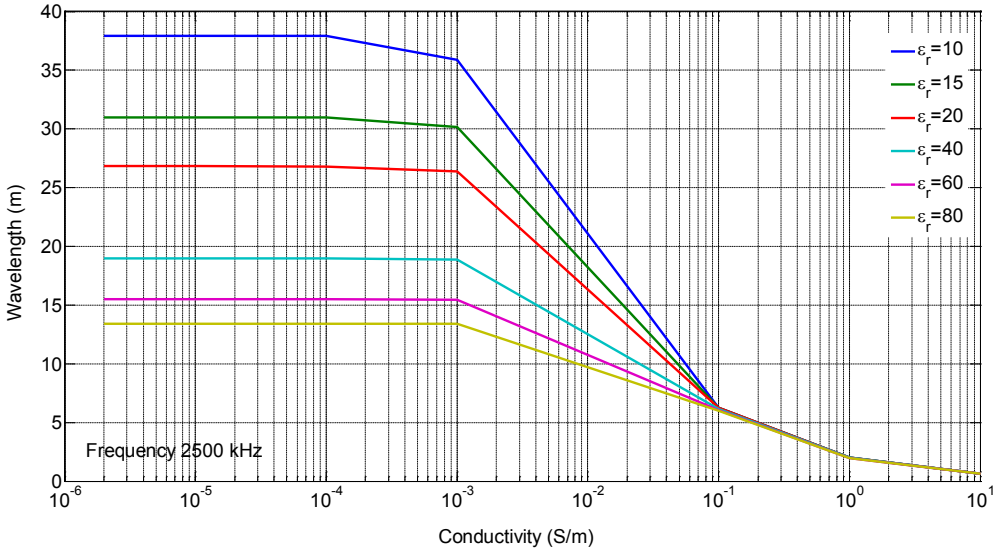

Fig. 28. The theoretical wavelengths for different material properties (2500 kHz). The electric conductivity of the background (host) ranges from 10 S/m to 10^{-6} S/m and the relative permittivity from 10 to 80. Non-magnetic material is assumed ($\mu = \mu_o$). In a sufficiently resistive environment ($\sigma < 10^{-4}$ S/m), the used antennas (20 m) are very close half-wave dipoles.

hole PYS127, the transmitter depth ranges from 170 m to 220 m (coloured circles under the borehole label correspond to depths) and from 150 m to 175 m in PYS113, respectively. Signals (dashed lines) registered in borehole PYS113 are very low from 180 m to 300 m, and low resistivity material (attenuating) must exist between the boreholes. The reverse measurement in borehole PYS127

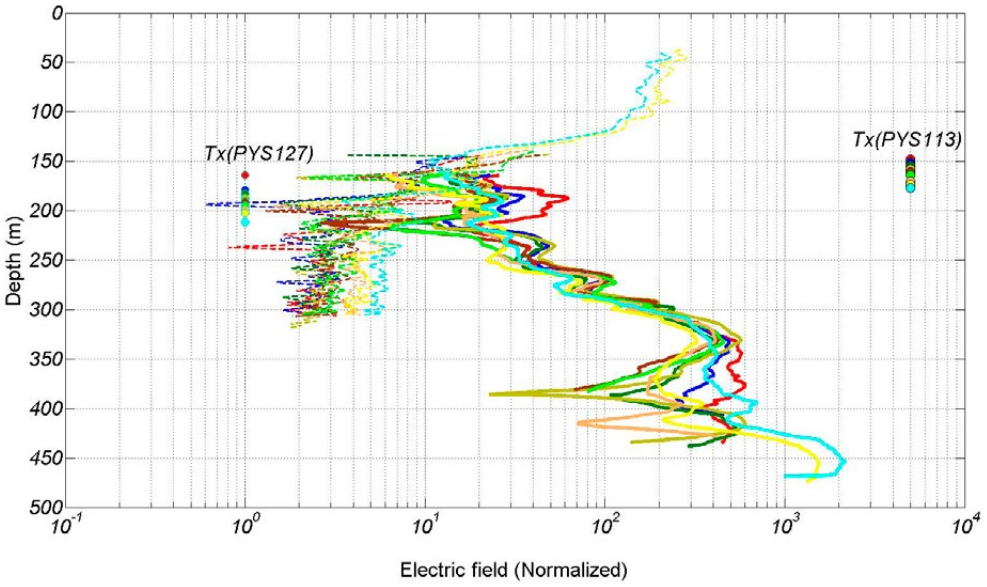

Fig. 29. a) The electric fields from borehole section PYS127-PYS113 are gathered in the same figure (2500 kHz). Bold lines correspond to the scannings in PYS127 (150-470 m) with the transmitter in PYS113 (145-175 m) and dashed lines in PYS113 (45-320 m) with the transmitter in PYS127 (170-220 m), respectively. The amplitudes of the electric field are low at the depth level of ~200-225 m in both of the measurements due to attenuating material, and the material extends downwards in the vicinity of borehole PYS127. The target is more likely closer to PYS127, because the transmitter in PYS127 is effectively screened by the unknown target and operates hardly above noise level. Coloured circles below the borehole labels represent the corresponding transmitter depths.

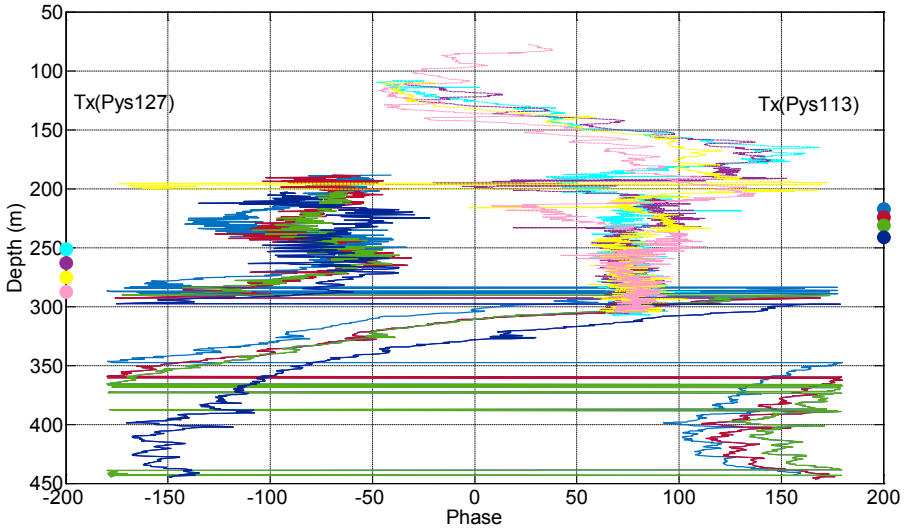

Fig. 29. b) The relative phases (borehole section PYS127-PYS113) are gathered in the same figure (2500 kHz). Bold lines correspond to the scannings in PYS127 (180-450 m) when the transmitter is in PYS133 (220-240 m) and dashed lines correspond to the scannings in PYS113 (70-320 m) when the transmitter is in PYS 127 (250-280 m), respectively. An increase of 200 degrees in the phase occurs during the receiver movement of 50 m (dashed lines) due to attenuating material at the depth level of ~180-225 m, after which the phase detection hardly functions due to attenuating material near PYS127. The same behaviour in the phase detection can also be seen in the reverse measurement (bold lines) during the receiver movement from 180 to 275 m. The phase keeps changing during the rest of the scanning (275-450 m). The attenuating material extends downwards and the target is more likely closer to PYS127. Coloured circles below the borehole labels represent the corresponding transmitter depths. The abrupt changes (at 180 ° and -180 °) occur due to the presentation format of the phase.

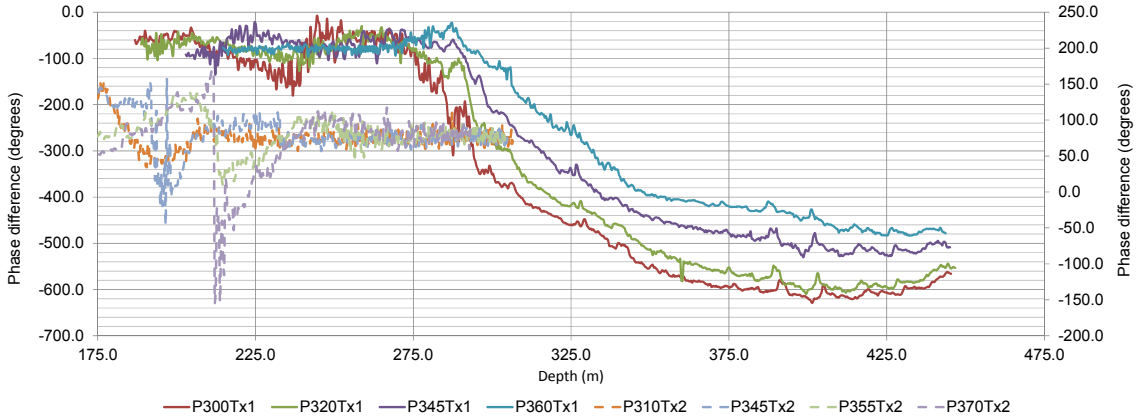

Fig. 29. c) The relative phases (borehole section PYS127-PYS113) are plotted in a monotonous format (2500 kHz). Bold lines correspond to the scannings in PYS127 (180–450 m) when the transmitter is in PYS133 (Tx1: 300–360 m) and dashed lines correspond to the scannings in PYS113 (70–320 m) when the transmitter is in PYS 127 (Tx2: 310–370 m), respectively. An increase of 200 degrees in the phase occurs during the receiver movement of 50 m (dashed lines) due to attenuating material at the depth level of ~180–225 m, after which the phase detection hardly functions due to attenuating material near PYS127. The same behaviour in the phase detection can also be seen in the reverse measurement (bold lines) during the receiver movement from 180 to 275 m. However, the phase keeps changing dramatically during the rest of the scanning (275–450 m). The attenuating material extends downwards and the target is more likely closer to PYS127. The wavelengths should not be greater than 40–50 metres at the frequency of 2500 kHz. However, the phase changes much too slowly. This results from the unknown initial phases of the local oscillators, and because the oscillators are not synchronized, the phase measurement is unreliable.

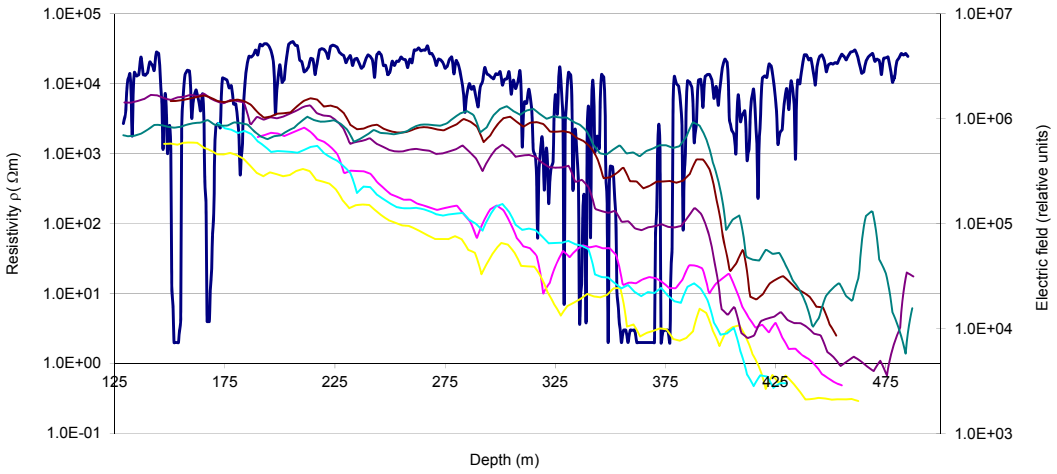

Fig. 29. d) The electric fields in PYS113 (borehole section PYS127-PYS113) are compared with the electrical logging result in PYS113. The dark blue line corresponds to the resistivity data.

(bold lines) has the same behaviour. Signal levels are slightly higher than in borehole PYS113, but still low at the depth level of 150–220 m, increasing strongly to the depth level of 350 m (Fig. 29a).

Electrical resistivity logging of boreholes is a widely used prospecting technique for identifying mineralised zones near the boreholes. Resistivity logging results (dark blue lines) in boreholes PYS113 and PYS127 are displayed in Figures 29d-e with the measured electric fields. The electric fields transmitted in PYS127 and received in PYS113 are presented in Figure 29d. The resistivity and electric field data coincide well at some depths but there are also differences between the data sets. A strong contact with low resistivity material is evident at the 150–180 m level, but the electric field values remain at an almost constant level. A sudden and local decrease in field values just before the level of 300 m correlates well with the resistivity data. Low resistivity material is evident at the 350–400 m

level, and below the 300 m level the field values also decrease. The descending trend is followed by a slight increase in electric fields at depths of up to 400 m before a rapid decrease to the noise level, but the resistivities remain at high values.

The reverse EMRE measurement when the transmitter and receiver are interchanged indicates rather similar behaviour (Fig. 29e). The resistivities are at a fairly high level, decreasing slightly when the depth increases. There is a local reference from conductive material in the electric data at the 150 m level, but no electric field data were available. Electric field values have an increasing trend, meaning that attenuating material between the holes might be dipping downwards from PYS113 towards PYS127.

Thus, RIM measurements may have the same distinct and even highly localized features as electric logging data (Figs. 28d-e). However, one has to remember that electric logging senses the close vicinity of boreholes, and an electric field strong enough to be registered by the EMRE system will most likely result from geological formations in the first Fresnel zone, the volume between the boreholes (Buursink et al. 2008, Seybold 2005, Spetzler & Snieder 2004). Radio wave attenuation in rocks corresponds to electrical conductivity, but the measured signal levels are not only increased or decreased by changes in the attenuation constant. The relationship between the antenna and borehole environment may change greatly from point to point, having an effect, for instance, on the scattering parameter s_{11} (Gustrau & Manteuffel 2006, Ludwig & Bretchko 2009), polarization and reflection losses (Zhang & Li 2007), and signal levels being combined with the material attenuation (Seybold 2005). In the amplitude geotomography, the decayed amplitudes can be directly converted to the attenuation distribution (Holliger et al. 2004, Holliger & Maurer 2004, Jackson & Tweeton 1996, Pears & Fullagar 1998, Zhou et al. 1998, Zhou & Fullagar 2001). Data reduction is completed to provide the attenuation distribution (dB/m) by using, for instance, well-known special purpose reconstruction methods such as the algebraic reconstruction technique (ART) (Kaczmarz 1937, Kak & Slaney 1998, Popa & Zdunek 2004, Tanabe 1971) and the simultaneous iterative reconstruction technique (SIRT) (Jackson & Tweeton 1996, Lakshminarayanan & Lent 1979). In the EMRE system, the power the antenna radiates to the rock is unknown, but the unknown source strength can be estimated by a linear regression of reduced amplitudes in a homogeneous medium (ImageWin 2012, Sharif 2013). In a homogeneous environment, the global source strength can be used for all transmitter positions. In situations where proximity to the borehole wall changes from one transmitter position to another, resulting in large variations in antenna impedance, local source strengths can be used. Because antenna impedance is sensitive to the electrical properties of the material near the borehole, the radiated power can also differ considerably from one transmitter position to another. The attenuation distribution can be converted to the conductivity distribution (S/m) using an equation presented by (Zhou et al. 1998):

$$\sigma = \frac{2500 \cdot \alpha^2}{\pi^2 \cdot f}, \tag{37}$$

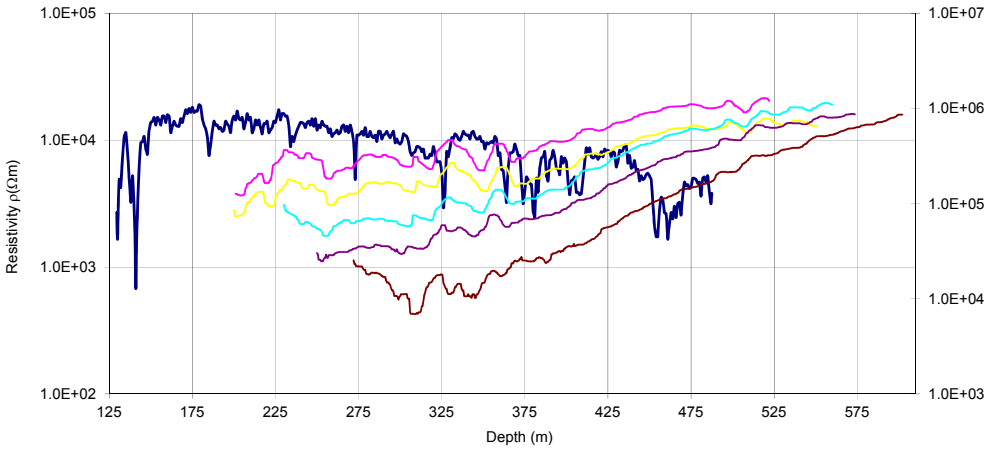

Fig. 29. e) The reversed electric fields in PYS127 (borehole section PYS127-PYS113) are compared with the electrical logging result in PYS127. The dark blue line corresponds to the resistivity data.

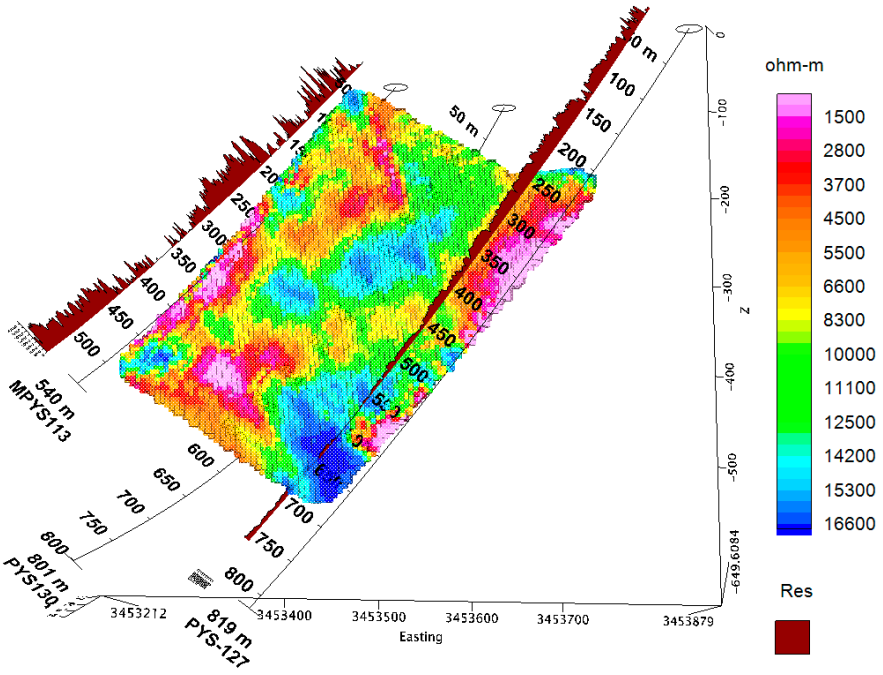

Fig. 29. f) Resistivity reconstruction of the section at a frequency of 2500 kHz by ImageWin (2012). Electrical logging results are displayed beside the boreholes as filled profiles (brown).

where α is the attenuation in Nepers/m and f the frequency in kHz. Eq. 37 is a plane wave solution that is satisfied in the far-field domain. In Figure 29f, the attenuation–conductivity conversion is completed, and furthermore, the conductivities (S/m) are transferred to resistivities (ohm-m). The utilized reconstruction technique was SIRT. The electrical logging results are attached to the boreholes. In MPYS113, at the depth levels of 100–200 m and 300–450 m, the low resistivity sections of electrical loggings coincide well with the tomographic reconstruction. In addition, in PYS127, the correlation between the electric logging results and the tomographic reconstruction is fine at the depth level of 550–600 m.

The geometry of the cross-borehole technique used in RIM measurements is a restrictive factor in the inversion. The problem is referred to as a limited angle problem, and the attenuating object may smear strongly in the horizontal direction. The horizontal smearing is always a common feature of the geotomographic reconstructions due to the low angle coverage in that direction. On the contrary, the vertical direction does not suffer from smearing. Normally, the highest ray path densities are found in the central parts of the section, resulting in a better and more reliable reconstruction in these regions (Fig. 30). The long ray paths due to small angles may lead to misleading high attenuation values, and they should therefore be removed. In addition, because of the limited angle geometry, the ray densities can be extremely low in the top and bottom parts of the section. When sensing a multipath wave, a sharp and localized change in the measured phase difference immediately tells the operator the difference in the lengths of ray paths, or how much longer a path the multipath wave has travelled. In addition, the phase difference between the direct and reflected wave may interfere in such a manner that the amplitude may increase or decrease. Because sharp changes cannot be taken into account in the linear reconstruction techniques, they must first be removed from data, but with great care. Before one can remove a distinct feature from one frequency, a careful comparison with all frequencies must be performed, and if the feature is missing from the other frequencies, it may be removed (I, Fig. 10). Due to the insulation layer of the antenna ($\varepsilon_I \sim 1\text{–}2$, $\sigma \sim 0$), charges cannot escape from the antenna to the surroundings, and the current distribution is less sensitive to the electrical properties of the surroundings ($\varepsilon_r >> \varepsilon_i$, $\sigma \neq 0$) if the electrical properties of the insulation are far from those of the surrounding rock. However, although the diagnostic power of the insulated antennas is highly reduced, their usage, for instance, in geoto-

mography is highly justified. One environment where the electrical properties of the insulation and surroundings are quite similar is ice (King et al. 1981). The sensitivity of the borehole antennas is highest to features near the boreholes. This may generate additional artifacts in the reconstruction and should be taken into account in the interpretation. The resolution decreases as a function of decreasing frequency (longer wavelength), and the images become more smeared. The reconstruction of the section PYS127-PYS113 with the highest EMRE frequency is good (Fig. 29f). The background resistivity of the host material is estimated correctly, but the properties of the attenuating targets are underestimated, as is usually the case in geotomography. Despite this, the shape and location of highly attenuating regions are quite accurate and they coincide well with the results from other methods used in the section (I).

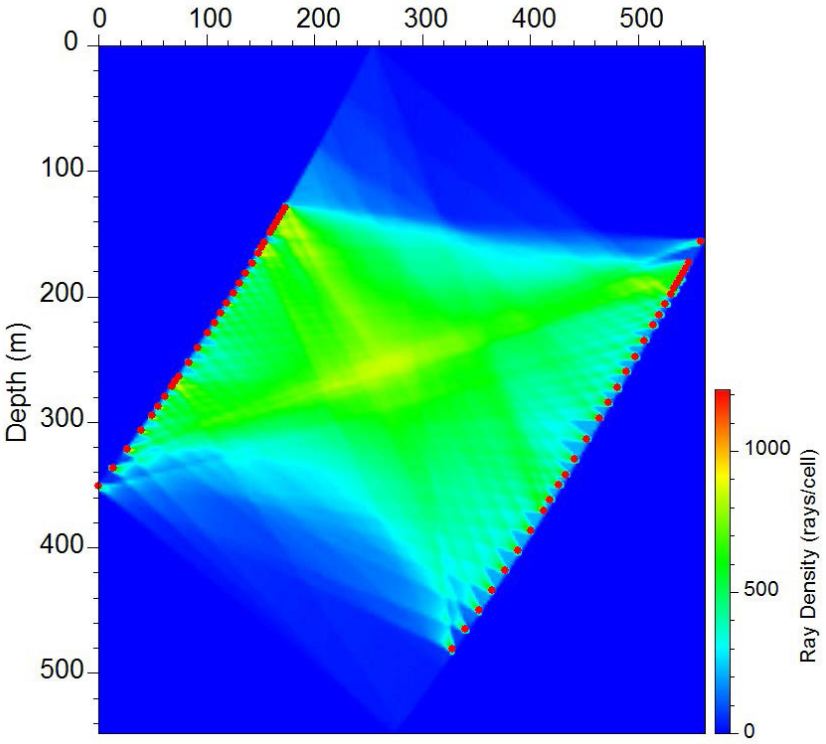

Fig. 30. Ray densities in borehole section PYS127-PYS113. The red dots correspond to the transmitter positions in the boreholes. The highest densities occur in the central parts of the section resulting in more reliable reconstruction. Geotomography can be referred to as a limited angle problem, and thus the densities in the upper and lower parts of the section may be extremely low, resulting in possible artifacts in the reconstruction. Long ray paths (low angle data) may result in especially high attenuation values, and their removal must therefore be considered. The sensitivities of the borehole antennas are highest to features near the boreholes, so this must also be taken into account in the interpretation.

6 CONCLUSIONS AND DISCUSSION

In this thesis, attention has focused on presenting providing the basic principles of the radio imaging method (RIM), from measurement to interpretation. Although most of the issues discussed in this thesis are in no sense novel, the thesis provides a unique overview of the fundamental aspects of borehole radar imaging and our first experiences with RIM in Finland. It also examines the use of RIM in conjunction with other methods for future deep ore prospecting. All methods have their own limitations, advantages and disadvantages. The drilling costs of a new drillhole are high and deep boreholes exist at long intervals. However, a RIM survey can have several benefits over ground-level EM sounding methods. When having the transmitter in the borehole, boundary effects due to the ground surface and the strong attenuation

emerging from soils are easily eliminated. The vertical resolution remains the same from the top of the borehole to the bottom. A borehole survey also brings the survey closer to the targets, and higher frequencies can be used, which also means better horizontal resolution. Viewing of the target from different angles and directions also means better reconstruction results, and deep boreholes are thus necessary to ensure the essential angle coverage. Formations (e.g. massive sulphide deposits, fractures filled with conductive water) between the boreholes produce distortions in the measured data and lead to higher attenuation values. As a result of a full tomographic survey in which the transmitter is interchanged in the boreholes during the research, and when the amplitude of the electric field is the only measurement parameter, the attenuation distribution of the section can reliably be reconstructed with simple traditional tomographic techniques. In addition, the interpretation of the section can even be started at the measurement site because these techniques are rapid, and the direction of the measurements can thus easily be changed, even during the survey. This is not usually possible with other borehole methods due to the much more complicated interpretation techniques utilized.

The spectrum of geophysical prospecting methods is diverse, and classification into passive and active methods is made according to the sources (natural or man-made sources). Measurements can also be carried out in the time domain, e.g. MT, AMT, GPR, or in the frequency domain, e.g. Slingram, RIM. Generally, natural field methods are used in deep studies, whereas active sources are limited to shallow targets and most often used in near-surface applications or in boreholes. Although some ore deposits outcrop, making the investigation much easier, there are more targets that are obscured by surficial materials (e.g. soil, shallow water). The use of boreholes eliminates the boundary effects related to the ground surface and the strong attenuation emerging from soil deposits, but due to the high drilling costs of deep boreholes, borehole methods are seldom used in the initial stages. However, even today, when high accuracy devices are utilized, the recognition of a world-class ore deposit is very demanding at even quite reasonable depths using only one data type. Thus, combination with other possible data types may help in the research. Although the sensitivity of these methods to various parameters is different, their combined use is complementary. This novel approach is referred to as joint inversion, where different data are inverted simultaneously. In general, a common factor for different data sets is needed or the methods used should be sensitive to the same physical property. In deep ore prospecting, the delineation of favourable host rock for ore and the utilization of the rock structures (e.g. faults, fractures and fissures) are important, because certain kinds of mineral deposit are only found in specific types of rocks or are associated with certain geological structures. Furthermore, the appearance of an indicator mineral, even few grains, may indicate the presence of a specific type of mineralization.

Rocks are highly complex compounds of different minerals (pure elements or chemical compounds) and can generally have a crystal structure. Their properties are determined to a large extent by the properties of the existing constituent minerals and textures. The conductivity of rocks is highly variable and can span over 20 orders of magnitude. The relative permittivities can range from ~4–5 to 40–50. Both of the properties strongly depend on the water content in porous rock. The magnetic susceptibilities are generally low, depending on the content of ferromagnetic materials, and thus small amounts of, for instance, iron sulphide minerals or iron oxides can significantly increase the volume susceptibilities. The same behaviour can also occur in resistivities and relative permittivities. For instance, when small amounts of pyrite are involved, a decrease in resistivity and an increase in permittivity is possible. Conversely, the conductivities of typical rock types (e.g. granite, quartzite) increase with increasing frequency, while the relative permittivities remain at constant values.

The solution of Maxwell's equations yields quantities that describe the propagation of electromagnetic waves in the wave number k. The field also depends on the distance r from the source. Certain characteristics of an electromagnetic field dominate at one particular distance from the antenna, while a completely different behaviour can dominate at another location. The wave number k multiplied by the distance r de-

fines the behaviour. The general expressions for the attenuation rate α and phase constant and β are functions of frequency, conductivity, electrical permittivity and magnetic permeability. The attenuation rates can be determined either by *in situ* measurements or by using theoretical equations. Direct measurements under *in situ* conditions are the most accurate. Generally, the relative permeability μ_r has a minor effect on the attenuation rates in a non-magnetic medium in the EMRE band (312.5–2500 kHz), but electric conductivity σ and permittivity ε_r are the main properties that can effectively influence the transillumination ranges. Increasing conductivity always means higher attenuation rates, but an increase in permittivities decreases the attenuation rates. Publication III reports the essential issues when handling the behaviour of the electromagnetic field in different conditions, and it also presents theoretical estimates for the maximal distances when the EMRE system is utilized in RIM measurements. According to simple theoretical modelling studies, the greatest transillumination distances can be as long as ~800–1000 m in a highly resistive environment. RIM measurements conducted in a conic borehole section are also closely reported. The measurement geometry was quite challenging and far from the optimal one, and thus the transmitter and receiver were not maximally coupled, but the reconstructed low and high resistivity zones and their apparent shapes and orientations were in good agreement with geological and other geophysical results. Despite the used frequency band being much lower than in GPR, RIM has good sensitivity and relatively high resolution to assess the integrity of the rock mass, as increased electrical conductivity is often associated with deformation of the rock mass.

Rock is a challenging environment for any antenna system, because widely changing conditions in the electric and magnetic properties of the earth's subsurface are extremely difficult to take into account in a proper way. The input impedance of the antenna is an important factor. Under optimal conditions with no impedance mismatch ($Z_G = Z_o = Z_L$), the input impedance should only consist of a real component, the resistance, and the maximal power is transferred from the antenna into the surroundings. Consequently, effective impedance matching to minimize losses can be extremely challenging, if not impossible. This is especially important in the transmitter, whereas in the receiver, impedance matching is not such an important property if the signal levels are high enough and above the noise level. In publication II, numerical studies were conducted when the antennas were situated in the borehole environment. As a result, the insulated antennas proved to be very suitable in the frequency band of 312.5–2500 kHz. Only the highest frequency of 2500 kHz could suffer in typical borehole conditions, resulting in low s_{11} scattering parameters. Vogt's results also confirmed that insulated antennas are well suited to RIM measurements. The diagnostic power of a bare dipole antenna is highly reduced when the antennas are covered with an insulation layer, because the electrical properties of insulation differ significantly from the corresponding properties of the surrounding rock, and the interpretation of the input impedance of the antenna in terms of accurate material parameters is difficult.

Coal mines were the first platforms for which the RIM technique was applied to define the continuity of seams of coal. We carried out an electromagnetic cross-borehole survey as a feasibility target for the radiowave imaging method (RIM) in a possible area for a repository of spent nuclear fuel in Finland to reveal the properties of the crystalline bedrock. This interesting case has been presented in publication IV. The results verified that the method can be used to delineate and follow sulphide-bearing formations between boreholes in such challenging environments where no massive ore body exists. The detected low and high resistivity zones and their apparent shapes and orientations were in fair agreement with geological and other geophysical results. The material properties differed from those recorded in seismic researches from the same location, although the reflections partly described the boundaries of domains differing in electrical properties. Using borehole geometry, similar but more detailed information is obtained compared to electric and electromagnetic measurements from the ground surface.

As the amplitude of the electric field is the directly measurable parameter, it can be used to estimate attenuation, bearing in mind the following. The far-field condition is assumed where the

source and transmitter are separated by several wavelengths. This may not be completely true in all RIM surveys, but the approximation makes the interpretation much easier. The attenuation is formulated for the $\vec{E}_\theta$ component, having r^{-1} dependency in the intermediate and far field region. In the near field, a radial $\vec{E}_r$ component with a different attenuation rate and the static field behaviour, having a dependency of r^{-3}, should be considered. The lack of a modern numerical forward solver for the RIM environment is the main reason why new powerful interpretation tools are not available. Thus, the traditional linear imaging reconstruction techniques (SIRT, ART) are still in normal use when geotomographic data are handled. Although they can give quite good results in certain circumstances, true 3D numerical modelling techniques with a full waveform are needed to obtain more precise reconstructions of borehole sections when realistic losses an electric and magnetic losses in the earth's subsurface could be taken into account. The rapid linear results could still be useful in serving as seeds for these modern methods. When using SIRT or ART, the reconstructions generally reveal the shape and location of highly attenuating targets quite accurately. The resolution decreases as a function of decreasing frequency, and the images become more smeared when the frequency is reduced. The smearing effect in the horizontal direction is always a common feature of geotomographic reconstructions due to the low angle coverage in that direction. On the contrary, the vertical direction does not suffer from smearing. The background resistivity of the host material is also generally estimated correctly, but the properties of the attenuating target are always underestimated. Off-plane attenuating targets will also strongly influence the field results. It is an internal property of the EMRE system to always sense the strongest signal in the first Fresnel zone. The first Fresnel zone is the region around a ray that mostly influences the propagation of the signal.

Inspired by the positive results with RIM, the future development of the EMRE system would be reasonable with enhancements of the device. An additional high frequency option (5000 kHz) would markedly improve the resolution in the resistive cases. Both the transmitter and receiver should be designed to work more effectively and to sense weaker signals (~0.1 μV). A broader dynamic range of 60 dB would increase the usefulness of the device. The angular resolution of the present device is ~10 degrees, but a resolution of ~2 degrees would be possible. These improvements could be achieved, for example, by improving the frequency synthesis and minimizing phase losses using a TCXO (temperature controlled crystal oscillator) in both the transmitter and receiver. The digitalization of data in the borehole receiver could make it possible to exploit data in a more effective way. In addition, to improve the operation level of the receiver, the present mixer technique must be modernized. The input impedance of the transmitter antenna and the return loss should be measured accurately to obtain the output power fed to the rock. The return loss of an antenna is the negative value of scattering parameter s_{11}, and it determines how well the antenna is matched to the transmission line and gives the part of the incident power that is reflected due to mismatch. In general, an antenna meets the minimum requirements for proper functioning with a return loss ≥10 dB or s_{11} ≤−10 dB, meaning that 90% of the incident power should go to the antenna for radiation. This requirement is, however, seldom met with RIM antennas due to mismatching problems or because the maximum power (resonance) to be sent to the antenna is difficult to put into practice. With minor developments of this kind, the EMRE system could become a much more powerful tool that could also be used in large rock building projects to more precisely determine the structural integrity of the rock.

REFERENCES

Airo, M.-L. & Hyvönen, E. 2008. Petrophysical data coupled with airborne magnetic, conductive and radiometric signatures identifying bedrock conductors. Proceedings of the 5th International Conference on Airborne Electromagnetics, Porvoo, Haikko, Finland.

Airo, M.-L. & Säävuori, H. 2013. Petrophysical characteristics of Finnish bedrock. Geological Survey of Finland. Report of Investigation 205. 33 p.

Annan, A. P. 2003. Ground penetrating radar: Principles, Procedures & Applications. Subsurface imaging. Solutions. Mississauga: Sensors & Software Inc. Notes.

Buhrke, V. E., Jenkins, R. & Smith, D. K. 1998. A practical guide for the preparation of specimens for X-ray fluorescence and X-ray diffraction analysis. New York: John Wiley & Sons, Inc.

Buselli, G. 1980. Electrical geophysics in the USSR. Geophysics, 45, 1551-1562.

Buttler, D. K. 2005. Near-surface geophysics. Investigations in Geophysics No. 13. First edition. Society of Exploration Geophysicists.

Buursink, M. L., Johnson, T. C., Routh, P. S. & Knoll, M. D. 2008. Crosshole radar velocity tomography with finite-frequency Fresnel volume sensitivities. Geophys. J. Int., 172, 1-17.

Cao, J., He, Z., Zhu, J. & Fullagar, P. K. 2003. Conductivity tomography at two frequencies**.** Geophysics, 68, 516-522.

Chave, A. D. & Jones, A. G. 2012. The magnetotelluric method. Cambridge: Cambridge University Press.

Claassen, D. M. 1995. Electromagnetic characterization of a wideband borehole radar imaging system. PhD thesis, University of Oxford, UK.

Collin, E. R. & Zucker, F. J. 1969. Antenna Theory. Part 1. New York: McGraw-Hill Book Company.

Daniels, D. J. 1996. Surface Penetrating Radar. IEEE Radar, Sonar, Navigation and Avionics series 6. London: The Institution of Electrical Engineers.

deBettencourt, J. T. & Surcliffe, R. A. 1962. Studies in deep strata radio communication. Final report. Norwood: Raytheon Company. AD0407840. Available at: http://www.dtic.mil/dtic/tr/fulltext/u2/407840.pdf

Dixon, C. J. 1979. Atlas of economic mineral deposits. Netherlands: Springer. Available at: https://dx.doi.org/10.1007/978-94-011-6511-2

Erkan, K. 2008. A comparative overview of geophysical methods. Report No. 488. The Ohio State University. Geodetic Science and Surveying. Columbus Ohio. Available at: https://earthsciences.osu.edu/sites/earthsciences.osu.edu/files/report-488.pdf

Fullagar, P. K., Livelybrooks, D. W., Zhang, P., Calvert, A. & Wu, Y. 2000. Radio tomography and borehole radar delineation of the McConnell nickel sulfide deposit, Sudbury, Ontario, Canada. Geophysics, 65, 1920-1930.

Geological Survey of Finland 2013. XRD (X-Ray Diffraction) Laboratory. Available at: http://en.gtk.fi/research/infrastructure/researchlaboratory/XRD.html

Gill, R. 1997. Modern analytical geochemistry. Singapore: Longman Singapore Publishers (Pte) Ltd.

Gustrau, F. & Manteuffel, D. 2006. EM Modeling of Antennas and RF Components for Wireless Communication Systems. Berlin, Heidelberg: Springer.

Hansen, P. C. 1998. Rank-Deficient and Discrete Ill-Posed Problems: Numerical aspects of linear inversion. Mathematical modeling and computation. Philadelphia: SIAM.

Harrison, R. M., deMora, S. J., Rapsomanikis, S. & Johnston, W. R. 1991. Introductory chemistry for the environmental sciences. Cambridge: Cambridge University Press.

Henney, K. 1950. Radio engineering handbook. Fourt edition. New York: McGraw-Hill Book Company, Inc.

Holliger, K. & Maurer, H. 2004. Effects of stochastic heterogeneity on ray-based tomographic inversion of crosshole georadar amplitude data. Journal of Applied Geophysics, 56, 177-183.

Holliger, K., Musil., M. & Maurer, H. R. 2004. Ray-based amplitude tomography for georadar data: a numerical assessment. Journal of Applied Geophysics, 47, 285-298.

Holloway, G. L. 1998. Radiofrequency Communication Principles. Module 17. NAVEDTRA 14189. Published by Naval education and training professional development and technology center. Available at: http://www.richardmcwhorter.com/NavyTraining/NEETS-v17-RFPrinciples.pdf

Hülsmeyer, C. 1904a. Verfahren zur Bestimmung der Entfernung von metallischen Gegenständen (Schiffen o. dgl), deren Gegenwart durch das Verfahren nach Patent 165546 festgestellt wird. Patentschrift 169154. Berlin: Kaiserliches Patentamt.

Hülsmeyer, C. 1904b. Verfahren, um entfernte metallische Gegenstände mittels elektrischer Wellen einem Beobacher zu melden. "Hertzian-wave projecting and receieving apparatus adapted to indicate or give warning of the presence of a metallic body, such as a ship or a train, in the line of projection of such waves." Patentschrift 165546. Berlin: Kaiserliches Patentamt.

Hunt, C. P., Moskowitz, B. P. & Banerjee, S. K. 1995. Magnetic properties of rocks and minerals. In: Ahrens, T. J., Rock Physics **&** Phase Relations: A Handbook of Physical Constants. Washington, DC: American Geophysical Union.

Hunt, G. R., Johnson, G. R., Olhoeft, G. R., Watson, D. E. & Watson, K. 1979. Initial report of the petrophysics laboratory. Circular 789. United States Department of the Interior. Reston: U.S. Geological Survey. Available at: http://pubs.usgs.gov/circ/1979/0789/report.pdf

ImageWin 2012. ImageWin geophysical tomography. Blackmans Bay: Fullagar Geophysics Pty Ltd. Available at: http://www.fullagargeophysics.com/download_imagewin.html

Iskander, M. F. & DuBow, J. B. 1983. Time- and frequency-domain techniques for measuring the dielectric properties of rocks. Journal of Microwave Power, 18, 55-74.

Jackson, M. J. & Tweeton, D. R. 1996. 3DTOM: Three-dimensional geophysical tomography. Report of investigations 9617. Minneapolis: United States Department of the Interior, Bureau of Mines.

Jankiraman, M. 2007. Design of Multi-Frequency CW radars. SciTech Publishing Inc.

Jol, H. M. 2009. Ground penetrating radar: Theory and applications. First edition. Amsterdam: Elsevier Science.

Kaczmarz, S. 1937. Angenaherte Auflosung von Systemem linearer Gleichungen. Bull. Int. Acad. Pol. Sci. Lett. A., 355-357.

Kak, A. C. & Slaney, M. 1998. Principles of Computerized Tomographic Imaging. The Institute of Electrical and Electronics Engineers, Inc. New York: IEEE Press Books.

Kearey, P., Brooks., M. & Hill, I. 2002. An Introduction to Geophysical Exploration. Third edition. Oxford: Blackwell Science Ltd.

King, R. W. P., Smith, G. S., Owens, M. & Wu, T. T. 1981. Antennas in Matter: Fundamentals, Theory, and Applications. Cambridge: The MIT Press.

Kittel, C. 1976. Introduction to solid state physics. Fifth edition. New York: John Wiley & Sons, Inc.

Knoll, M. D. 1996. A petrophysical basis for ground penetrating radar and very early time electromagnetics: Electrical properties of sand-clay mixtures. Doctoral dissertation, Department of Earth and Ocean Sciences, The University of British Columbia.

Kukkonen, I., Heikkinen, P., Paananen, M., Elo, S., Paulamäki., S., Heinonen, S., Laitinen, J. & HIRE Working Group of the Geological Survey of Finland 2010. HIRE Seismic reflection survey in the Olkiluoto area, western Finland. Geological Survey of Finland, archive Report Q23/2009/53.

Kukkonen, I. T., Heinonen, S., Heikkinen, P. & Sorjonen-Ward, P. 2012. Delineating ophiolite-derived host rocks of massive sulfide Cu-Co-Zn deposits with 2D high-resolution seismic reflection data in Outokumpu. Geophysics, 77, WC213-WC222. Available at: http://dx.doi.org/10.1190/geo2012-0029.1

Lafleche, P. T. 1985. Underground UHF-EM Transillumination: A feasibility study. Doctoral dissertation. The Department of Geological Sciences. Montreal: McGill University.

Lager, D. L. & Lytle, R. J. 1977. Determining a subsurface electromagnetic profile from high frequency measurements by applying reconstruction technique algorithms. Radio Science, 12, 249-260.

Lakshminarayanan, A. V. & Lent, A. 1979. Methods of least squares and SIRT in reconstruction. J. Theor. Biology, 76, 267-295.

Lee, T. J., Suh, J. H., Kim, H. J., Song, Y. & Lee, K. H. 2002. Electromagnetic traveltime tomography using approximate wavefield transform. Geophysics, 67, 68-76.

Lowrie, W. 2007. Fundamentals of Geophysics. Second edition. New York: Cambridge University Press.

Ludwig, R. & Bretchko, P. 2009. RF circuit design: Theory and application. Upper Saddle River: Prentice Hall.

Lytle, R. J. 1973. Measurement of Earth medium electrical characteristics: Techniques, Results and applications. Sensor and Simulation Notes 188. Livermore: Lawrence Livermore Laboratory.

Lytle, R. J., Laine, E. F., Lager, D. L. & Davis, D. J. 1979. Using cross-borehole electromagnetic probing to locate high contrast anomalies. Geophysics, 44, 1667-1676.

Macintury, S A. 1999. Magnetic field measurements. Chapter 48. In: Webster, J. G., The measurement, instrumentation, and sensors handbook. CRC Press LLC.

Mahrer, K. D. 1995. Review of the radio frequency (RIM) method and its utilization in near-surface investigations. The Leading Edge, April, 249-256.

MALÅ GPR Resource Center 2014. Available at: http://www.malags.com/resources/software-download/

McClenaghan, M. B. 2005. Indicator mineral methods in mineral exploration. Geochemistry: Exploration, Environment, Analysis, 5, 233-245.

Meles, G. A. 2011. New developments in full waveform inversion of GPR data. Doctoral dissertation. DISS. ETH NO. 19768. Zurich: ETH Zurich.

Moore, R. K. 1963. Effects of a surrounding conducting medium on antenna analysis. IEEE Transactions on Antennas and Propagation, 12, 216-225.

Mukhopadhyay, P. K. 2005. Three-dimensional borehole radar imaging. Doctoral dissertation, University of Cape Town.

Murphy, E. J. & Morgan, S. E. 1937. The dielectric properties of insulating materials. Bell System Technical Journal, 16, 493-511.

Murphy, E. J. & Morgan, S. E. 1938. The dielectric properties of insulating materials. Bell System Technical Journal, 17, 640-669.

Murphy, E. J. & Morgan, S. E. 1939. The dielectric properties of insulating materials: III Alternating and direct current conductivity. Bell System Technical Journal, 18, 502-537.

Musil, M., Maurer, H. R. & Green, A. G. 2003. Discrete tomography and joint inversion for loosely connected or unconnected physical properties: application to crosshole seismic and georadar data sets. Geophys. J. Int., 153, 389-402.

Nabighian, M. M. 1987. Electromagnetic methods in applied geophysics. Investigations in geophysics No. 3. Tulsa: Society of Explorations Geophysicists.

Naidu, G. D. 2012. Magnetotellurics: Basic Theoretical Concepts. Chapter 2. In Deep Crustal Structure of the Son–Narmada–Tapti Lineament, Central India. Springer thesis. Berlin, Heidelberg: Springer-Verlag. DOI: 10.1007/978-3-642-28442-7_2.

Naprstek, T. 2014. Modelling radio imaging method data using electrical dipoles in a homogeneous whole space. Master of Science thesis, Laurentian University, Sudbury, Ontario, Canada.

Naprstek, T. & Smith, R. S. 2016. The effect of dielectric permittivity on the fields radiated from a radio-frequency electric dipole in a homogeneous whole space. Geophysics, 81, K1-K8.

Olaffson, G. & Quinto, E. T. 2006. The Radon Transform, Inverse Problems, and Tomography. American Mathematical Society, 63.

Olhoeft, G. R. 1976. Electrical properties of rocks. In: Strens, R.J.G., The Physics and Chemistry of Rocks and Minerals. London: Wiley, 262-278.

Orfanidis, S. J. 2004. Electromagnetic waves and antennas. ECE Department. Rutgers University. Piscataway. Availabe at: http://www.ece.rutgers.edu/~orfanidi/ewa/.

Paige, C. & Saunders, M. 1982. LSQR: An algorithm for sparse linear equations and sparse least squares. ACM on Trans. Math. Software,8, 43-71.

Parasnis, D. S. 1973. Mining geophysics. Second revised and up-dated edition. Methods in Geochemistry and geophysics, 3. Amsterdam: Elsevier Scientific Publishing Company.

Parasnis, D. S. 1986. Principles of applied geophysics. Fourth edition. New York: Chapman and Hall.

Parkhomenko, E. I. 1967. Electrical properties of rocks. New York: Plenum Press.

Pears, G. A. & Fullagar, P. K. 1998. Weighted tomographic imaging of radio frequency data. Exploration Geophysics, 29, 554-559.

Pellerin, L. & Wannamaker, P. E. 2005. Multi-dimensional electromagnetic modeling and inversion with application to near-surface earth investigations. Computers and Electronics in Agriculture, 46, 71-102.

Popa, C. & Zdunek, R. 2004. Kaczmarz extended algorithm for tomographic image reconstruction from limited-data. Math. Comput. in Simulation, 65, 579-598.

Pralat, A. & Zdunek, R. 2005. Electromagnetic geotomography – selection of measuring frequency. IEEE Sensors Journal, 5, 242-250. Available at: http://dx.doi.org/10.1109/JSEN.2005.843897

Puranen, M. 2009. Pulsed radar measurements and related equipment. Doctoral dissertation. Espoo: Helsinki University of Technology.

Redko, G. V., Lebedkin, L. V., Shuval-Sergeev, A., Stevens, K. & Kazda, G. 2000a. Borehole electromagnetic geophysical methods in ore and coal deposits. A paper at the International Conference "300 years of Russian mine-geological service", Saint-Petersburg (Russia). Availabe at: http://www.farasystem.ru/Pubs/Spb1998_Text_E.pdf

Redko, G. V., Ratnikov, K. D., Savitsky, A. P., Fedorov, A. B. & Shuval-Sergeev, A. N. 2000b. Method of cross-hole radiowave surveying in ore deposits. A paper at the International Conference "300 years of Russian mine-geological service", Saint-Petersburg (Russia), 2000. Available at: http://www.farasystem.ru/Pubs/Spb2000_Text_E. pdf

Reintjes, J. F. & Coate, G. T. 1953. Principles of radar. Third edition. New York: McGraw-Hill Publishing Company Ltd.

Ruffet, C., Gueguen, Y. & Darot, M. 1991. Complex conductivity measurements and fractal nature of porosity. Geophysics, 56, 758-768.

Saksa, P., Heikkinen, E. & Lehtimäki, T. 2005. Geophysical radar method for safeguards application at Olkiluoto spent fuel deposal site In Finland. STUK report STUK-YTO-TR 213.

Salisbury, M. H., Milkereit, B., Ascough, G., Adair, R., Matthews, L., Schmitt, D. R., Mwenifumbo, J., Eaton, D. W. & Wu, J. 2000. Physical properties and seismic imaging of massive sulfides. Geophysics, 65, 1882-1889.

Seybold, J. S. 2005. Introduction to RF propagation. New Jersey: John Wiley & Sons, Inc.

Sharif, L. K. 2013. Application of the cross-hole radio imaging method in detecting geological anomalies, Maclennan township, Sudbury Ontario. Master of Science thesis, Laurentian University, Sudbury, Ontario, Canada. (dissertation)

Sheriff, R. E. & Geldart, L. P. 1995. Exploration Seismology. Second edition. Cambridge: Cambridge University Press.

Smith, G. S. 1977. An introduction to classical electromagnetic radiation. Cambridge: Cambridge University Press.

Somerstein, S. F., Berg, H., Chang, D., Chung, H., Johson, H., Richardson, B., Pizzicara, J. & Salisbury, W. W. 1984. Radio frequency geotomography for remotely probing the interiors of operating mini and commercial sized oil shale retorts. Geophysics, 49, 1288-1300.

Spetzler, J. & Snieder, R. 2004. The Fresnel volume and transmitted waves. Geophysics 69, 653-663.

Stevens, K., Watts, A. & Redko, G. 1998. In-Mine Applications of the Radiowave Method in the Sudbury Igneous Complex. A paper at the Annual SEG Conference, Calgary (Canada), 2000. Available at: http://www.farasystem.ru/Pubs/papr0398.pdf

Stolarczyk, L. G. & Fry, R. C. 1986. Radio imaging method (RIM) or diagnostic imaging of anomalous geologic structures in coal seam waveguides. Society for Mining, Metallurgy and Exploration Inc. Transactions, 288, 1806-1814.

Tanabe, K. 1971. Projection method for solving a singular system of linear equations and its applications. Numer. Math., 17, 203-214.

Thompson, S. & Hinde, S. 1993. Bringing geophysics into the mine: Radio attenuation imaging and mine geology. Exploration Geophysics, 24, 805-810.

Touloukian, Y. S., Judd, W. R. & Ho, C. Y. 1981. Physical properties of rocks and minerals. Data series on material properties. McGraw-Hill/Cindas. II-2. New York: McGraw-Hill Book Company.

Turner, G. & Siggins, A. F. 1994. Constant Q attenuation of subsurface radar pulse. Geophysics, 59, 1192-1200.

Vogt, D. 2000. The modelling and design of radio tomography antennas. University of York (United Kingdom) Available at: http://www.opengrey.eu/item/display/10068/624370

Wait, J. R. 1969. Electromagnetic fields of sources in lossy earth. Chapter 23. In: Collin, R. E. & Zucker, F. J. Antenna Theory. New York: McGraw-Hill.

Ward, S. H. 1987. Electrical methods in geophysical prospecting. In: Sammis, C. G. & Henyey, T. L. Methods of experimental physics. Volume 24 - part B. Geophysics: Field measurements. New York: Academic Press, Inc.

Yu, L., Chouteau, M., Boerner, D. E. & Wang, J. 1998. On the imaging of radio-frequency electromagnetic data for cross-hole mineral exploration. Geoph. J. Int., 135, 523-541.

Zhang, K. & Li, D. 2007. Electromagnetic Theory for Microwaves and Optoelectronics. Second edition. Berlin, Heidelberg: Springer-Verlag.

Zhou, B. & Fullagar, P. K. 2001. Delineation of sulphide ore zones by borehole radar tomography at Hellyer mine, Australia. Journal of Applied Geophysics, 47, 261-269.

Zhou, B., Fullagar, P. K. & Fallon, G. N. 1998. Radio frequency tomography trial at Mt Isa Mine. Exploration Geophysics, 29, 675-679.

ORIGINAL PUBLICATIONS

The four publications presented in the appendix form an entity in which the basics of the radio imaging method (RIM) are explained, consisting of the device properties, basic mathematics and field cases. In the first publication, "*Geotomographic studies for ore explorations with the EMRE system*", the fundamentals of the EMRE device are presented, including basic mathematics using a plane wave approximation resulting in common equations for the attenuation and phase constant. RIM results from an ore district are compared with electric logging and TEM results. The second paper concentrates on the functioning of insulated electric dipole antennas in borehole conditions, "*Borehole antenna considerations in the EMRE system: Frequency band 312.5–2500 kHz*". The third paper, "*Characterization of geotomographic studies with the EMRE system*", clarifies the basic properties of the EMRE system and determines its performance level using a simple geometric model. The scattering parameter s_{11} is determined and the behaviour of s_{11} is examined under various conditions. An interesting field case from the Olkiluoto site is also examined. The fourth paper, "*Radiowave imaging (RIM) for determining the electrical conductivity*

of the rock in borehole section OL-KR4–OL-KR10 at Olkiluoto, 2005", concentrates on a special field case at the Olkiluoto site.

Paper I

Korpisalo, A. 2014. Geotomographic studies for ore explorations with the EMRE system. Measurement, Vol. 48, 232–247.

A new geophysical borehole prospecting method has been taken into use at the Geological Survey of Finland (*GTK*), known as the radiofrequency imaging method (RIM). RIM is a high-resolution technique and useful for second-stage explorations and ore body delineations, assisting, for instance, in strategic mine planning and large rock building projects to determine the structural integrity of the rock in the area of interest. It is a computerized tomography method that is based on the attenuation of radiowaves between boreholes, making it possible to reconstruct the attenuation distribution of the borehole section (*tomographic image*). Under certain conditions, it may also be possible to convert the high p domain attenuation to electric conductivity and use it to determine the relative permittivity in the low p domain. The system consists of a continuous wave (*CW*) borehole transmitter and borehole receiver. The transmitter and receiver deploy insulated dipole antennas to radiate and receive electromagnetic energy. The borehole transmitter of the system is the core, where the four measurements frequencies (*312.5, 625, 1250, 2500 kHz*) and the vital references frequency (*156.25 kHz*) are generated. The reference is important in the proper detection of the phase difference and amplitude. This paper presents the first experiences with the RIM device in Finland, dealing with the technical characteristics of the instrument and comparisons with results measured by other systems (resistivity logging and transient electromagnetic method). Presently, the device is the main part of a borehole system known as EMRE (*electromagnetic radiofrequency echoing*).

Paper II

Korpisalo, A. 2013. Borehole antenna considerations in the EMRE system: Frequency band 312.5–2500 kHz. The Open Geology Journal, Vol. 7, 63–79.

The electromagnetic radiofrequency echoing (EMRE) system is utilized in radiofrequency imaging (RIM) measurements between two deep boreholes. It is based on radiowave attenuation, making it possible to reconstruct the attenuation distribution of the borehole section (tomogram). The main parts of the EMRE system are a continuous wave (CW) transmitter and superheterodyne-type receiver. The insulated dipole antennas are the transducers between the device and environment, or together they form a transmission line. The system is bistatic because the antennas are placed in separate boreholes. When an antenna is situated in a dissipative medium, e.g. in a deep borehole, its performance becomes highly environmentally sensitive. Direct measurements of the feed-point current and radiative characteristics are impossible, and numerical models must therefore be used to investigate the borehole effects. A generalized transmission line model of an insulated antenna is a simple and useful way to examine the antenna-related properties. A drawback is that the borehole water must be excluded from the models due to the high wave number of water. The commercial simulation package FEKO is a numerical modelling package and a powerful tool when constructing more realistic antenna and borehole models. FEKO models and transmission line models (WKG, CHEN) were compared and the results coincided in the frequency band of 312.5–2500 kHz. According to the FEKO studies, the influence of borehole water and the location of the antenna in the borehole, i.e. centric or eccentric, did not appear to have a significant effect. The scattering parameter s_{11}, the ratio of forward and returned power, is a useful antenna parameter to estimate the power level that is radiated from the antenna to the surrounding rock. According to the FEKO models, the highest measurement frequency (2500 kHz) of the EMRE system appears to suffer the most under the borehole conditions due to the low values of s_{11} (~–2dB). The performance level of the system determines the maximum distances (transillumination distance) at which the signals are still detectable. According to the results using a simplified measurement geometry, the EMRE system can operate at distances of <1000 m when the host rock has resistivities of >10 000 Ωm and the lowest frequency of 312.5 kHz is used. At minor distances of 400–600 m, the system operates well at all frequencies.

Paper III

Korpisalo, A. 2014. Characterization of geotomographic studies with the EMRE system. International Journal of Geophysics, Vol. 2014. Article ID 401654. 18 p.

Posiva Oy carries out research and development on spent nuclear fuel disposal in Finland. A repository will be constructed deep in the crystalline bedrock of Olkiluoto Island in Eurajoki. Posiva Oy and ANDRA (*France*) have actively cooperated in examining methods for revealing the properties of granitic bedrock. One of the considered methods was an electromagnetic cross-borehole survey, and RIM measurements were conducted in 2009. Olkiluoto migmatitic bedrock has undergone polyphasic ductile-brittle deformation and resistivity in the bedrock varies strongly in the range of tens to tens of thousands of Ωm. Fieldwork was successfully performed in one borehole pair, and the results are presented in this paper. The tomographic reconstruction of the borehole section is based on the far-field approximation of the electric field. The results prove that the method can be used between boreholes to delineate and follow sulphide-bearing horizons. The detected low and high resistivity zones and their apparent shapes and orientations are in fair agreement with geological and other geophysical results. The obtained information can be used, for example, in assessing the integrity of the rock mass, as increased electrical conductivity is often associated with rock mass deformation (*clay and water bearing fractures, sulphide and graphite bearing zones*).

Paper IV

Korpisalo, A. & Heikkinen, E. 2014. Radiowave imaging (RIM) for determining the electrical conductivity of the rock in borehole section OL-KR4–OL-KR10 at Olkiluoto, Finland. Exploration Geophysics, Vol. 46. Published online: 14 May 2014.

We carried out an electromagnetic cross-borehole survey as a feasibility target for the radiowave imaging method (RIM) in a possible area for a repository of spent nuclear fuel in Finland to reveal the properties of the granitic, i.e. crystalline bedrock. The resistivity of the bedrock varies strongly in the range of tens to tens of thousands of ohm metres due to sulphide bearings. Because increased electrical conductivity is often associated with rock mass deformation (clay and water-bearing fractures, sulphide- and graphite-bearing zones), the obtained information could be used, for example, in determining the integrity of the rock mass.

This paper describes the fieldwork, as well as the interpretation and comparison of the results of radiowave imaging with other geophysical results in one borehole section at the 200–600m depth level from 2005. The results verified that the method can be used to delineate and follow sulphide-bearing horizons between boreholes. The detected low and high resistivity zones and their apparent shapes and orientations are in fair agreement with geological and other geophysical results. The material properties differ from those recorded in seismic tomography from the same location, although the reflections partly describe the boundaries of domains differing in electrical properties. Using borehole geometry, similar but more detailed information is obtained compared with electric and electromagnetic measurements from the ground surface. Our first experience with RIM convinced us that it can also be utilized in such challenging environments as at Olkiluoto, and not only when massive sulphide deposits exist.

All GTK's publications online at hakku.gtk.fi

Our knowledge of the earth's subsurface systems and structures is still quite limited, and thus new methods and interpretation techniques are continuously being developed to better understand geological systems. This Ph.D. thesis comprises a synopsis and four original papers dealing with the essential issues concerning the radio imaging method (RIM) and attenuation measurements, providing an overview of the fundamental aspects of RIM and presenting novel results from the combination of RIM with other borehole methods. Medium radiofrequencies are high enough to give much better resolution and sensitivity to conductive targets in the subsurface than traditional ground-level and borehole methods, but at the same time, radiofrequencies are low enough for translumination depths of even 1,000 m to be reached. Formations (e.g. massive sulphide deposits) between boreholes produce distortions in the measured data and lead to higher attenuation values. The attenuation distribution of a section can reliably be reconstructed with simple traditional tomographic techniques. In addition, the interpretation of the section can even be started at the measurement site, because these techniques are rapid, and the direction of the measurements can thus easily be changed, even during a survey. This thesis deepens our understanding of the physical characteristics of electromagnetic fields in a lossy medium and has proven the potential of RIM in exploration geophysics.

ISBN 978-952-217-359-1 (PDF version without articles)
ISBN 978-952-217-358-4 (paperback)